Graduate Theses, Dissertations, and Problem Reports

2000

Refined turbulence models for simulation of IC -engine cylinder flows

Ibrahim Yavuz
West Virginia University

Follow this and additional works at: https://researchrepository.wvu.edu/etd

REFINED TURBULENCE MODELS FOR SIMULATION OF IC-ENGINE CYLINDER FLOWS

Ibrahim Yavuz

**Dissertation submitted to the
College of Engineering and Mineral Resources
at West Virginia University
in partial fulfillment of the requirements
for the degree of**

**Doctor of Philosophy
in
Aerospace Engineering**

**Ismail Celik, Ph.D., Chair
John Kuhlman, Ph.D.
Harry Gingold, Ph.D.
Christopher Atkinson, Sc.D.
Alberto Ayala, Ph.D.**

Mechanical and Aerospace Engineering Department

**Morgantown, West Virginia
2000**

Keywords: Computational Fluid Dynamics, IC Engines, KIVA, LES

ABSTRACT

Refined Turbulence Models for Simulation of
IC-Engine Cylinder Flows

Ibrahim Yavuz

Turbulence and turbulent mixing are two of the most important factors that influence the efficiency and emissions level in internal combustion (IC) engines, particularly for diesel engines. This study has been performed with the premise to accurately predict in-cylinder turbulence by employing the large eddy simulation (LES) technique. In order to assess the turbulence scales involved correctly, a review of measured and computed scales relevant to IC engines is conducted. An assessment of these is made in comparison with the self-imposed scales of the engine itself. This assessment focuses on the influence of combustion, compression ratio, initial conditions and numerical mesh on predicted turbulence scales. It was found that the turbulence scales predicted by employing the commonly used k-ε turbulence model were in good qualitative agreement with experimental observations and could be used as a guide to determine the degree of resolution needed in LES.

To establish a base to improve existing Reynolds averaged Navier-Stokes (RANS) models, a comparative study of the commonly used RANS models applied to IC engines was conducted, using an experimental benchmark case, which is an isothermal, incompressible flow within a piston-cylinder arrangement motored without combustion. This study has lead to a new hybrid turbulence model, namely, the Smagorinsky based eddy viscosity (SEV) model, which is self-adjusting between an eddy viscosity model and subgrid-scale model, depending on the grid size, continuously from RANS to LES. It was tested against the above-mentioned experimental benchmark. The predicted velocity profiles and streamlines are in good agreement with experiments. The new model is a viable alternative to the k-ε model in predicting the mean flowfield in IC engines.

Furthermore, the relative importance of the turbulence generation mechanisms in IC engines has been studied using LES. First, the compression and expansion strokes of a piston-bowl configuration are thoroughly investigated using a fine 2-D axisymmetric grid and a 3-D grid. Next, the flow dynamics during the intake stroke has been examined using a full 3-D configuration of an engine with valves and a typical bowl. The results show that a significant portion of the inertial sub-range in the energy spectra can be resolved using a moderately fine grid with about 300,000 vertices. The calculated spectra display about the same energy content up to $f \approx 10^4$ Hz, which is on the same order of maximum frequency resolved in typical experiments. It is shown via the LES technique, that significant turbulence is likely to be generated by a carefully designed bowl; and that the more energetic intake turbulence generated during the intake stroke decays rapidly during the compression stroke.

I dedicate this study to my family,
whose love and continuous support
made it possible for me to see the end of this endeavor.

ACKNOWLEDGEMENTS

I am extremely grateful to Dr. Ismail Celik, my advisor, for his friendship and guidance throughout this endeavor. Without his mentorship, helpful advice, and patience, I would not have been able to conduct this research. I would also like to extend my gratitude to Dr. John Kuhlman, Dr. Harry Gingold, Dr. Christopher Atkinson, and Dr. Alberto Ayala, who were supportive and helpful while serving on my graduate committee.

I am grateful to all my colleagues and friends for their support and inspiration during my continued education.

Finally, I would like to thank my wonderfully supportive parents and my brothers and sisters, whose encouragement made it a little easier to live far away from my beloved ones.

TABLE OF CONTENTS

LIST OF FIGURES

LIST OF TABLES

Chapter 1

OBJECTIVE

The objectives of this research are to develop new or refine existing models to improve the turbulent flow solution capabilities of a widely-used engine code, KIVA, and to improve the capabilities of this tool to perform large eddy simulations while considering to build a synergism of LES and RANS models. The long-term goal is to enhance the understanding of turbulence generation in IC-engines and provide insight for achieving higher efficiency and environmentally acceptable emissions levels.

Chapter 2

INTRODUCTION

Realistically simulating and predicting the mixing and combustion phenomena relevant to IC engines still heavily depends on accurate prediction of in-cylinder turbulence. As it is also demonstrated in this work, the shortcomings of the classical turbulence models, particularly the two-equation models, are the primary factors for poor predictions. This study has been performed with the premise that some of these turbulence-modeling issues can be addressed by employing the large eddy simulation (LES) technique to predict in-cylinder flow dynamics. In the LES approach the most important (energetic), large turbulent scales are resolved, while only the effect of unresolved small scales are modeled. For the present simulations the existing KIVA family (versions 2, 3, and 3V) of codes originated from Los Alamos National Labs was utilized. The 3-D, unsteady KIVA codes, which were designed specifically for internal combustion engines, have been modified for LES.

First, the order of magnitudes of the important length and time scales which are relevant to both the engine geometry and speed, and the resulting turbulent flow field are established. If these scales are correctly assessed, the understanding of the turbulent flow field will improve, which in turn will lead to better modeling strategies. A review of

measured and computed scales relevant to IC engines is presented, and an assessment of these is made in comparison with the self imposed scales of the engine itself. This assessment includes axisymmetric calculations using the KIVA-3 code (Amsden, 1993) for a typical IC engine, and focuses on the influence of combustion and numerical mesh on predicted turbulence scales. RANS (Reynolds Averaged Navier Stokes) simulations have also revealed that the turbulence length scale indicated by the k-ε model provide a good base line for deciding on the degree of resolution needed for LES simulations.

Another goal of this research is to improve existing RANS models when applied to IC-engines. To achieve this a study is performed on a benchmark flow, which resembles that of a motored IC-engine to assess the performance of various turbulence models. As expected the models do not perform uniformly well over all flow regimes. Significant differences were observed among various models as the engine speed increased. A new hybrid model has been proposed which tends to RANS calculations with an eddy viscosity model and to LES with a Smagorinsky SGS model, in the limits of coarse and fine girds, respectively. This is especially suitable for engine simulations because most engine simulations are inherently three-dimensional and transient as in LES.

Much work has focused on the compression and expansion strokes under motored conditions, due to the complications introduced by the valve dynamics during the intake stroke. A comparison of the results using different subgrid-scale (SGS) models showed that the simulations with a SGS model produced an energy cascade, derived from a spectral analysis of the fluctuating data, that qualitatively resembled experimental trends. To achieve this, the numerical errors needed to be carefully controlled using small time

3

steps with second order convection schemes. The predicted turbulence intensity was low but showed the same trend (roughly a linear relationship with mean piston speed) as experiments. This lower intensity can be partly attributed to approximations of the unknown initial conditions inside the cylinder, which may be influenced significantly by the intake stroke.

During the compression and expansion strokes, turbulence is induced primarily by the geometry of the piston-cylinder assembly, in particular the piston-bowl. Most of the turbulence in a real engine is induced during the intake stroke. For the next level of realism, simulations of the intake and subsequent expansion and compression strokes were performed for a typical two-valve cylinder assembly using the KIVA-3V (Amsden, 1997) code. A multi block structured mesh was set up for a general engine geometry. A study was performed using different sub-grid scale and RANS turbulence models including the k-ε model, no turbulence model, and a Smagorinsky model. The study showed that the growth and the subsequent decay of turbulence during the intake phase predicted with the Smagorinsky subgrid-scale model agreed well with experiments. The power density spectra of the fluctuating velocity components were compared with those obtained from the measurements. This comparison showed that a significant portion of the inertial range dynamics is captured in the simulations.

Chapter 3

LITERATURE REVIEW

Turbulence and turbulent mixing are two of the most important factors which influence the efficiency and emissions level in internal combustion (IC) engines, particularly for diesel engines (see Hentschel, 1996; Reynolds, 1980; Heywood, 1987). The mean flow field is also a critical factor controlling the combustion process. Together they control the fuel-air mixing and burning rates, influence the mechanisms by which emissions form, and govern the heat transfer rate to the cylinder walls. These flows are extremely complex: they are turbulent, unsteady (in the mean), and three-dimensional. The flow field is further complicated by the presence of swirl, squish, tumble, phase change (of fuel droplets), chemical reactions, density fluctuations and acoustic phenomena. According to Hentschel (1996), swirl is a dominant flow structure in the piston bowl, and tumble and turbulence are essential for perfect mixing which is a prerequisite for high power output at a low soot level. A good understanding of the physical processes of fluid motion in diesel chambers is critical in developing engine designs and control diagnostics with the most desirable operating efficiency and emissions characteristics.

The classical multidimensional modeling approach is to use some semi-empirical turbulence model (e.g. the well-known k-ε model) to close Reynolds/Favre Averaged Navier-Stokes (RANS) equations of motion. These models have serious shortcomings in that they introduce ad hoc assumptions, which are not validated or verified by experiments. One such assumption is the local isotropy of turbulence inherent to eddy viscosity models. For example, in the standard k-ε model the eddy viscosity is isotropic, and the dissipation rate, ε, equation is modeled using the local isotropy assumption (see e.g. Hossain and Rodi, 1982). In addition to local isotropy, this model uses a single length scale and a time scale (locally) to represent a whole spectrum of turbulent length and time scales ranging from the large eddies (proportional to the size of the combustion chamber) down to the Kolmogorov scales. Moreover, most of these models require that the turbulent stress tensor be aligned with the mean rate-of-strain tensor, which is not valid for many complex flows such as those observed in IC-engines. An important defect in the k-ε model is that it gives a completely unrealistic representation of the normal stresses, failing to reproduce the strong normal stress anisotropy observed essentially in all shear flows. Many of the shortcomings and assumptions made in RANS simulations can be eliminated by employing the Large Eddy Simulation (LES) technique which has been widely tested for simple flows, and has recently been extended for predicting complex turbulent flows encountered in realistic engineering applications.

The LES technique solves the three dimensional, transient Navier-Stokes equations after applying a spatial filtering which is similar to time averaging. Depending on the filter width, which is usually a function of the numerical mesh size used, LES can capture the most important large-scale fluctuations in the flow quantities, leaving only the

relatively small scales to be modeled empirically. The finer the grid size, the better is the resolution of turbulence scales, and the less important are the modeling assumptions. The small-scale structures in turbulence are believed to be more isotropic; hence the usual eddy-viscosity type models are more appropriate. If LES can be successfully applied to engine flows it should provide insight to the above-mentioned controversies and enhance the understanding of in-cylinder turbulence generation and control. In particular, it will help to resolve the outstanding questions relevant to integral length and time scales, heat and mass transfer rates, reaction rates, and cycle-to-cycle variations. It will also provide data that can be used to refine the classical turbulence models.

As far as RANS modeling is concerned, there is an extensive amount of literature on internal combustion engines (Bo et al., 1997; Celik et al., 1992, 1997; Reitz and Rutland, 1991; Han et al., 1997; Ramos, 1989; O'Rourke and Amsden, 1987; Bashay et al., 1986; Gosman, 1985). Most of the current computational studies utilize some version of the so-called k-ε turbulence model. Because of the multiple eddy structures and the strongly elliptic nature of the governing equations, low-order (i.e. zero-equation) models do not work well. Some studies use algebraic stress models (ASM), but the improvements over the k-ε model and its variants (e.g. low Reynolds number k-ε model; RNG k-ε, Lien and Leschziner, 1994, Han et al., 1996) are marginal and there is no consensus in the literature as to which model performs better. The isotropic eddy viscosity concept and gradient diffusion model, where the turbulent stresses are related solely to the local strain rates, are central to the k-ε model. It is well known (see e.g. Reynolds, 1980) that in most cases relevant to engine combustion chambers the above assumptions are not correct. Due to this fact, the performance of the k-ε model has not

been fully successful, and the predictions are not as accurate as is desirable; in some cases performance is very poor. The comparisons presented by Leschziner (1991), Celik et al. (1987), and Mongia et al. (1986), confirm the above arguments. The applications of second moment closure models (i.e. Reynolds stress transport-RST models) to three dimensional turbulent flows are scarce in the literature for the obvious reason that six additional non-linear partial differential equations must be modeled and solved. RST models were applied to engine-like geometries in a recent study by Yang et al. (1998). Although this study shows some promise it remains to be fully validated. This study also shows significant differences between k-ε and RST model results. Leschziner (1991) has demonstrated that while considerable improvement can be gained from second moment-closure, predictive performance is not consistently satisfactory.

State-of-the-art experimental techniques are also available and they are being applied to measure in-cylinder turbulence. Some recent studies in this field are: Catania et al. (1995, 1996, 1997); Corcione and Valentino (1990); Valentino et al (1998); Lee and Farell (1992); and Himes and Farell (1998). There are also attempts to deduce some of the relevant scales from measurements (see e.g. Catania et al. 1997; Arcoumanis et al., 1994; Subramaniam et al., 1991; Corcione and Valentino, 1990, 1994a&b, Witze, 1977 and Lancaster, 1976). Not only are these measurements difficult and time consuming, but they are also limited in the sense that only point data can be obtained in case of hot-wire and LDV measurements. The PIV techniques are still in a stage of development (Reuss et al., 1995; Choi and Guezennec, 1998). Measurement techniques that can withstand the harsh combustion environment inside the engine cylinder are very rare, and require glass (quartz) windows for optical access. The above mentioned studies point to the importance

of integral turbulence length scales and time scales in determining the dynamics of in-cylinder flow and combustion processes.

In the last decade a substantial effort has been put into advancing the prediction of turbulence in compressible non-reacting flows by application of LES (Reynolds, 1989; Galperin and Orszag, 1993; Ragab and Piomelli, 1993; Rodi et al., 1997; and Piomelli, 1998). The same technique has also been applied to turbulent reacting flows with considerable success (see e.g. Garrick, 1995; Erlebacher and Hussaini, 1993; Menon and Jou, 1991; Sykes et al., 1990, 1994). Reynolds (1980) suggested that LES was probably the best way to model combustion in reciprocating engines. The application of LES to internal combustion engine (ICE) cylinder flows is rare because of complications introduced by compressibility, complex cylinder and valve geometries with moving boundaries, and particularly the complication due to turbulence-combustion interaction. One of the early attempts of LES for engine flows was presented by Naitoh et al. (1992). This extensive study even with a relatively coarse grid, and first order Euler time marching scheme has shown the great potential of LES for ICE applications. Another study using a finite volume CFD code is by Haworth (1998) who reported encouraging results in predicting the ensemble averaged trends for an experimental axisymmetric, motored engine cylinder at a relatively low speed of 200 RPM.

3.1   Turbulence and Turbulence Modeling

One of the pioneers in the study of turbulent flows, Osborne Reynolds, named this type of motion "sinuous motion".

Although it is difficult to give a precise definition of an irregular motion like turbulent flow, Hinze (1975) defined turbulence as:

"Turbulent fluid motion is an irregular condition of flow in which the various quantities show a random variation with time and space coordinates, so that statistically distinct average values can be discerned."

Moreover, Bradshaw (1971) defined turbulence in a more satisfactory way as:

"Turbulence is a three-dimensional time-dependent motion in which vortex stretching causes velocity fluctuations to spread to all wavelengths between a minimum determined by viscous forces and a maximum determined by the boundary conditions of the flow. It is the usual state of fluid motion except at low Reynolds numbers."

3.1.2 Properties of Turbulence

For a better understanding of turbulence a list of the characteristics of turbulent flows is summarized below:

- One characteristic of all turbulent flows, is the irregularity, or apparent randomness. This leads one to rely on statistical methods, since a deterministic approach to turbulence problems is impossible.

- The diffusivity of turbulence is perhaps the most important feature of turbulence from an engineering point of view. Turbulent diffusion causes rapid mixing, and greatly enhances the transfer of momentum, mass and energy. Several orders of magnitude larger stresses develop in turbulent flows than in corresponding laminar flows. As far as applications are concerned: it prevents boundary-layer

separation on airfoils at fairly large angles of attack, it raises heat transfer rates in machinery, etc.

- High Reynolds numbers are common in turbulent flows. An analysis of the solutions to the Navier-Stokes equations, show that turbulence often originates as an instability of laminar flows if the Reynolds number becomes too large. The instabilities are related to the interaction of viscous terms and nonlinear inertia terms in the equations of motion (Tennekes and Lumley, 1972).

- Turbulence is rotational and three-dimensional. The characteristic fluctuating vorticity in turbulent flows is maintained by vigorous stretching of vortex lines (Wilcox, 1993; Tennekes and Lumley, 1972), which is missing in two-dimensional flow. Nevertheless, two-dimensional turbulence is studied, as of its simplicity and as a basis for three-dimensional turbulence. However, Batchelor (1969) expresses his concerns as:

   "Motion in two dimensions has the simple property that vorticity of a fluid element is unchanged (i.e., in 2-D although $\omega = 0$ and $\frac{\partial}{\partial z} = 0$, vorticity, $\underline{\nabla} \times \underline{V} \neq 0$), except by molecular diffusion, as the element follows the motion. And precisely because of this special characteristic of 2-D motion, we should be wary of assuming too close a relation between two- and three- dimensional turbulence."

- Turbulence is dissipative in nature. The viscosity effects in real fluids will result in an increase of the internal energy of the fluid at the expense of kinetic energy

11

of turbulence. The continuous generation of turbulent motion depends on a continuous supply of energy; otherwise it will decay.

- The time-dependent, three-dimensional Navier-Stokes equations govern the physics of turbulent flow. This leads to the fact that turbulence is a continuum phenomenon. Even the smallest scales present in a turbulent flow are far larger than any molecular length scale (Tennekes and Lumley, 1972).

- Turbulence consists of a continuous spectrum of scales, i.e. turbulence is a broad-band process with a continuous spectrum where all scales ranging from largest to smallest interact (Schumann, 1993). For a better understanding one is referred to the concept of eddies. A turbulent eddy can be described as a local swirling motion with a characteristic dimension of the local turbulence scale. On one end of the spectrum are the large, energy containing eddies. As the turbulence decays, the kinetic energy of the highly anisotropic larger eddies is transferred to the isotropic smaller eddies. The smallest eddies then dissipate into heat via molecular viscosity interaction. Therefore, turbulence becomes more homogeneous and independent of direction with the effect of viscosity.

- A common source of energy for turbulence is shear in the mean flow and buoyancy. But mostly other factors, like rotational or irrotational mean flow straining of turbulence and initial and boundary conditions, determine the eddy structure (Hunt, 1990).

3.1.2 Turbulence Modeling

Attempts of modeling turbulence started more than a century ago, when Boussinesq (1877) introduced the concept of an eddy viscosity, i.e. the Boussinesq eddy viscosity approximation. After Prandtl (1925) introduced the mixing length and a method for computing the eddy viscosity in terms of the mixing length, the horizon for turbulence modeling was broadened. A mixing length model is usually referred to as an algebraic model or a zero-equation model of turbulence. The birth of the one-equation model of turbulence had to wait until 1945 when Prandtl postulated a model in which the eddy viscosity depends upon the kinetic energy of the turbulent fluctuations, k. This improvement takes into account that the eddy viscosity is affected by the flow history. However, even with this development, turbulence models that do not provide a length scale are incomplete (Wilcox, 1993).

A complete model of turbulence should be of a kind that does not require any prior knowledge of any property of the turbulence. The first one was introduced by Kolmogorov (1942), the so-called k-ω model. In this model ω has a differential equation similar to the one for k. Thus, this model is termed a two-equation model of turbulence.

Second order closure models were founded by Rotta (1951), which do not make use of the Boussinesq approximation. Instead, they use a model for the turbulent stresses, i.e. the Reynolds-stress tensor. These models take effects like streamline curvature, rigid body rotation and body forces into account, which is not the case in eddy viscosity models.

All of the models mentioned above are the so-called RANS (Reynolds Averaged Navier Stokes) models. There are four main classes of techniques for dealing with turbulent flows:

1) Analytical

2) Direct numerical simulation (DNS)

3) Reynolds averaged Navier-Stokes (RANS)

4) Large eddy simulation (LES)

For highly idealized situations like isotropic and homogeneous flow, analytical methods can be employed (Aldama, 1990). These studies have proven to provide information about the dynamic behavior of small scales of turbulence.

In direct numerical simulation the solution of the Navier-Stokes equations are sought without averaging and approximation. Though there will be some errors from the numerical discretization, they can be estimated and controlled. Basically, all scales of the motion contained in the flow are resolved. DNS is used for developing an understanding of the physics of the flow and deployed in developing turbulence models for simple flows. However, from an engineering point of view, it provides far more information than an engineer needs, and it is simply too expensive to be employed on a regular basis. Moreover, on present machines it is restricted to low Reynolds numbers.

Most engineering flows of interest are turbulent in nature and it is not a trivial task to do accurate numerical simulations of these flows. The mixed quality of the results gained with RANS simulations and the ever-decreasing cost of doing computations has led to the recognition of large eddy simulation (LES) as a tool for prediction of turbulent

flows. Large eddy simulations are three-dimensional, time-dependent and expensive but much less costly than direct numerical simulations. Thus, LES is preferred when the Reynolds number is high or the geometry is relatively complex for the application of DNS. A detailed discussion of large eddy simulations will be presented later.

3.2   Turbulence Scales

It is important to establish the order of magnitudes of the important length and time scales which are relevant to both the engine geometry and speed, and the resulting turbulent flow field.

The relevant length and time scales pertaining to both the geometry and to turbulence are reviewed by Reynolds (1980) and Heywood (1987), and computed by Shah and Markatos (1986). The length scales exhibit a wide spectrum of sizes from the size of the combustion chamber down to the Kolmogorov microscale $l_K = \left(\nu^3/\varepsilon\right)^{1/4}$. In between are the thickness of the wall boundary layers, the width of the intake jet, the integral length scale of turbulence, and the Taylor microscale as relevant length scales which must be considered. The important time scales include the integral time scale of turbulence, large eddy turnover time, the flow-pass time (a measure of time required for a fast moving fluid eddy to travel the length of the shear layer), and development time (time required for a boundary layer to reach equilibrium). Since burning occurs at the smallest scales, it is desirable that these scales are either resolved or modeled (e.g. via sub-grid scale models) to accurately predict the flame structure and propagation. The time scale associated with the smallest eddies is the Kolmogorov time scale.

The two most important scales of turbulence, namely, the integral length scale and the Taylor microscale show significant variations over a complete engine cycle, as well as cycle-to-cycle. Shah and Markatos (1987) demonstrated that the length scales predicted by different versions of the k-ε model are significantly different; here k is the turbulent kinetic energy and ε is the dissipation rate of k. However, it was not investigated which scales were more appropriate for the engine simulations, and they were not compared to the relevant scales imposed by the engine itself. With liquid fuels, the length scales associated with the fuel jet, and the droplet size and distribution, including the evaporation velocity must all be accounted for. For example, the droplet turbulence interaction time (or turbulence-droplet correlation time) is usually taken to be the minimum of eddy turnover time (proportional to the integral time scale of turbulence) and the droplet residence time in a large-scale eddy. The droplet residence time in turn is a function of the droplet relaxation time, the slip velocity, and the gas-phase velocity fluctuations.

There is an extensive amount of information available in the literature concerning turbulence intensity, length scales and turbulence in general. However this information, which comes from discrete experiments which are engine or problem specific, have rarely been assessed together under the realm of theory and engine simulations using turbulence models. Here, only the most relevant literature has been reviewed and a summary of findings is presented. These are relevant to the selected topic, namely, turbulence modeling and combustion in IC engines.

One of the earlier papers in the area of turbulence characterization of motored spark ignition (SI) engines is due to Lancaster (1976) where proper measurements and

16

averaging techniques are discussed for non-stationary turbulent flows observed in SI engines. He showed that the turbulence energy spectrum deviated from the Kolmogorov distribution (i.e. -5/3 slope) in the lower frequency regions with a slope closer to -2. Only about 30% of the energy is contained at frequencies above 1.0 kHz. The turbulence frequencies were less than about 13 kHz for the engine conditions tested for speeds on the range 1000 - 2000 RPM (revolutions per minute). The turbulence intensity was found to scale with the mean engine speed as well as the volumetric efficiency, engine speed having the strongest effect. The turbulence intensity is naturally correlated with intake flow parameters (e.g. volume flow rate) near the top dead center (TDC). The temporal length scales increased with crank angle during the intake and compression strokes. The mean temporal microscale decreased with increasing mean engine speed. The in-cylinder turbulence near TDC of compression is nearly isotropic. By applying Taylor's hypothesis he obtained spatial micro scales in the range 0.63 to 0.84 mm, and 0.86 to 1.68 mm with non-shrouded and shrouded valves, respectively. Lancaster questions the applicability of Taylor's hypothesis to non-stationary engine flows. His assessment of the literature showed that the integral length scale, l_I , varied between 0.2 to 3.5 mm, and the Taylor microscale, l_T, can be estimated from $l_T = l_I / 4$.

The paper by Hoult and Wong (1980) sheds light on certain aspects of turbulence generation in IC engines. Here the authors apply rapid distortion theory to quantify turbulence intensity and energy spectrum. Comparisons with experiments indicate that this theory can indeed predict the correct trends during the compression and expansion phases. The theory works best during the combustion phase when the gases are compressed rapidly. The results show that the size of the main vortex generated during

the intake is scaled with the valve diameter, and its position remains approximately fixed relative to the piston position. The finding of Hoult and Wong is important in that they indicate that the viscous effects can be neglected at high Reynolds numbers and some kind of a conservation of vorticity perturbation law can be used, ignoring the nonlinear interactions of fluctuating quantities, to characterize the turbulent flow structure including flame propagation. Heywood (1987) points out that in the absence of dissipation, the rapidly imposed distortions during compression would nearly conserve angular momentum, and hence they should lead to an increase in vorticity and turbulence intensity. However, in some cases the dissipative effects can be large enough to render the above conclusion invalid.

An extensive review of the literature on IC engines turbulence is presented by Heywood (1987). He reiterates the fact that during the intake the turbulent flow is neither homogeneous nor isotropic. However, near TDC (at the end of the compression) the turbulence is nearly homogeneous, and in the absence of intake generated swirling flow the turbulence is essentially isotropic, and turbulence experiences a rapid decay process lasting until intake valve closing. With the swirl and bowl-in-piston geometry, the flow is expected to be more complex. It would be interesting to evaluate the influence of intake swirl on the turbulence generated by the intake flow. There are indications that swirl might either enhance or damp the turbulence level depending on the character of the swirl velocity profile. According to Heywood when the swirl velocity is of the solid-body rotation type the turbulence intensity almost always decreases. He also suggests that the maximum turbulent intensity at TDC is approximately equal to 50% of the mean piston speed. Concerning the turbulence length and time scales, Heywood's review reveals the

summary shown in Table 3.1. Another important piece of information pertaining to the length scales in engines is that the maximum wall boundary layer thickness on the cylinder head and piston surfaces could be as high as 5 mm at moderate engine speeds. The flow regimes inside the boundary layer as well as the main vortex motion inside the cylinder can be characterized by a Reynolds number defined as $Re = V_pL/\nu$; where V_p is the mean piston speed, L is the stroke, and ν is the kinematic viscosity.

Fraser et al. (1986) present direct measurements of lateral integral length scale using laser Doppler velocimetry (LDV). This length scale ranges between 2 to 3.5 mm for crank angles between 320 to 380 degrees ATDC with a local minimum at the TDC. When the same data is normalized by the instantaneous clearance height the non-dimensional value increases from 0.1 to 0.2 at TDC and remains approximately fixed after that. Lancaster's measurements agree with those by various other authors within a factor of two. The previous work reviewed by Lancaster along with his work seem to indicate that the relative integral length scale of turbulence should be function of the engine speed, swirl ratio, and compression ratio. He also points out that the longitudinal and lateral length scales could be significantly different; for homogeneous, isotropic turbulence the former is about two times the latter (a consequence of Taylor's hypothesis).

Corcione and Valentino (1990) presents some direct measurements of lateral length scale inside the combustion chamber of a diesel engine during the compression stroke at 600 and 1000 RPM. They calculate indirectly the lateral length scale using Taylor's hypothesis, however due to the uncertainty involved in this analysis, only the direct measurements are considered here. The measured lateral length scales were in the

19

order of 1 to 2.5 mm and decrease during the compression stroke (330 to 370 degree crank angles). These authors showed that the cylinder geometry had a significant influence on turbulence length scales.

Table 3.1 Estimated length and time scales for an automotive-size engine at a speed of 1000 RPM (Deduced from Heywood, 1987)

	Estimated Value	Process, location	Comments
l_I (Integral length scale)	10.0 mm	during intake	scales with valve lift
l_I (min) (Integral length scale)	2.0-5.0 mm	end of compression	scales with clearance height, varies little with engine speed
l_T (Taylor micro length-scale)	1.0 mm	end of compression	varies little with engine speed
l_K (Kolmogorov length scale)	0.01 mm	end of compression	
τ_I (Integral time scale)	1.0 ms	end of compression	decreases with increasing engine speed
τ_T (Taylor micro time-scale)	0.1 ms	end of compression	decreases with increasing engine speed

Detailed measurements of root mean square (RMS) turbulent velocity fluctuations using a state-of-the-art LDV system are reported by Arcoumanis et al. (1994) for a 1.9 liter direct injection (DI) diesel engine. The RMS values of the swirl velocity fluctuations are very high (about $4 \cdot Vp$, Vp being the mean piston speed) during the intake due to counter-rotating jets, and they decay to about Vp near the BDC. The RMS axial velocity

fluctuations attain peak values of about 4·Vp during early induction. Both swirl and axial velocity fluctuations show as much as three fold spatial variation with radial position at a dimensionless distance x/S = 0.l (here x is the axial distance and S is the stroke) from the cylinder head indicating that the turbulence is strongly non-homogeneous. The detailed mean velocity measurements reported in this paper can be used for validation of multi-dimensional computational models.

3.3   Large Eddy Simulation

Most engineering flows of interest are in the turbulent regime, which contains a wide range of length and time scales. In large eddy simulation (LES) the large eddies are computed and the smallest eddies are modeled, as the large-scale motions are more energetic than the small scale ones and are responsible for most of the transport. The small-scale turbulence serves mainly to drain energy from the large scales through the cascade process, and is more universal and nearly isotropic, which makes it more suitable to be modeled.

To apply LES, the Navier-Stokes equations are filtered to obtain the equations for the large-scale motion. However, the non-linearity of the Navier-Stokes equations makes it impossible to obtain an exact closed equation for any filtered quantity (Rodi et al., 1997). The filtered out small scales then have to be represented by a RANS-like model that relates their effects to the resolved large scales to close the equation. The main difference between RANS and LES approaches lies in the fact that only the mean flow is resolved in RANS and the whole spectrum of turbulence is modeled with a limited number of scales.

3.3.1 Filtering for LES

To separate the large scales from the small scales, LES is based on the filtering operation. For a one-dimensional and time dependent arbitrary function $f(x,t)$, the filtered variable $\bar{f}(x,t)$ can be defined as

$$\bar{f}(x,t) = \langle f(x,t) \rangle = \int_{-\infty}^{\infty} h_s(x-x')f(x',t)dx' = h_s(x) * f(x,t) \qquad (3.1)$$

where h_s is the filter function, and $\langle \ \rangle$ or overbar indicates spatial filtering. The convolution of h_s and f gives the filtered signal $\bar{f}$, then in Fourier space

$$\hat{\bar{f}}(k,t) = \hat{h}_s(k)\hat{f}(k,t) \qquad (3.2)$$

There are three popular types of filters: the box filter, the sharp-cutoff filter, and the Gaussian filter, the properties of which are shown in Fig. 3.1
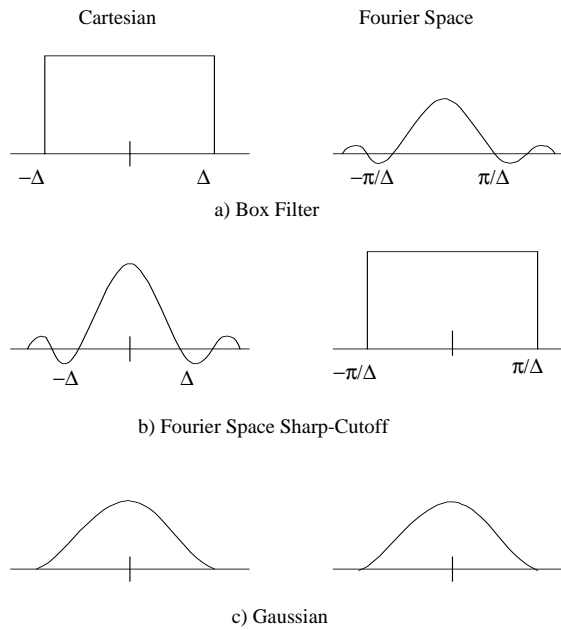
Figure 3.1 LES filter types

Consider for example, for the Gaussian filter,

In Cartesian space, $\quad h_s(x) = \dfrac{\sqrt{\gamma}}{\pi \lambda_f} e^{-\gamma(x/\lambda_f)^2}$

In Fourier space, $\quad \hat{h}_s(k) = e^{-\dfrac{\lambda_f^2 k^2}{4\gamma}}$

where λ_f is a characteristic filter width and γ is a constant.

3.3.2 Governing Equations for Incompressible Turbulent Flows

The filtered continuity, momentum and energy equations for incompressible flow can be written as follows

$$\frac{\partial \overline{u}_i}{\partial x_i} = 0 \tag{3.3}$$

$$\frac{\partial \overline{u}_i}{\partial t} + \frac{\partial \overline{u}_i \overline{u}_j}{\partial x_j} = -\frac{1}{\rho} \frac{\partial \overline{P}}{\partial x_i} - \frac{\partial \tau_{ij}}{\partial x_j} + \nu \frac{\partial^2 \overline{u}_i}{\partial x_j \partial x_j} \tag{3.4}$$

$$\frac{\partial \overline{T}}{\partial t} + \frac{\partial \overline{u}_i \overline{T}}{\partial x_j} = \alpha \frac{\partial^2 \overline{T}}{\partial x_j \partial x_j} - \frac{\partial q_j}{\partial x_j} \tag{3.5}$$

where u is the normal velocity, P the pressure, T the temperature, ν the kinematic viscosity and α the thermal diffusivity. These equations can then be solved if one introduces models for τ_{ij} and q_j which are defined as

$$\tau_{ij} = R_{ij} - \frac{1}{3} R_{kk} \delta_{ij} \tag{3.6}$$

$$R_{ij} = \overline{u_i u_j} - \overline{\overline{u}_i \overline{u}_j} \tag{3.7}$$

23

and

$$q_j = \overline{u'_i T'} \tag{3.8}$$

3.3.3   Governing Equations for Compressible Turbulent Flows

For compressible flows it is appropriate to define a Favre-filtered (i.e density weighted average) variable $\tilde{f}(x,t)$ as

$$\tilde{f}(x,t) = \frac{\overline{\rho f}}{\overline{\rho}} \tag{3.9}$$

The filtered compressible Navier-Stokes equations can then be written as

$$\frac{\partial \overline{\rho}}{\partial t} + \frac{\partial \overline{\rho}\,\overline{u}_i}{\partial x_i} = 0 \tag{3.10}$$

$$\frac{\partial \overline{\rho}\,\tilde{u}_i}{\partial t} + \frac{\partial \overline{\rho}\,\tilde{u}_i \tilde{u}_j}{\partial x_j} = -\frac{1}{\rho}\frac{\partial \overline{P}}{\partial x_i} + \frac{\partial G_{ij}}{\partial x_j} \tag{3.11}$$

$$\frac{\partial \overline{\rho}\,\tilde{e}}{\partial t} + \frac{\partial}{\partial x_j}\left(\overline{\rho}\,\tilde{e} + \overline{P}\right)\tilde{u}_j = \frac{\partial H_j}{\partial x_j} \tag{3.12}$$

$$\overline{P} = \overline{\rho}\,R\tilde{T} \tag{3.13}$$

where x_i represents the Cartesian coordinates (i = 1,2,3), $\tilde{u}_i$ are the Cartesian components of the filtered velocity, $\overline{p}$ is the mean presssure, $\overline{\rho}$ is the mean density, G_{ij} is the total stress, H_j is the energy flux due to heat transfer and work done by the total stress, and $\overline{\rho}\,\tilde{e} = \overline{\rho}c_v\tilde{T} + 1/2\,\overline{\rho}\,\tilde{u}_i\,\tilde{u}_i + \overline{\rho}k$ is the filtered total energy per unit volume where

$k = 1/2 \left(\overline{u_i u_i} - \tilde{u}_i \tilde{u}_i \right)$ is the subgrid scale turbulence kinetic energy per unit volume. Note that double overbar and tilda both have the same meaning in the notation used here.

The total stress is defined as

$$G_{ij} = \tau_{ij} + \overline{\sigma}_{ij} \tag{3.14}$$

$$\tau_{ij} = -\overline{\rho} \left(\overline{u_i u_j} - \tilde{u}_i \tilde{u}_j \right) \tag{3.15}$$

where τ_{ij} is the subgrid scale stress tensor and $\tau_{ii} = -2\rho k$. The molecular viscous stress tensor $\overline{\sigma}_{ij}$ is approximated (Moin et al., 1991) by

$$\overline{\sigma}_{ij} = \mu \left(-\frac{2}{3} \frac{\partial \tilde{u}_k}{\partial x_k} \delta_{ij} + \frac{\partial \tilde{u}_i}{\partial x_j} + \frac{\partial \tilde{u}_j}{\partial x_i} \right) \tag{3.16}$$

where μ is the molecular viscosity based on the Favre-filtered static temperature $\tilde{T}$. The total heat transfer is given by

$$\vartheta_j = Q_j + \overline{q}_j \tag{3.17}$$

where Q_j is the subgrid scale heat flux

$$Q_j = -c_p \overline{\rho} \left(\overline{u_j T} - \tilde{u}_j \tilde{T} \right) \tag{3.18}$$

$$\overline{q}_j = k_T \frac{\partial \tilde{T}}{\partial x_j} \tag{3.19}$$

and $\overline{q}_j$ is the molecular heat flux and k_T is the molecular thermal conductivity based on the Favre-filtered static temperature $\tilde{T}$. The energy flux (Knight, 1998) is expressed as

$$H_j = Q_j + G_{ij}\tilde{u}_i \qquad (3.20)$$

Then, the closure of this system needs models for the subgrid scale stress τ_{ij} and heat flux Q_j.

3.3.4 Smagorinsky Model

Smagorinsky (1963) was the first to postulate a model for the subgrid scale stresses (SGS). The model assumes the SGS stresses follow a gradient-diffusion process, similar to molecular motion. Most sub-grid scale models are based on the definition of a SGS stress in the form

$$\tau_{ij}^s - \frac{1}{3}\tau_{kk}^s = \nu_t\left(\frac{\partial \overline{u}_i}{\partial x_j} + \frac{\partial \overline{u}_j}{\partial x_i}\right) = 2\nu_t \overline{S}_{ij} \qquad (3.21)$$

where ν_t is the eddy viscosity and $\overline{S}_{ij}$ is the large-scale strain rate tensor which is defined as

$$\overline{S}_{ij} = \frac{1}{2}\left(\frac{\partial \overline{u}_i}{\partial x_j} + \frac{\partial \overline{u}_j}{\partial x_i}\right) \qquad (3.22)$$

Assuming equilibrium of production and dissipation of subgrid energy, a mixing length type model in the form of the subgrid scale eddy viscosity is then defined as

$$\nu_t = C_s\Delta^2\left|\overline{S}\right| \qquad (3.23)$$

where C_s is the model parameter, Δ is the filter width (usually taken as characteristic subgrid scale representing the largest subgrid scale eddies), and

$|\overline{S}| = (\overline{S}_{ij}\overline{S}_{ij})^{1/2}$ is the contraction of resolved stresses. In general C_s is not constant; it may

be a function of non-dimensional parameters like the Reynolds number and may differ

according to the flow situation. For example, Lilly (1966) suggested for homogeneous

isotropic turbulence $C_s = 0.17 \sim 0.23$, Bardina (1983) used values of 0.09 to 0.20 for

homogeneous and sheared flows, and $C_s = 0.065 \sim 0.1$ for channel flow.

The filter length scale Δ is usually calculated as the average cell size in finite

volume or finite difference simulations, i.e.

$$\Delta = (\Delta_x \Delta_y \Delta_z)^{1/3} \tag{3.24}$$

Another important issue is the treatment of the regions near solid surfaces, where

the value of C_s has to be reduced. One suggestion is to use the van Driest damping that

has been used to reduce the near-wall eddy viscosity in RANS models (Ferziger and

Peric, 1997),

$$C_s = C_s' \left(1 - e^{-y_w^+/A^+}\right)^2 \tag{3.25}$$

where A^+ is a constant usually taken as 25 and y_w^+ is the distance from the wall in

viscous wall units ($y_w^+ = y_w u_\tau / \nu$, where u_τ is the shear velocity).

Chapter 4

AN ASSESSMENT OF TURBULENCE SCALES RELEVANT TO IC ENGINES

4.1   Introduction

It is important to place the expected orders of magnitude of the important length and time scales which are relevant to both the engine geometry and speed, and the resulting turbulent flow field. If these scale magnitudes are correctly assessed, the understanding of the turbulent flow field will improve, which in turn will lead to better modeling strategies, especially for large eddy simulations. Moreover, turbulence intensity and the length scales play dominant roles in turbulent flame propagation and hence in temperature distribution and combustion processes in internal combustion engines. In spite of this due emphasis is not focused on investigating the primary factors which influence these scales. The consequences of the length scale variations are not investigated either. Experimental work relevant to this subject, i.e. direct measurement of lateral and axial length scales, dates back 20 years and is based on hot wire data. More recent experiments using laser Doppler velocimetry (LDV) technique focus more on determining the mean flow field with very rare attempts to measure length scales directly. In this work most relevant experimental work on this topic has been reviewed and are

compared with those scales implied by the standard k- ε turbulence model. The influence of combustion and the numerical mesh size on predictions is investigated. This assessment is carried out via axisymmetric calculations using the KIVA-3 code (Amsden, 1993) for a typical IC engine, and focuses on the influence of combustion and numerical mesh on predicted turbulence scales. The present results will serve as a prelude and as a guide to determine the mesh size in the anticipated large eddy simulations (LES) of diesel combustion chambers.

4.2   Combustion and Grid Effects on Turbulence scales

Here, the implied velocity and the length scales are summarized when the standard k-ε turbulence model is used in engine calculations. The integral velocity scale of turbulence is related to the turbulent kinetic energy, k, by assuming locally isotropic turbulence, as

$$u = (2k/3)^{1/2} \tag{4.1}$$

In what follows this velocity scale should be interpreted as the root mean square, u_{rms}, turbulence intensity. The integral length scale, ℓ_I, of turbulence is calculated from

$$\ell_I = u^3 / \varepsilon \tag{4.2}$$

Equation 4.2 should not be interpreted as a strict equality, but rather an approximation where the constant of proportionality is taken as unity. The integral time scale is calculated simply from the ratio

$$\tau_I = \ell_I / u \tag{4.3}$$

The smallest scales associated with dissipation of turbulent kinetic energy, k, by viscous effects are the Kolmogorov (micro) scales, and are given by

$$\ell_K = \left(\nu^3/\varepsilon\right)^{1/4} \qquad (4.4)$$

$$\tau_K = \left(\nu/\varepsilon\right)^{1/2} \qquad (4.5)$$

where ν is the kinematic viscosity, and ε is the dissipation rate of k.

The velocity scale u (= u_{rms}) of turbulence is related to the time, τ, and length, ℓ, scale by

$$u = \ell / \tau \qquad (4.6)$$

For example the Kolmogorov (micro) velocity scale is

$$u_K = \ell_K/\tau_K = \left(\nu\varepsilon\right)^{1/4} \qquad (4.7)$$

The various scales mentioned above can be related to each other by using the approximate relation

$$\varepsilon = u^3/\ell_I \qquad (4.8)$$

and the definition of a turbulence Reynolds number

$$Re_t = u\ell/\nu \qquad (4.9)$$

$$\ell_K/\ell_I = Re_t^{-3/4} \qquad (4.10)$$

$$\tau_K/\tau_I = Re_t^{-1/2} \qquad (4.11)$$

Under some restrictive conditions (e.g. homogeneous, stationary turbulence) the length and time scales can be related using Taylor's hypothesis.

$$\ell_I = U\tau_I \tag{4.12}$$

$$\ell_T = U\tau_T \tag{4.13}$$

where U is the mean velocity component in the direction in consideration.

The integral scales are associated with relatively large eddies and the Kolmogorov scales are associated with smallest eddies in a turbulent flow. The time τ, and velocity, u, scale of an eddy of size ℓ, is between ℓ_I and ℓ_k can be calculated if the assumption is that u and τ are functions of ε and ν only. Dimensional reasoning then leads to

$$\tau = \left(\ell^2/\varepsilon\right)^{1/3} \tag{4.14}$$

$$u = \left(\ell\varepsilon\right)^{1/3} \tag{4.15}$$

For large Re_t, turbulence can be assumed to be locally isotropic, in which case Taylor micro scale can be computed from (Tennekes and Lumley, 1992)

$$\ell_T/\ell_I = \frac{\sqrt{15}}{A}Re_t^{-1/2} \tag{4.16}$$

The Taylor's time scale can be calculated from

$$\tau_T = \left(\ell_T^2/\varepsilon\right)^{1/3} \tag{4.17}$$

The present calculations were performed utilizing a readily available computer code, KIVA-3 (Amsden, 1993), as described in Appendix A.

The geometry and the relevant parameters used for the engine simulated are shown in Figure 4.1. This is the engine, which is presented as the base case in the KIVA family manuals. The fuel used is gasoline represented as C_8H_{17}. Combustion was induced

by increasing the energy content of a certain number of cells to approximately emulate a spark ignition process. But the amount of the ignition energy seems to have a significant influence on the overall combustion process. Hence, this procedure needs to be handled with more caution in the future.

Four cases were simulated, namely, (1) the base case with a coarse grid, (2) base case without combustion, (3) the base case with approximately double the number of grids in each direction (with combustion), (4) the same as Case 3 but without combustion. The objective was to investigate the influence of combustion and numerical grid on turbulence scales in comparison with experiments. All of the cases were axisymmetric and had the same reaction rates, which were turned off for cases without combustion. The base case had about 333 grid nodes with the smallest grid size of 0.275 and 0.3 cm in the r-direction and the x-direction, respectively.

4.2.1   Results

Figure 4.2 shows the variation of temperature with crank angle at various points (see Figure 4.1 for the location of these points). Points 1&2 are fixed relative to the piston head, and points 3&4 are fixed relative to the cylinder head. Combustion is initiated at about 25 CA (crank angle degree) BTDC. The maximum temperature is around 2500 K. Points 2&4 are barely influenced by combustion as they are near the cylinder surface and away from the flame core. The influence of the combustion is seen most near the flame front (points 1&3) as expected. At points 2&4 the temperature is most probably dictated by the cylinder wall temperature and hence affected the least by the flame. A more interesting observation is that the temperature distribution is affected very little by the

mesh size except for point 1 towards the end of the expansion stroke. Here the grid doubling with combustion leads to about 250 K (25%) difference in temperature. With the finer mesh a sharper flame front is captured.
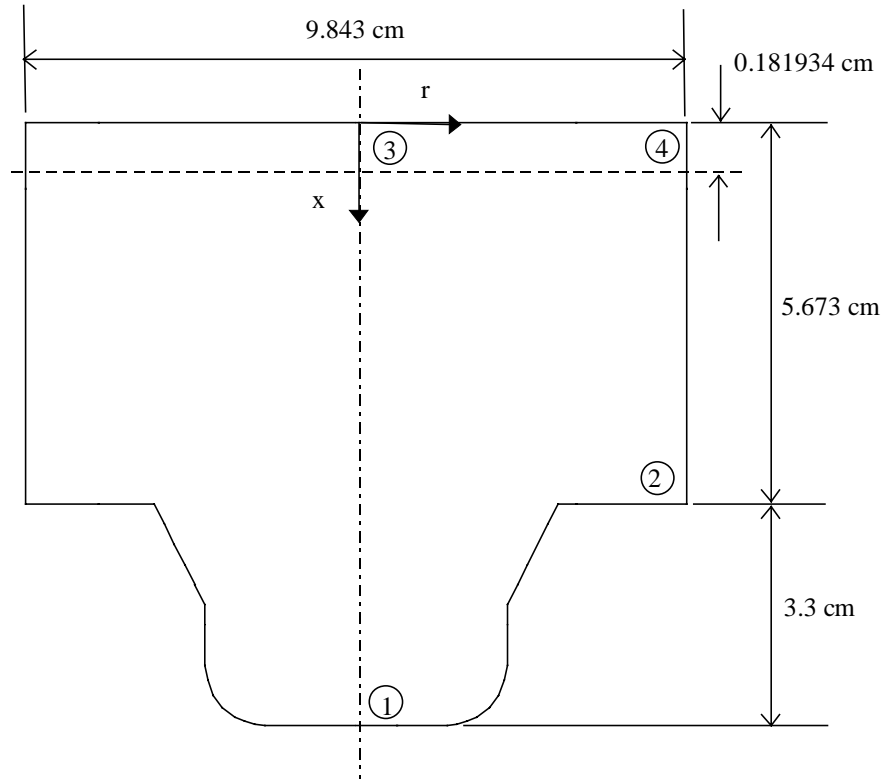
The Coordinates of nodes 1,2,3 and 4 are at -90 ATDC

Node	r (cm)	x (cm)
1	0.28	8.42
2	4.65	4.86
3	0.50	0.15
4	4.65	0.15

Bore	9.843 cm	Stroke	9.55 cm
Squish	0.181934 cm	Speed	1600 rpm
Mean Piston Speed	509.3 cm/sec		

Figure 4.1 The geometry of the simulated IC engine (-90 ATDC)

Figure 4.3 shows the variation of the root-mean-square (RMS) velocity fluctuations as predicted by the isotropic k-ε turbulence model. As expected, there is dramatic influence of combustion on velocity fluctuations away from the cylinder walls (see points 1&3). However, the influence of grid doubling is not as large as one would intuitively expect, given that the base grid is a fairly coarse grid at point 1. At point 2, however, the results are seen to be clearly grid dependent where u_{rms} changes as much as 60% as the grid is doubled with or without combustion. There is some change at points 2&4 towards the end of the expansion stroke which amounts to about 25%. Observing that there is little dependence of the temperature on the grid at point 3, and the significant changes seen in u_{rms} at point 3 leads to the conclusion that the k-equation (hence the other related turbulence quantities) is more grid sensitive. It is also noteworthy that away from the flame (points 2&4) the turbulence intensity seems to follow the trend of the piston speed, first increasing then decreasing as the TDC is approached; then increasing again. The intensity is much less during the expansion stroke compared to that of the compression stroke. The maximum value of u_{rms} is attained at point 3 about 30 CA deg. BTDC, and it is about twice the mean piston speed, Vp=276 cm/s. The maximum u_{rms} near the wall (point 4) decreases by about 50%. The measurements of Arcoumanis et al. (1994) in a DI diesel engine also showed similar trends but had different relative magnitudes. The maximum u_{rms} at TDC is about $2.0V_p$ in contrast to Heywood's (1987) suggestion that it is $0.5V_p$. It is puzzling to see that u_{rms} at point 3 starts increasing before the temperature at the same point starts increasing, indicating some kind of a phase shift between these two quantities!

The influence of combustion on the integral length scale is not monotonic, i.e. in some regions the length scale increases while in others it decreases with combustion; but mostly it is smaller with combustion. Again the influence of combustion is insignificant near the cylinder walls (points 2&3). There is also a significant influence of grid size. As the grid is refined the implied length scale by the k-ε model mostly increases; point 4 shows a reverse trend. The pseudo periodic variation seen at points 2&4 indicate that the length scale should scale with the clearance height as observed in the experiments (Fraser et al., 1986). The minimum length scale is observed near the TDC and varies from 1 to 5mm spatially which agrees well with experimental observations (see Table 3.1). The variation of the length scale seen at point 3 is very similar to those measured experimentally by Fraser et al. (1986); it decreases towards the TDC and then increases during the expansion. The maximum length scale is observed at point 1 at the end of the expansion stroke, which is about 30mm. This should correspond to the size of the large vortex (Hoult and Wong, 1980) which grows as the piston is expanding, and should scale with the clearance distance from the piston to the cylinder head as well as the cylinder bore length. The implied integral time scale can be computed from Equation 4.3, which varies from 1 to 10 ms being smaller near the TDC and larger elsewhere. More drastic variation occurs in the flame region. At points 2 and 4 it ranges from 1 to 2 ms. These values seem to be reasonable when compared to those observed experimentally (see Table 3.1). The smallest frequency $(1/\tau_I)$ computed from the k-ε model correspond to about 1.0 kHz which is certainly in the lower frequency range of the energy spectrum. The minimum Taylor and Kolmogorov length scales are in the order of 0.05mm and 0.01 mm, respectively, and they occur near TDC. For more detail see Celik and Yavuz (1997).
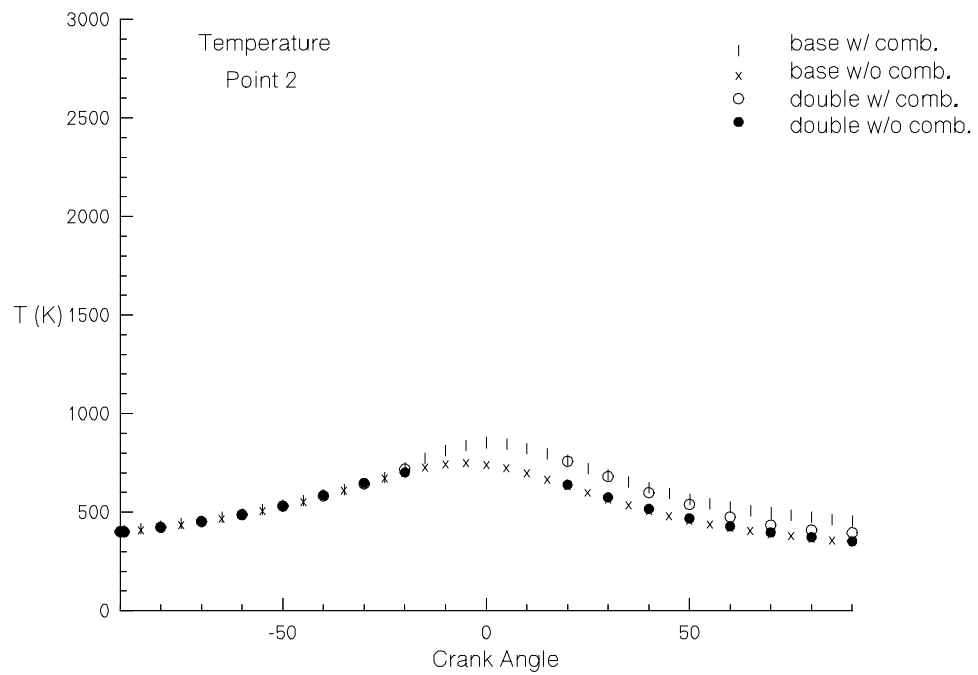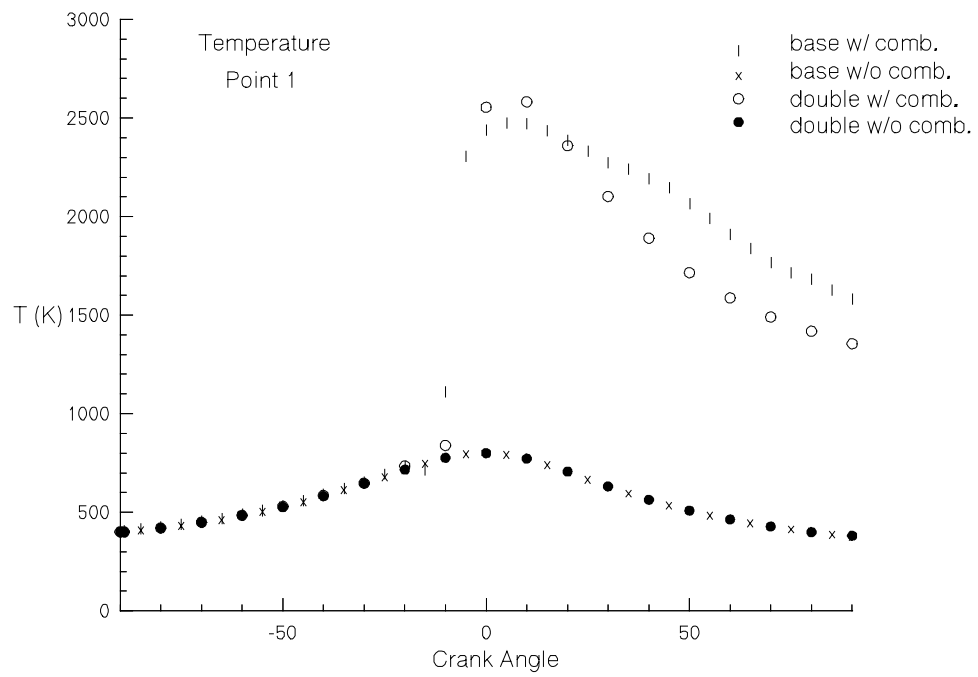
Figure 4.2a Temperature distribution for points 1 and 2

36
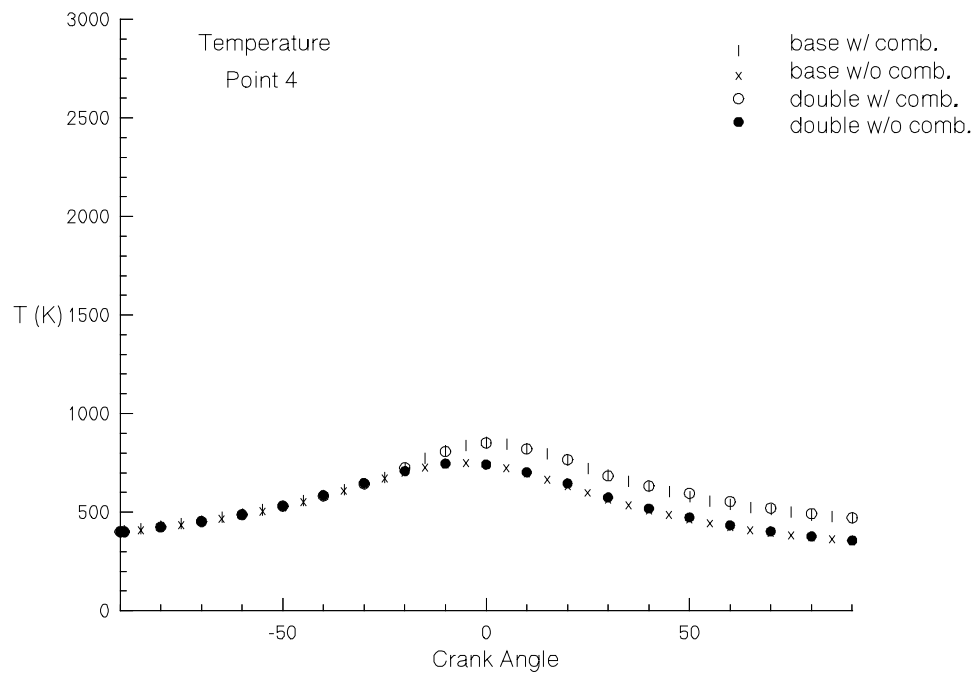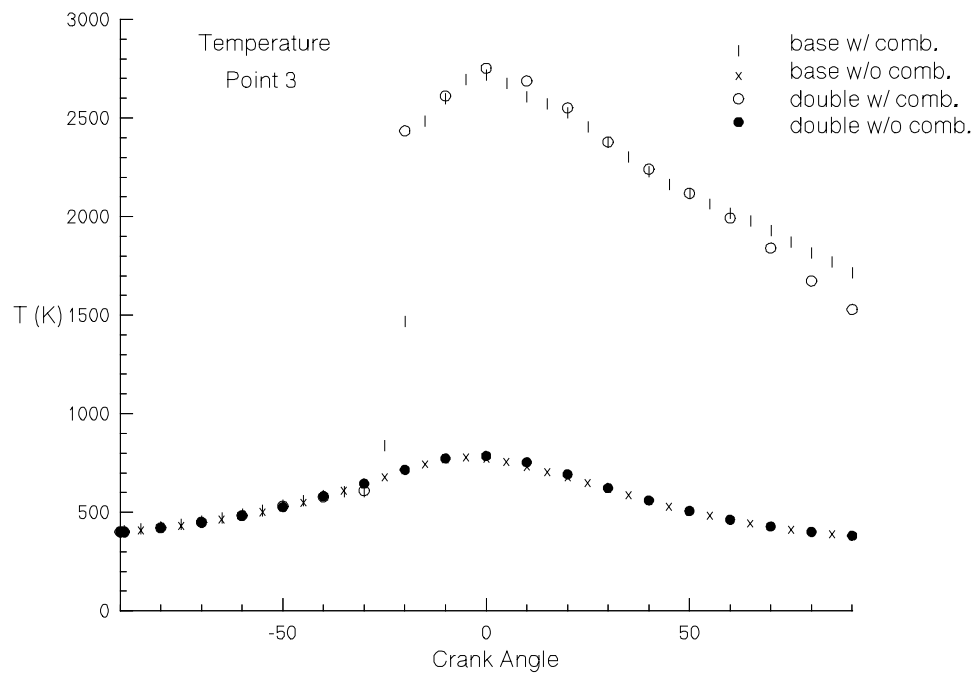
Figure 4.2b Temperature distribution for points 3 and 4
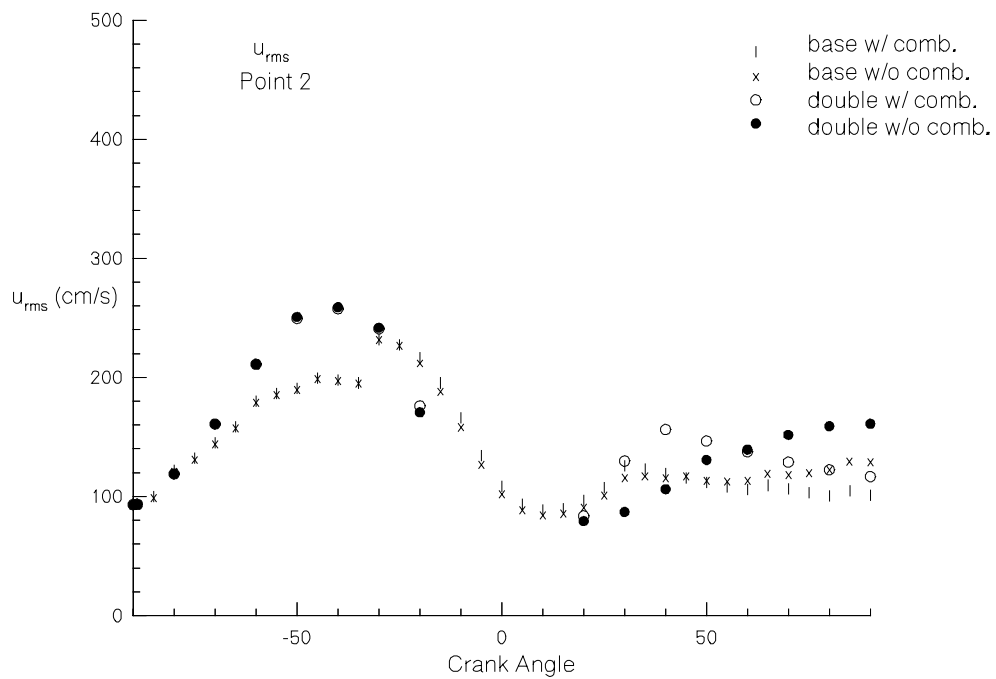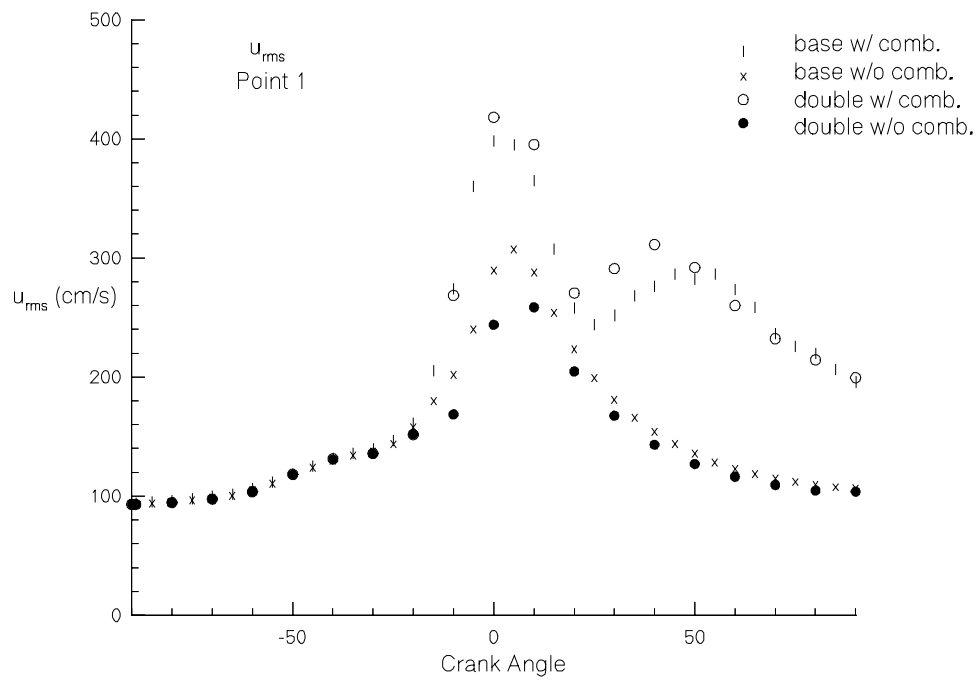
Figure 4.3a Root mean square velocity scale for points 1 and 2

38
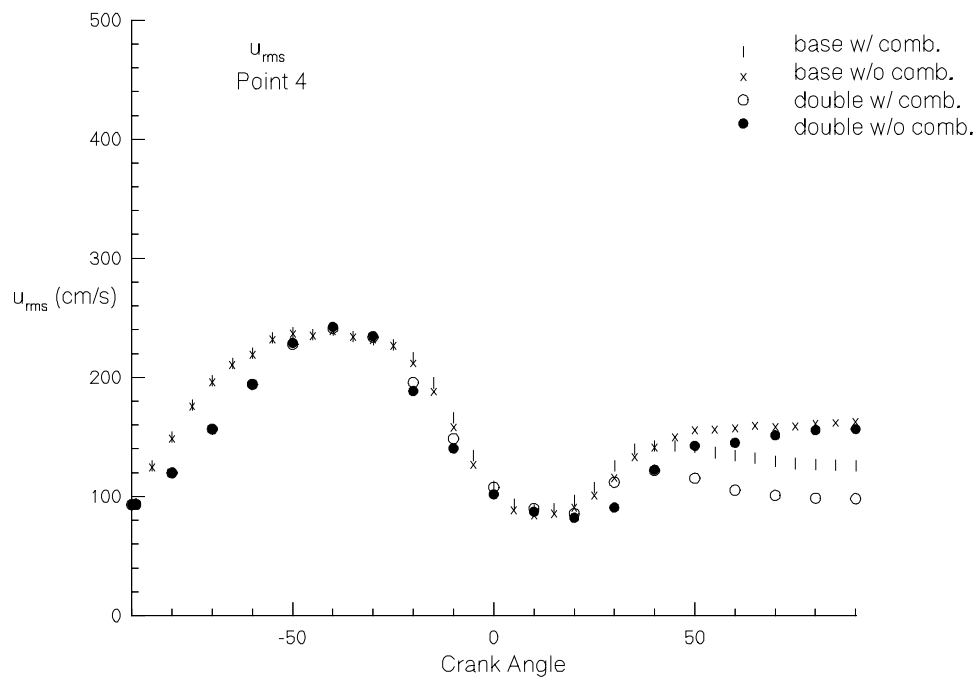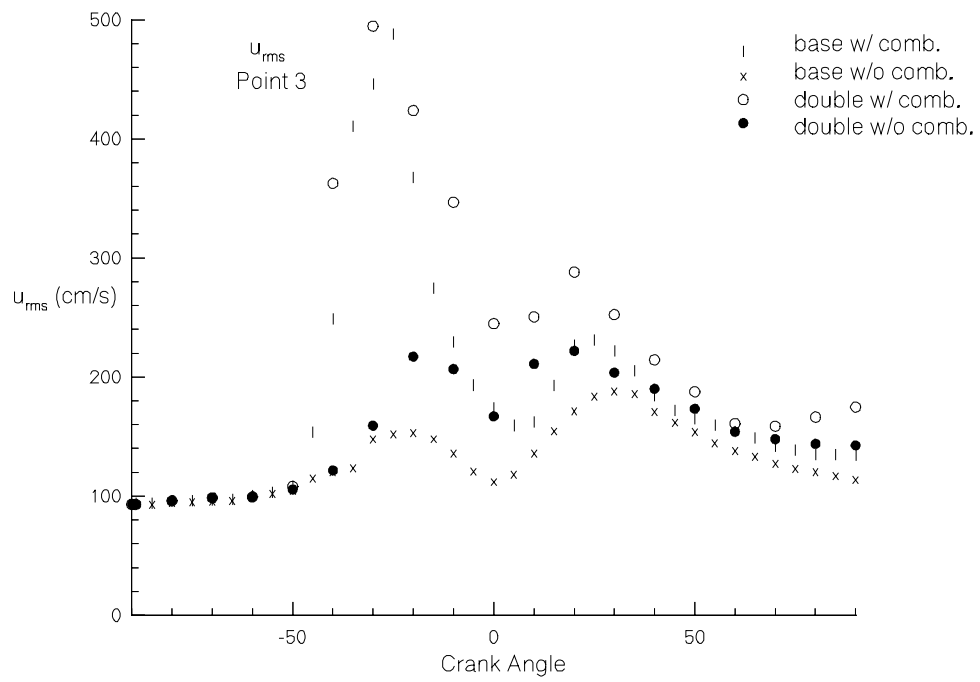
Figure 4.3b Root mean square velocity scale for points 3 and 4

39
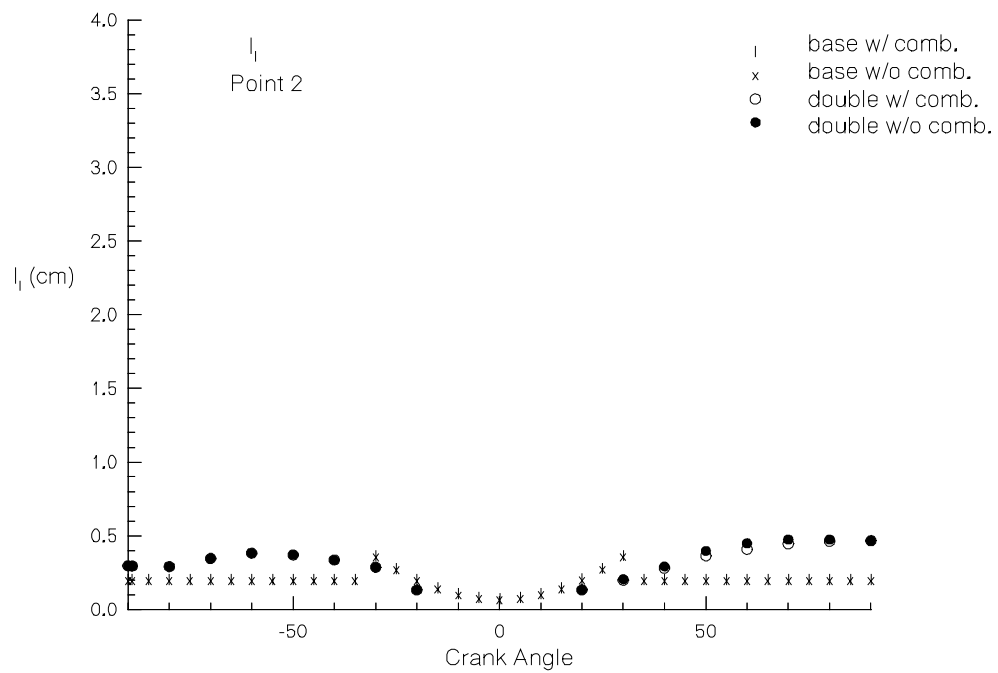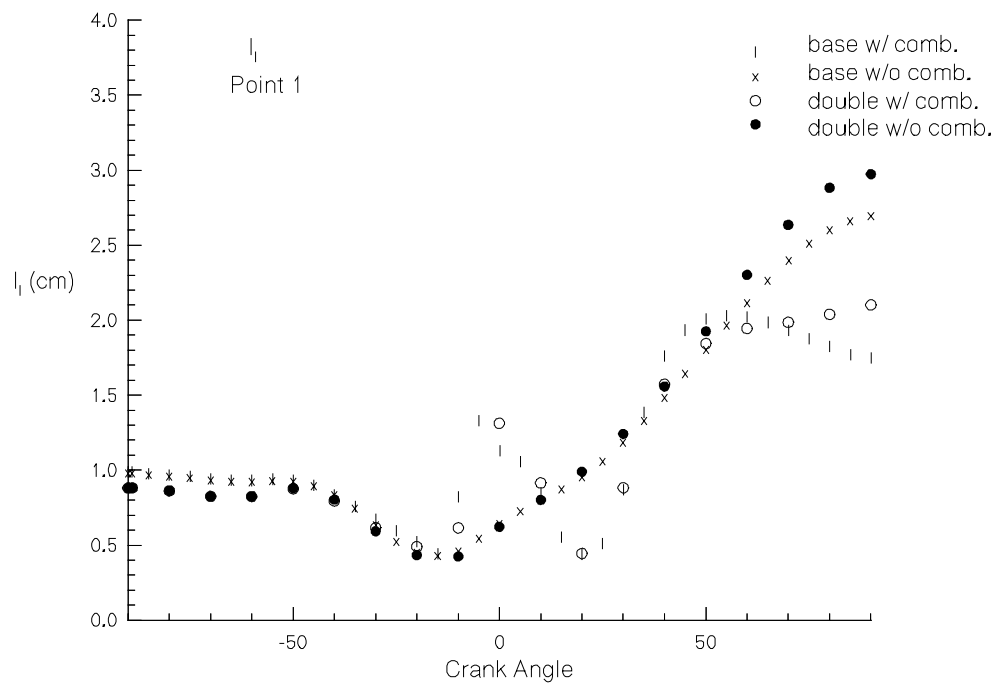
Figure 4.4a Integral length scale for points 1 and 2

40
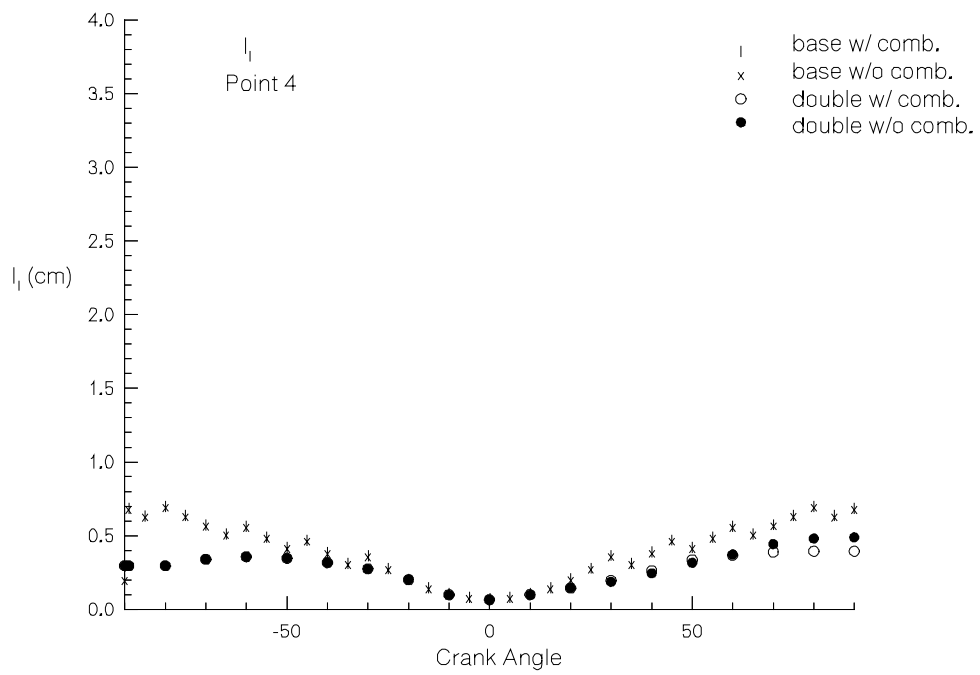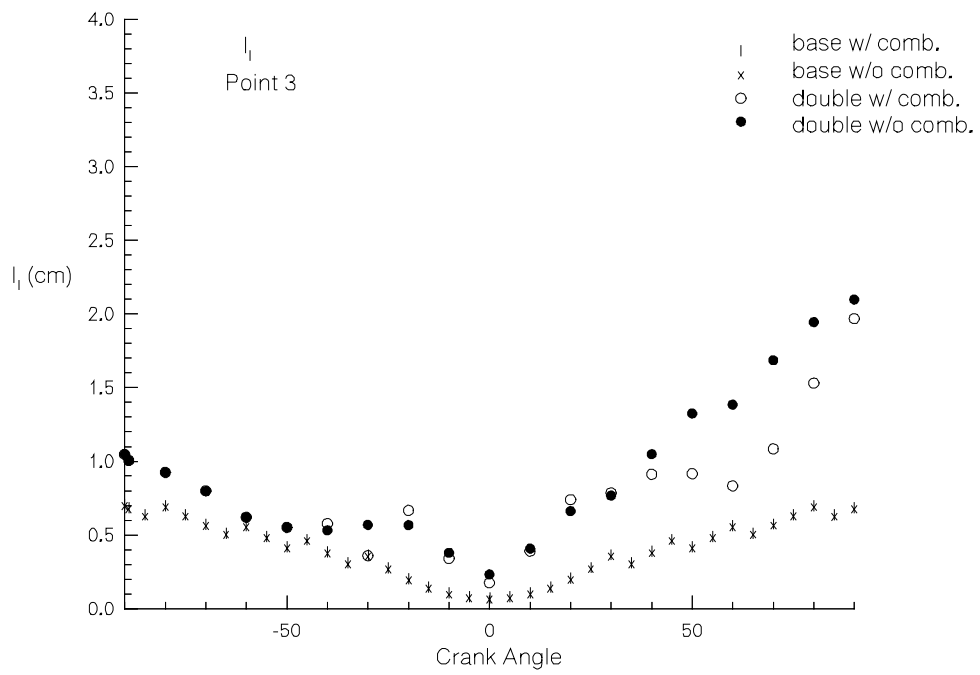
Figure 4.4b Integral length scale for points 3 and 4

41
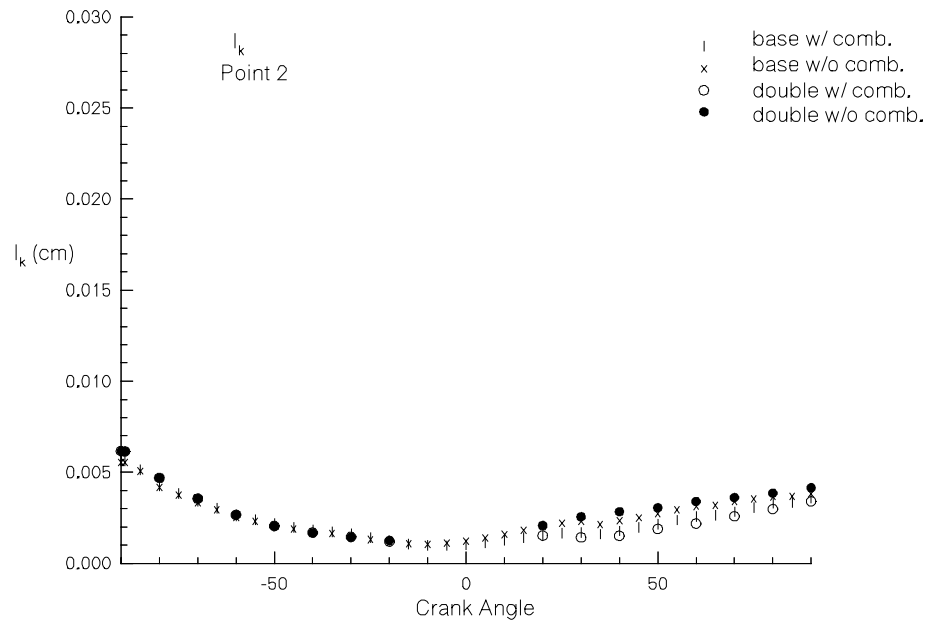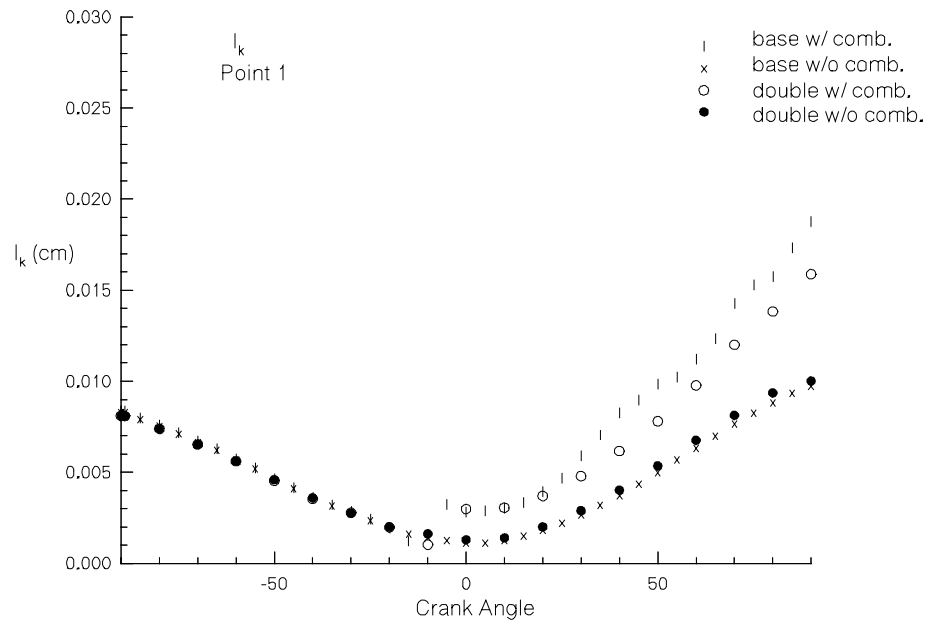
Figure 4.5a Kolmogorov length scale for points 1 and 2
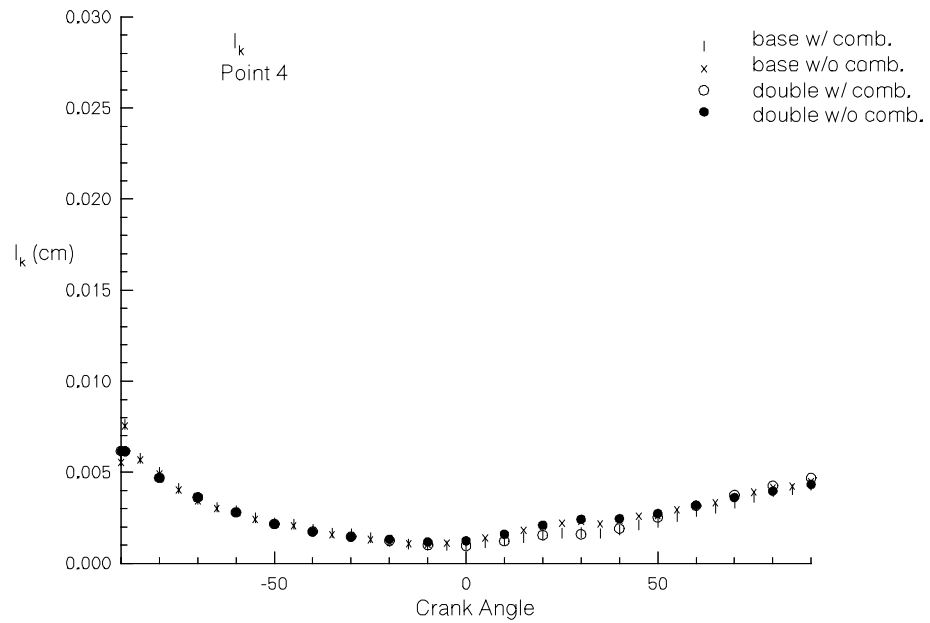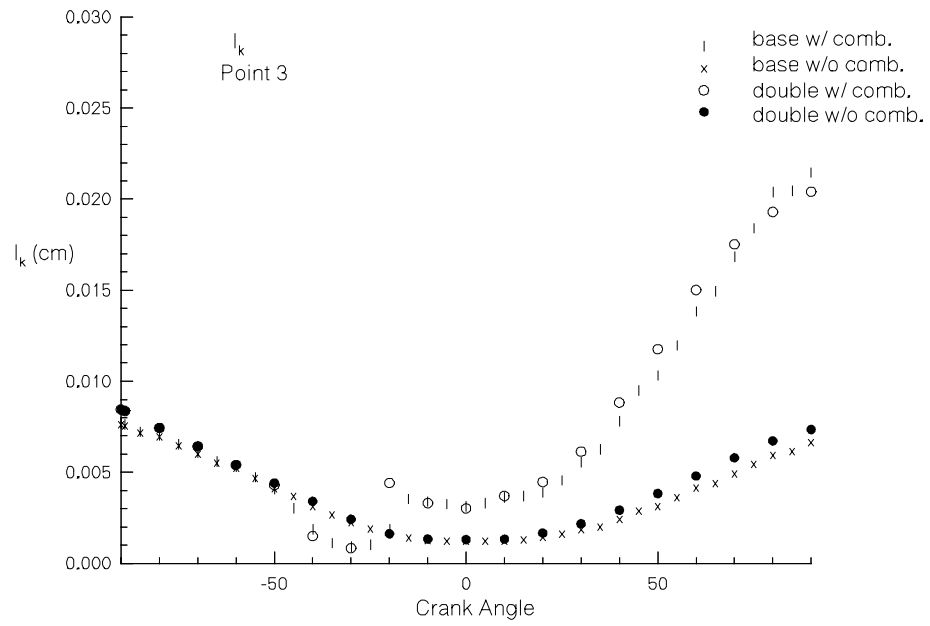
Figure 4.5b Kolmogorov length scale for points 3 and 4

43

These calculations gave good qualitative results in comparison to experiments. In particular the data of Fraser et al. (1986) from a motored IC engine for the dimensionless integral length scale showed the same trend and the magnitudes as the calculated length scale as shown in Figure 4.6. Fraser et al. (1986) presents direct measurements of lateral integral length scale using laser Doppler velocimetry (LDV). This length scale ranges between 2 to 3.5 mm for crank angles between 320 to 380 degrees ATDC with a local minimum at the TDC. When the same data is normalized by the instantaneous clearance height the non-dimensional values increase from 0.2 to 0.4 at TDC and remains approximately fixed after that. See also Section 4.3 for an interpretation of Fraser et al.'s measurements.
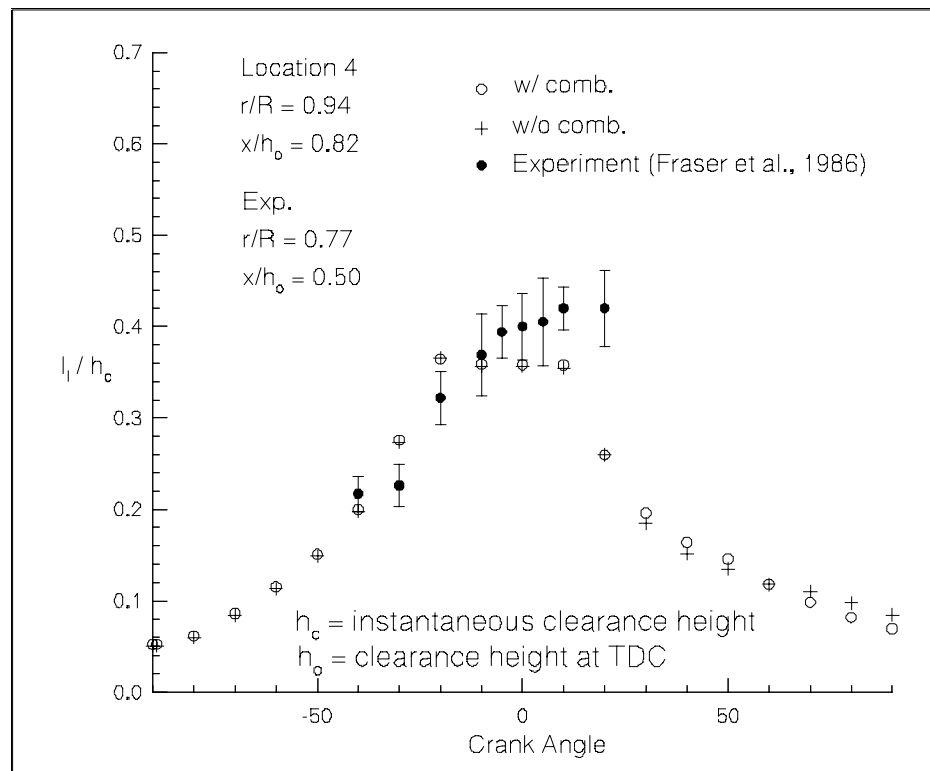
Figure 4.6 Non-dimensional Integral Length Scale versus Crank Angle (°)

4.3 Effect of Compression Ratio and Three-dimensionality on Turbulence scales

In this section the previous calculations are extended to three dimensions. The influence of compression ratio is investigated. An assessment of all velocity, length and time scales is made in comparison with the self imposed scales of the engine itself and in comparison with available experimental data.

The previous work reviewed by Lancaster (1976) along with his work seem to indicate that the relative integral length scale of turbulence should be function of the engine speed, swirl ratio, and compression ratio. He also points out that the longitudinal and lateral length scales could be significantly different; for homogeneous, isotropic turbulence the former is about two times the latter (a consequence of Taylor's hypothesis). It is noteworthy to mention that the lateral auto correlation coefficient measured by Fraser et al. (1986) can be represented well by an exponential function of the from

$$R(r^*) = a\ (1\text{-}br^*/2)\exp(\text{-}br^*) \tag{4.18}$$

where a and b are constants, r^* is the radial distance between the two points in consideration.

Here, it was assumed that the integral scale, ℓ_I, deduced from the k-epsilon model represented an average of the lateral, ℓ_g, and the longitudinal, ℓ_f, length scales, i.e.

$$\ell_I{}^2 = \ell_f{}^2 + \ell_g{}^2 \tag{4.19}$$

In the experiments only the lateral scale was measured. It was further assumed that $\ell_f = 2\ell_g$ as in homogeneous turbulence (Fraser at al., 1986).

The geometry and the relevant parameters for the engine simulated are the same as the previous case (Fig.4.1). The data was taken at different points, which are shown in Figure 4.7. This is the engine, which is presented as the base case in KIVA-II and KIVA-3 manual.
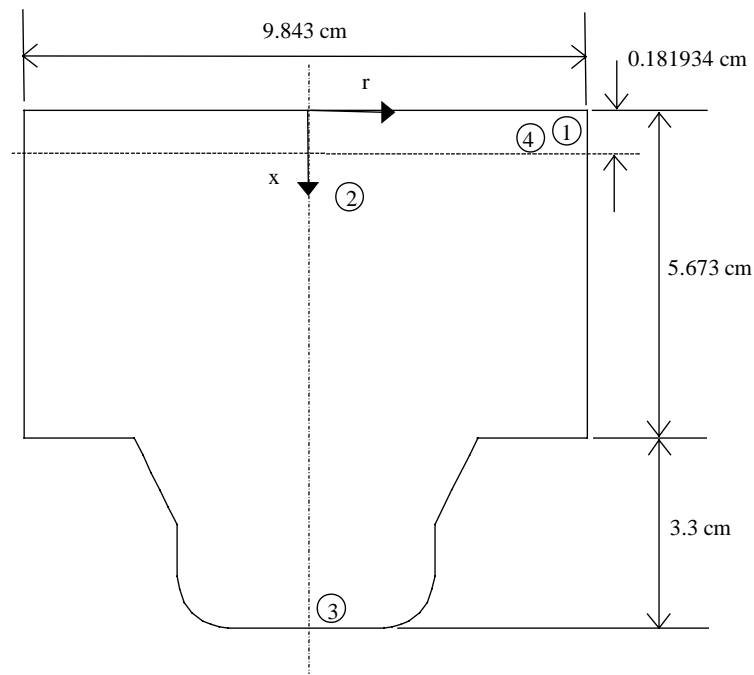
The Coordinates of nodes 1,2,3 and 4:

Node	r (cm)	x (cm)
1	4.79	0.052
2	1.00	3.03
3	0.28	8.42
4	4.65	0.15

Figure 4.7 The geometry of the simulated IC engine (-90° ATDC)

The base case had about 333 grid nodes. An additional case with a modified grid with 1336 grid nodes with the smallest grid size of 0.15 and 0.175 cm in the r-direction and the x-direction, respectively for the axisymmetric cases, and also 25 grid nodes in the θ direction for the polar grid of the 3-D case, was considered as shown in Figure 4.8.
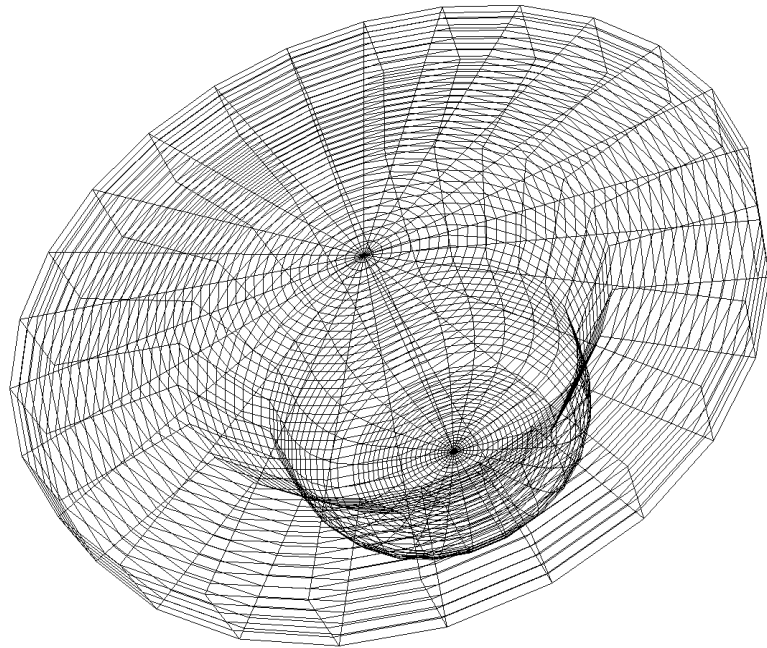
Figure 4.8 The computational 3-D grid of the simulated IC engine

4.3.1 Results

The simulation was done from 270° CA to 450° CA, where the TDC is at 360° CA. The computed length and time scales under different circumstances are given in Figures 4.9 and 4.10, respectively. Where the k-ε model is used as the turbulence model, and comparisons between different compression ratios, varying initial conditions and 3-D

effects are presented. Point 1 and 2 are chosen for these graphs, where the first one is very near the corner of the cylinder head and the second one further in the middle of the engine. The exact coordinates are given in Figure 4.7, where for Point 1 and 2, the coordinates are exact, however for Point 3 and 4, they are node values, and the exact coordinates may vary slightly.

As seen in Figure 4.9a, the effect of compression ratio on the length scale is not that significant in the vicinity of the cylinder wall, where it increases the Taylor's and Kolmogorov's scales a little. Outside this region an increase in the compression ratio from 11.0 to 20.4 increases the length scales all over the crank angle spectrum, sometimes up to 3 times its original value. The reaction of the time scales, see Figure 4.10a, is a little different, near the wall there is no much going on in a quantitative sense, except at the beginning of the compression stroke simulation, where it is affected by the initial conditions. If Point 2 is investigated, they underlay the original value before TDC, but have an increased trend after TDC.

The effect of turbulence intensity on the length scales is demonstrated in Figure 4.9b, where there is actually no effect at all, but as seen in Figures 4.10b, there is some effect on the time scales, but again induced by the initial condition, and the effect dies out after 40° CA after TDC in the near wall region, whereas it lasts until TDC in the middle region of the engine.

As the 3-D effects are concerned, the only difference caused by the three-dimensionality is the ignition region, where it is on one side of the engine only. The ignition starts 27° CA before TDC, in which range as seen on Figures 4.9c and 4.10c, the deviations of the length scales are introduced.
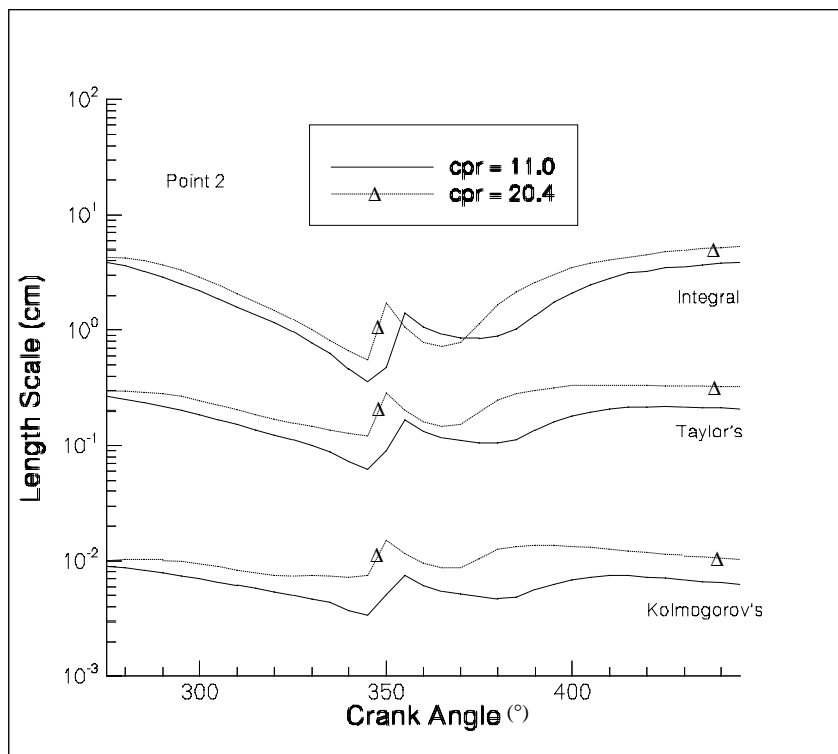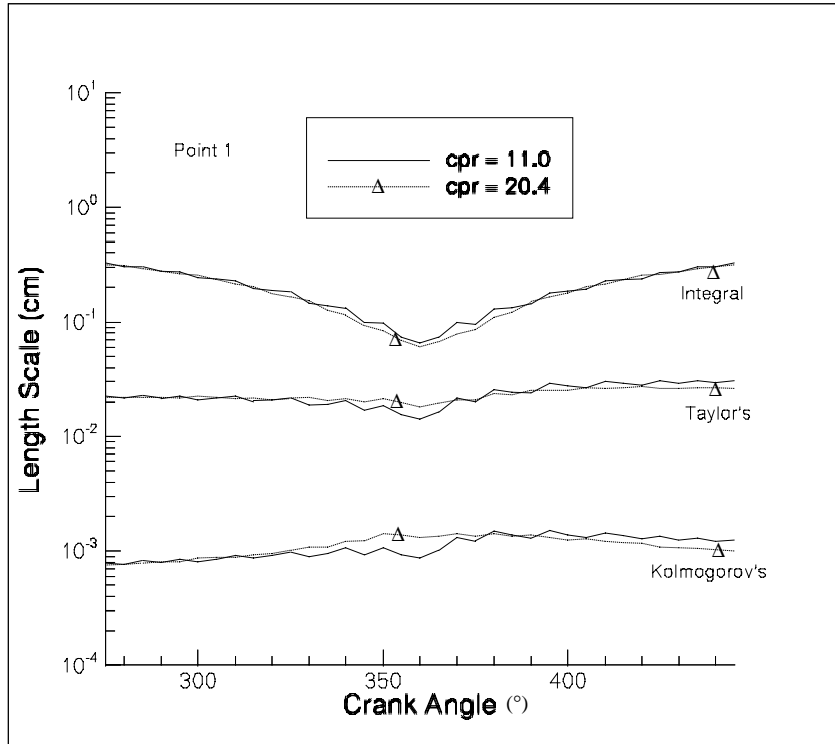
Figure 4.9a Length scale differences due to compression ratio
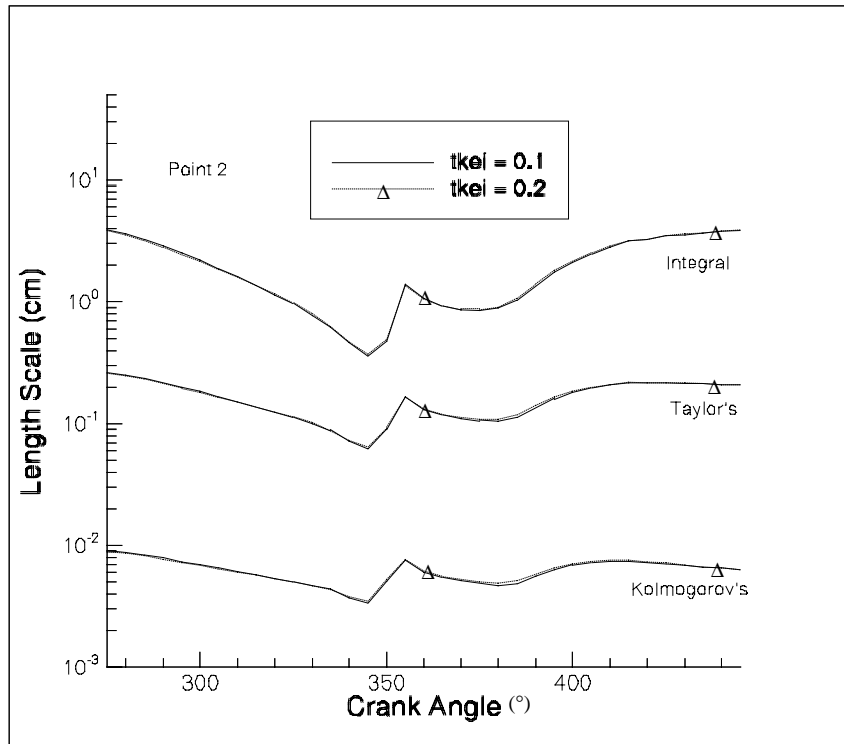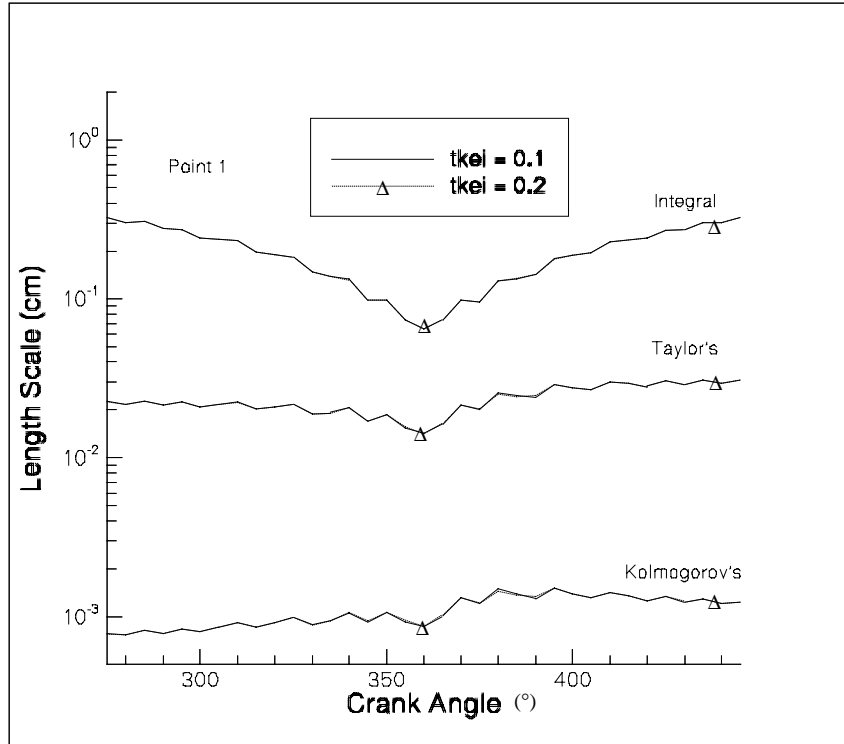
Figure 4.9b Length scale differences due to initial turbulence intensity
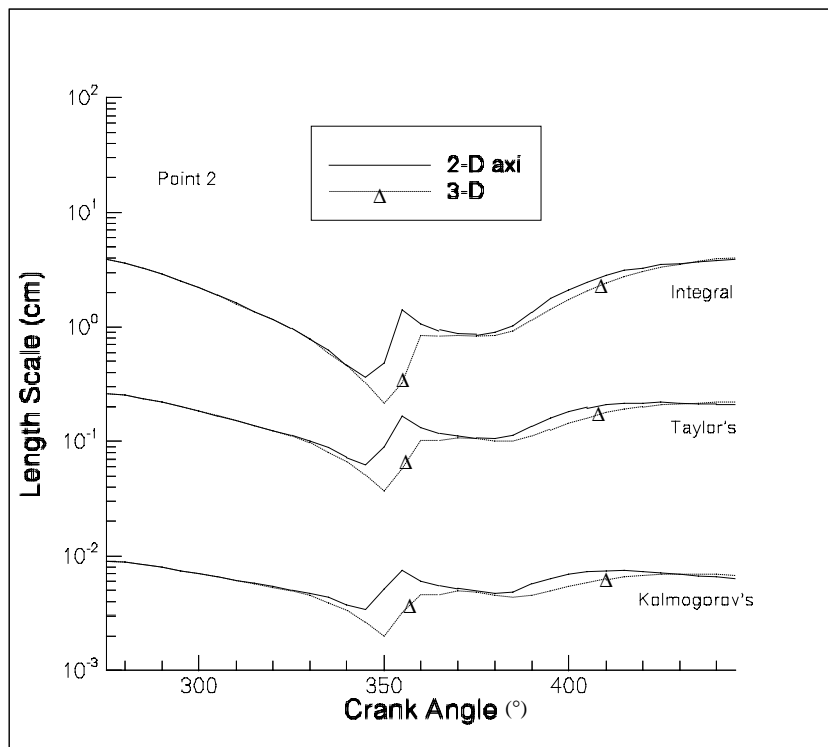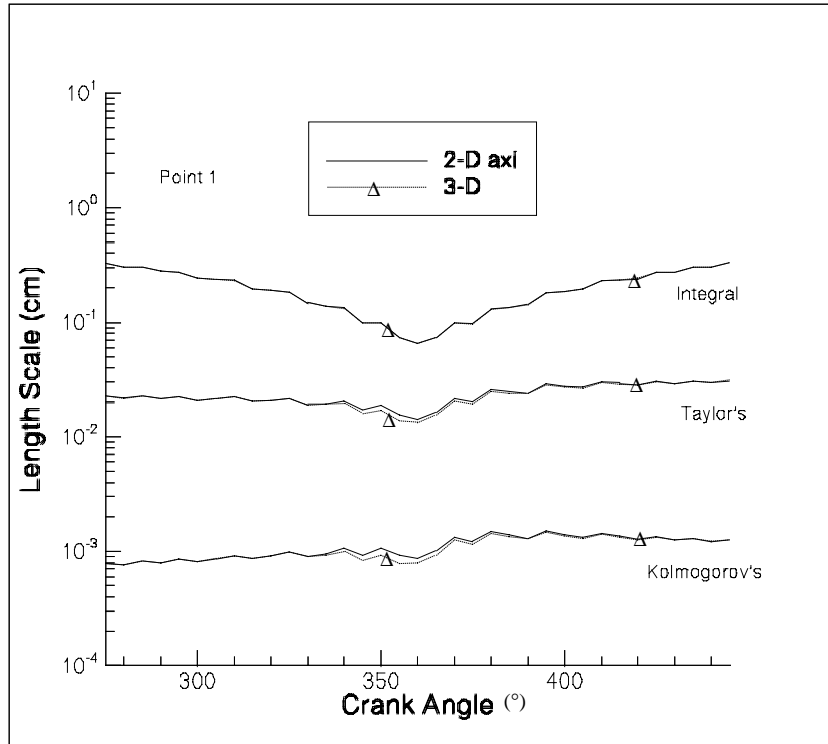
Figure 4.9c Length scale differences due to 3-D effects
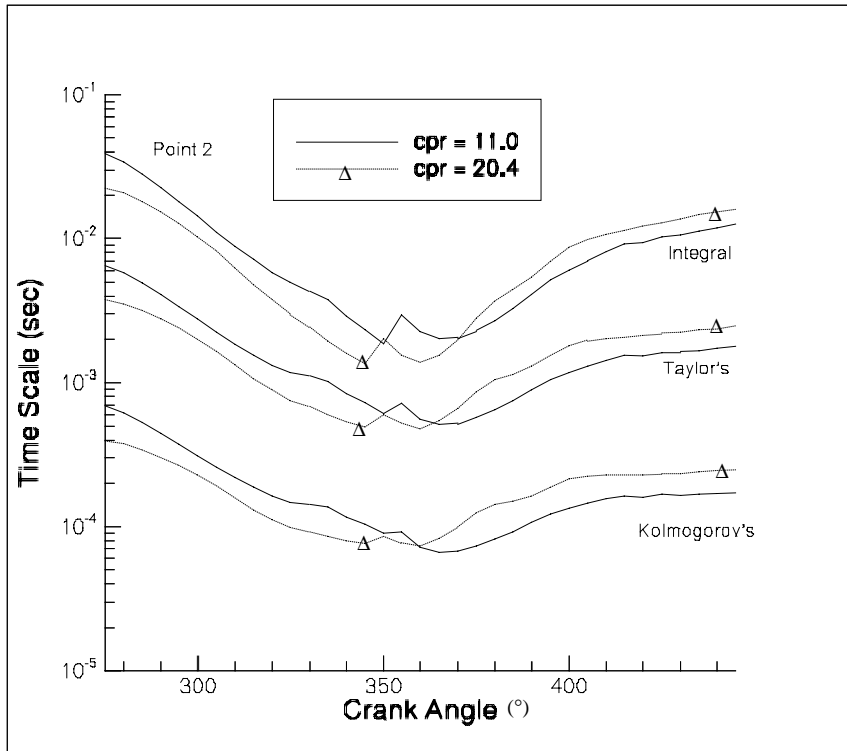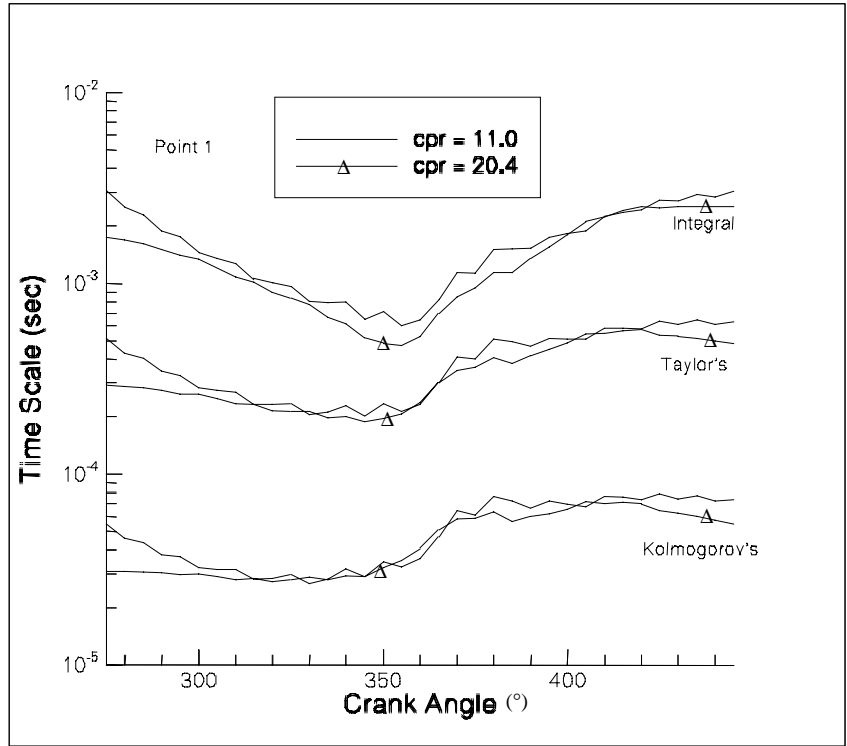
Figure 4.10a Time scale differences due to compression ratio
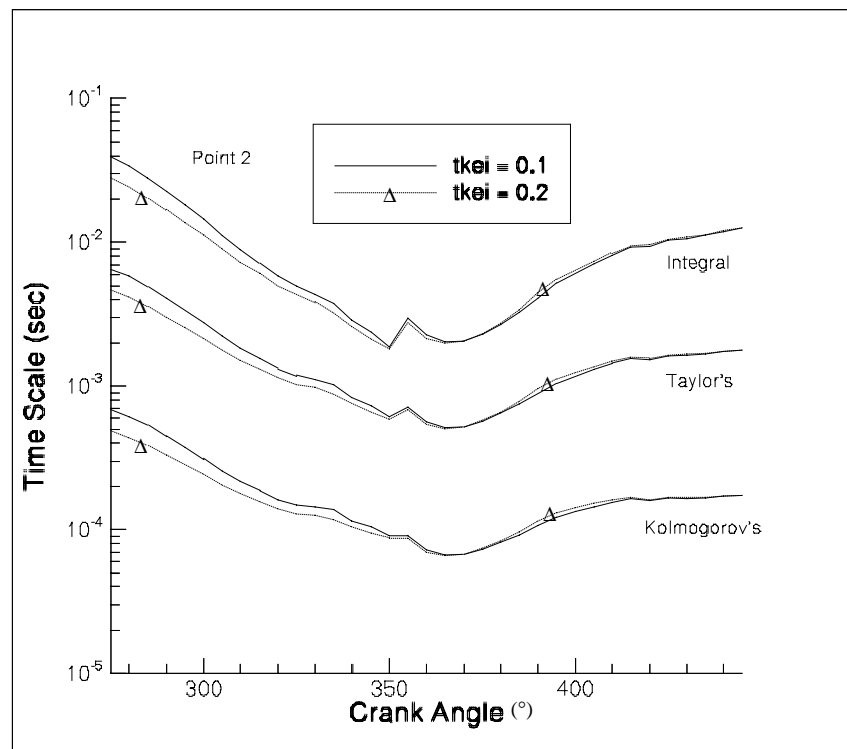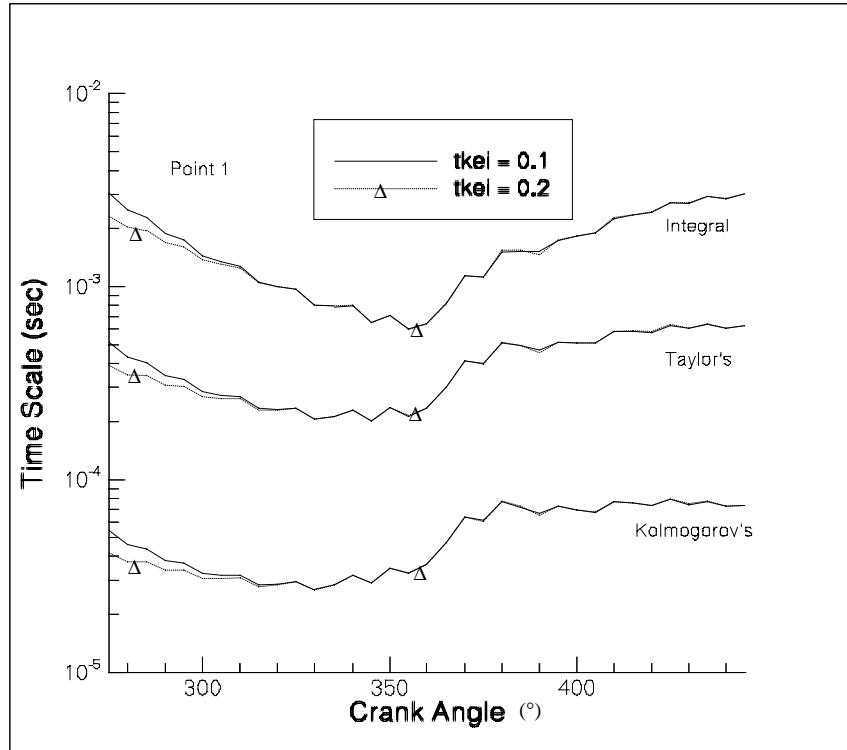
Figure 4.10b Time scale differences due to initial turbulence intensity
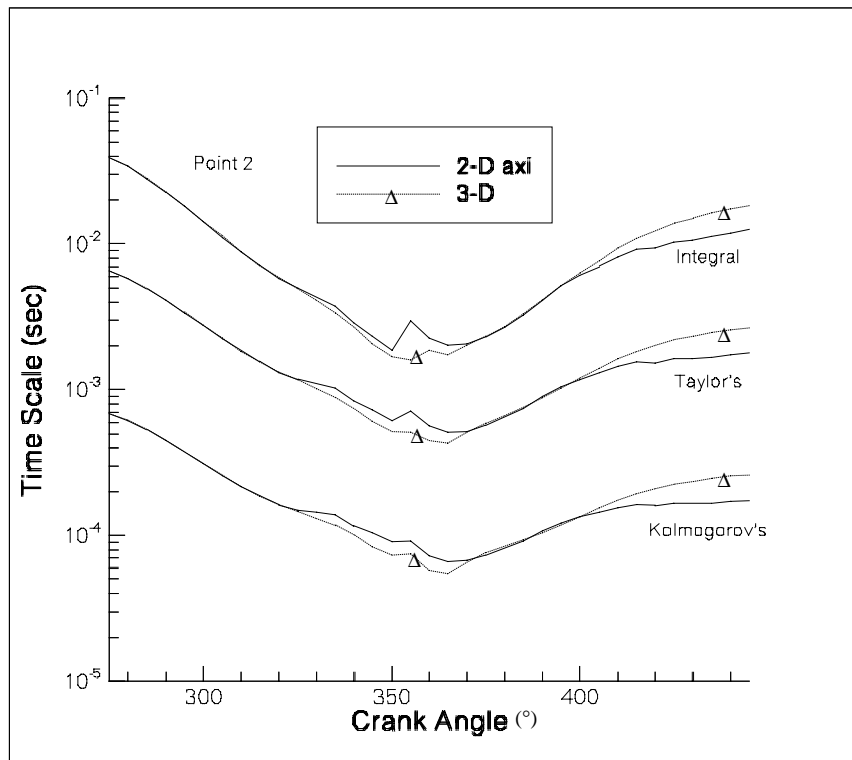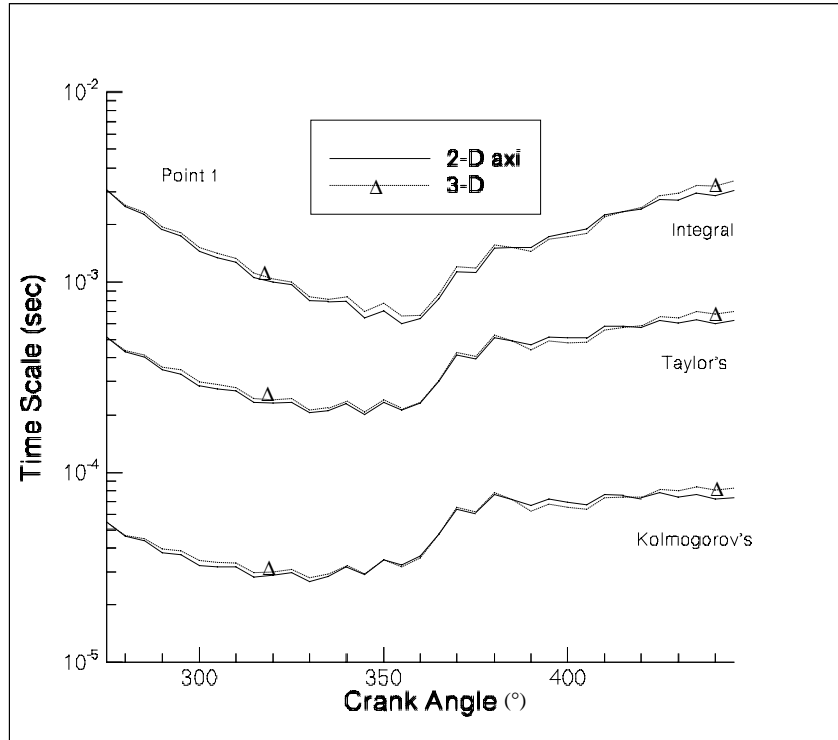
Figure 4.10c Time scale differences due to 3-D effects

In the near wall region, only the Taylor's and Kolmogorov's scales are affected within a small percentage, and the effect last only a few crank angle degrees after TDC. However, in the far wall case, the effect is much greater. There is a decrease to half of the original length scale values of the 2-D axisymmetric case in the TDC region. Note that, the place of the lowest length scale has shifted from -15° CA to -10° CA.

As for the time scales, again the 3-D effects are small in the near wall region, as given in Figure 4.10c. The 3-D effects are a few percents in the TDC region, but noticing that there is a considerable increase towards the end of the expansion stroke, one can say that three-dimensionality relaxes the flowfield causing a lower level of turbulence intensity.

4.4   Summary

An order of magnitude analysis of the scales present in the turbulent flow field inside an engine cylinder has been conducted and length and time scale magnitudes are assessed to be used in modeling strategies for large eddy simulations.

Literature most relevant to the subject of turbulence scales in IC engines have been reviewed. In this respect, the work by Lancaster (1976), Witze (1977), Fraser et al. (1986) and Arcoumanis et al. (1994) contain useful information. What seems to be lacking is the systematic assessment of these quantities in proper dimensionless forms using appropriate engine parameters as scaling parameters. Fraser et al. (1986) shows that the lateral integral length scale scales with the clearance distance between the piston and the cylinder head. Arcoumanis et al. (1984) uses the mean piston speed as scaling

parameter for the turbulence intensity. Future analysis should focus on appropriate dimensionless quantities. Otherwise it would be extremely difficult to reach conclusions with universal applicability, which do not change significantly from engine to engine.

The measured auto correlation coefficients, and the energy spectra can be used to calculate the cut-off frequency and length scales (eddy sizes) that are to be resolved by fine grid Navier-Stokes solutions or large eddy simulations. For example the observation made by Lancaster that only about 30% of the energy is contained beyond 1.0 kHz frequency is very useful.

The present computations are limited in that they only consider axisymmetric flow during the compression and expansion stroke of a typical IC engine. However, the results indicate that the standard k-ε model does seem to give the right orders of magnitude and even trends for the turbulence velocity and length scales. Needless to say this model assumes local isotropy, hence cannot predict the usually observed non-isotropic distribution of turbulence, especially during the intake and exhaust strokes.

The computational results further indicate that the turbulence intensity is very sensitive, but the integral length scale is not as much sensitive to combustion. Interestingly, the Taylor and Kolmogorov length scales are sensitive to combustion, and this influence manifests itself with a considerable lag with respect to the increase in temperature.

The minimum length scales (integral, Taylor, and Kolmogorov) are predicted near the TDC, and are 1 to 5 mm, 0.05 mm, and 0.01 mm, respectively, which are in good agreement with experimental observations. In this regard the k-ε can be used as a guide to

determine computational strategies for fine grid LES simulations. It seems that it would be logical to isolate the zone near top dead center and use many more spatial grid nodes in this zone as compared to other zones with accurate interpolation and/or extrapolation to continue the computations elsewhere.

Chapter 5

ASSESSMENT OF VARIOUS TURBULENCE MODELS

FOR IC-ENGINE APPLICATIONS

5.1   Introduction

The literature on applications of computational fluid dynamics (CFD) to internal combustion engines shows that the turbulence model of choice widely utilized are of the two-equation models based on isotropic eddy viscosity concept (see Celik et al., 1999, for a review). However, there is little information in the common literature as to the validation and performance comparison for various models of this type. Experience in the present work has been that these models do not give results consistent with each other when applied to realistic in-cylinder engine flows. It is found necessary to perform a comparative validation study among various models, which might benefit the CFD community involved with in-cylinder turbulent flow predictions.

In this study the commonly used conventional two-equation turbulence models based on the eddy viscosity concept, the standard k-ε model, the renormalization group theory (RNG) k-ε model, a typical Low Reynolds number k-ε model (Lam and

Bremhorst 1981), the Richardson number correction (RNC) k-ε model, and a Smagorinsky based eddy viscosity model are considered.

As a benchmark case an isothermal, incompressible flow within a piston-cylinder arrangement motored without compression at 200 RPM (Morse, 1979) is investigated. Then, a typical diesel-engine cylinder-bowl assembly (Catania et al., 1995) is considered under motored conditions (i.e., without combustion). Only the compression and expansion strokes are simulated for the latter case; hence cycle-to-cycle variations are not considered. Since this study was intended to be a preliminary study for complex engine simulations, at this stage the engine model was kept simple, i.e. axisymmetric and without valves.

The present calculations were performed utilizing a readily available computer code, KIVA-3 (Amsden, 1993) as described in Appendix A. In this study QSOU scheme was used exclusively.

5.2   Turbulence Models

The standard k-ε model that is implemented in KIVA-3 includes modifications for velocity dilatation, interactions with the spray, etc. (not included here). Moreover, modifications for Low Reynolds number turbulence models are implemented as follows:

$$\frac{\partial \rho k}{\partial t} + \nabla \cdot (\rho u k) = -\frac{2}{3} \rho k \nabla \cdot u + \underline{\underline{\sigma}} : \nabla u$$
$$+ \nabla \cdot \left[\left(\frac{\mu}{Pr_k} \right) \nabla k \right] - \rho \varepsilon$$

(5.1)

and

$$\frac{\partial \rho \bar{\varepsilon}}{\partial t} + \nabla \cdot (\rho u \bar{\varepsilon}) = -(\frac{2}{3} f_1 C_{\varepsilon_1} - C_{\varepsilon_3}) \rho \bar{\varepsilon} \nabla \cdot u + \nabla \cdot \left[\left(\frac{\mu}{Pr_\varepsilon} \right) \nabla \bar{\varepsilon} \right]$$

$$+ \frac{\bar{\varepsilon}}{k} \left[f_1 C_{\varepsilon_1} \underline{\underline{\sigma}} : \nabla u - f_2 C_{\varepsilon_2} \rho \bar{\varepsilon} \right] + \rho E \tag{5.2}$$

and the eddy viscosity is calculated from

$$\nu_t = f_\mu C_\mu \frac{k^2}{\bar{\varepsilon}} \tag{5.3}$$

$$\varepsilon = \bar{\varepsilon} + D \tag{5.4}$$

Here, E and D are additional functions for Low-Re k-ε models.

For the standard k-ε model, f_μ, f_1, and f_2 are unity, and D and E are equal to zero. For more details regarding the above equations the reader is referred to Amsden et al., (1989), and the standard k-ε model constants used in this model are $C_{\varepsilon 1}$ = 1.44, $C_{\varepsilon 2}$ = 1.92, C_μ = 0.09, σ_k = 1.0, σ_ε = 1.3.

The Low Reynolds number model of Lam-Bremhorst (1981) is utilized in this study, where E and D are zero, and

$$f_\mu = \left[1 - e^{-0.0165 Re_y} \right]^2 \left(1 + \frac{20.5}{Re_t} \right) \tag{5.5}$$

$$f_1 = 1 + \left(0.05 / f_\mu \right)^3 \tag{5.6}$$

$$f_2 = 1 - e^{-Re_t^2} \tag{5.7}$$

Also, the turbulence Reynolds number and wall Reynolds number are given as

$$Re_t = \frac{k^2}{\nu \bar{\varepsilon}} \quad \text{and} \quad Re_y = \frac{\sqrt{k} y}{\nu}$$

The Renormalization group theory (RNG) k-ε model (Orszag et al., 1993) was implemented in the KIVA-3 code as it was done by Han and Reitz, (1995); see also Amsden, (1997). Here, the ε equation requires an additional term that accounts for the turbulent to mean-strain time scale ratio through modification of the coefficient $C_{\varepsilon 1}$ (see Han and Reitz, 1995). The RNG k-ε model coefficients are as follows,

$$C_{\varepsilon 1} = 1.42 - \eta\,(1-\eta/\eta_o)\,/\,(1+\beta\eta^3)\;;\;\eta = \rho k/\varepsilon$$

$$C_{\varepsilon 2} = 1.68,\; C_{\mu} = 0.085,\; \sigma_k = 0.72\text{ and }\sigma_{\varepsilon} = 0.72.$$

The standard k-ε model poorly predicts non-equilibrium flows with high streamline curvatures with high swirl. For this, it has been subjected to a number of modifications to account for the streamline curvature effects. These modifications are usually introduced as corrections to the model of turbulent shear stress or as additions to the source term in the ε equation. The former tends to produce a relatively rapid response to the local curvature, while the latter may respond more slowly. The Richardson number corrections (analogous to buoyant flows) considered in this section belong to the latter type. They are most commonly used in dealing with swirl flows. The Richardson number correction (RNC) was implemented to KIVA by Smirnov, (1998) to account for this problem. The source term in the ε equation was modified as

$$S_{\varepsilon} = C_{\varepsilon_1} G \frac{\varepsilon}{k} - C_{\varepsilon_2} \left(1 - C_g R_g\right) \frac{\rho \varepsilon^2}{k} \qquad (5.8)$$

$$R_g = \frac{2\left(V_{t,r} + V_t/r\right)V_t/r}{V_{n,r}^2 + \left(V_{t,r} - V_t/r\right)^2} \qquad (5.9)$$

Here V_t and V_n, are the tangential and normal velocities to the streamline, respectively, r is the curvature, "," denotes a derivative, G is the production and $C_g = 0.008$, other constants are the same as in the standard k-ε model.

The turbulent shear stresses are modeled via

$$\tau_{ij}^s - \frac{1}{3}\tau_{kk}^s = \nu_t\left(\frac{\partial \overline{u}_i}{\partial x_j} + \frac{\partial \overline{u}_j}{\partial x_i}\right) = 2\nu_t \overline{S}_{ij} \tag{5.10}$$

where $\overline{S}_{ij}$ is the resolved large-scale strain rate tensor which is defined as

$$\overline{S}_{ij} = \frac{1}{2}\left(\frac{\partial \overline{u}_i}{\partial x_j} + \frac{\partial \overline{u}_j}{\partial x_i}\right) \tag{5.11}$$

Assuming local equilibrium of production and dissipation of subgrid energy, a mixing length type model in the form of the subgrid scale eddy viscosity is then defined as (Smagorinsky, 1963)

$$\nu_t = C_s\Delta^2\left|\overline{S}\right| \tag{5.12}$$

where C_s is the model parameter, Δ is the filter length, and $\left|\overline{S}\right| = \left(\overline{S}_{ij}\overline{S}_{ij}\right)^{\frac{1}{2}}$ is the contraction of resolved stresses. See Section 3.3.4 for the model constants.

Modifications were made to the KIVA code to allow a fairly simple Smagorinsky based eddy viscosity model (SEV) where the eddy viscosity is calculated from

$$\nu_t = \left(C_s L_{ch}\right)^2\left(\overline{S}_{ij}\overline{S}_{ij}\right)^{1/2} \tag{5.13}$$

$$L_{ch} = \min\left(\alpha \cdot \ell_{vo}, \ \lambda \cdot \text{Bore}/2, \ \left(\ell_p \cdot y_n\right)^{0.5}\right) \tag{5.14}$$

The Smagorinsky constant C_s was set equal to 0.1, which is in the lower range of the typical values used in the literature (see e.g. Rodi et al., 1997). The valve opening, l_{vo} is 0.4 cm, and the model parameter $\lambda = 0.2$ according to the classical boundary layer theory, y_n is the normal wall distance, $\alpha = 1$ and ℓ_p is the minimum of the distance from the cylinder head and the piston head. In the original Smagorinsky model L_{ch} is related to the grid size in the context of large eddy simulation.

The above turbulence models were used in conjunction with the commonly used law-of-the-wall boundary condition which is implemented in KIVA-3 (Amsden et al., 1989).

5.3   Case Specific Numerical Issues

An isothermal, incompressible flow within a piston-cylinder arrangement (Morse et al., 1979; Haworth, 1998) motored without compression at 200 RPM is investigated. The mean piston speed V_p was 40 cm/sec in these calculations. There was no swirl imposed. The computational mesh used in the 2-D simulations is shown in Fig.1. The seat angle was 60° with the horizontal axis. A time step of 1×10^{-5} seconds was used for time marching. A numerical mesh of 40,000 vertices was employed with a wedge angle of 0.5 degrees in the circumferential direction. The maximum cell size for the wedge calculations was 0.5x0.5 mm in the radial and axial direction inside the cylinder. The inlet pressure was atmospheric and the initial flow was at rest until the piston started to move away from TDC (0° CA).
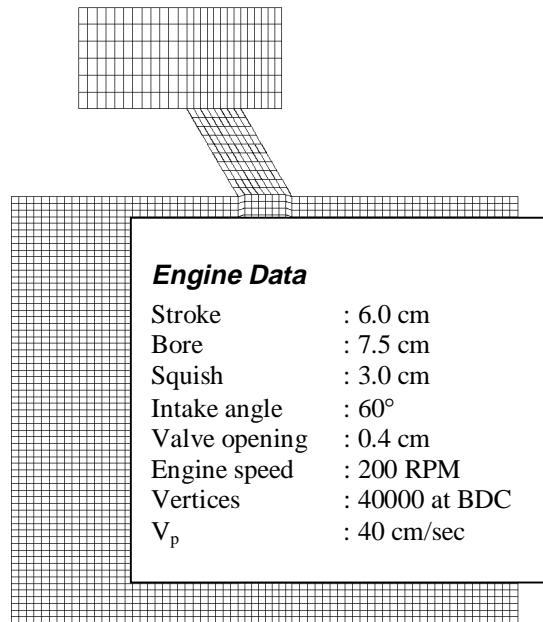
Figure 5.1 Computational mesh for case 1 (intake) and specific engine data (half

of cylinder geometry, left edge is symmetry line)
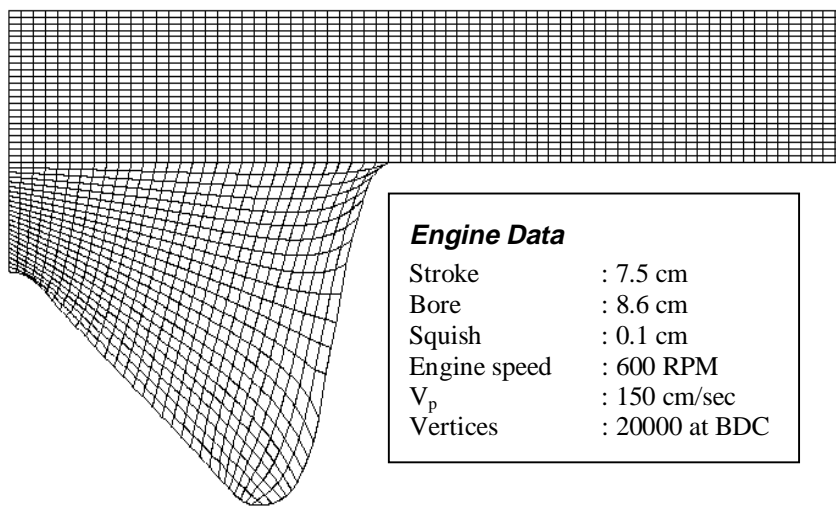
Figure 5.2 Computational mesh for case 2 (piston-bowl) and specific engine data (left

edge is symmetry line)

Also the flow field inside a typical piston-cylinder assembly (Catania et al., 1995) was simulated under motored conditions at 600 RPM, which implies a mean piston speed V_p =150 cm/sec. The numerical mesh used in these simulations is depicted in Figure 5.2. A numerical mesh of 20,000 vertices was used with a wedge angle of 0.5 degrees in the circumferential direction. The maximum cell size for the wedge calculations was 0.6x0.9 mm in the radial and axial direction. As reported by Celik and Yavuz (1997), the minimum integral length scale occurs at the end of the compression stroke in the order of squish clearance height. To investigate grid dependency another mesh with 70,000 vertices was used for the same case, which provided approximately the same results in the mean flow for the standard k-ε model.

The time step used in computing the results of the second case was $5x10^{-6}$ seconds. The simulations for the piston-bowl assembly were started at CA 90° BTDC. As an initial condition the radial velocity was taken as zero and the axial velocity varied linearly from piston velocity at the piston face to zero at the cylinder head. The tangential velocity was defined by the Bessel function dependent on engine speed as provided in the KIVA code with a swirl number equal to 2.

Although, these conditions are not realistic, the goal was to show the difference in predictions applying different turbulence models starting with the same initial conditions. Moreover, periodic boundary conditions were applied on the front and back face of the wedge, whereas the law of the wall was applied near the walls.

5.4   Results and Discussion

In Figures 5.3 to 5.5, the axial velocity profiles are compared at various stations inside the cylinder. The standard k-ε model and the Low-Re model results are essentially the same and compare well with the measurements. The Low-Re model seems to improve the results near the wall (as expected) as well as in the vicinity of the reattachment point at the wall. However, the SEV model and RNG k-ε model are deviating from these predictions in some regions favorably and in others not so favorably. It should be noted that the SEV model usually overpredicts the axial velocity very near the cylinder wall. This can be remedied by damping the mixing length according to boundary layer theory, i.e. $L_{ch} \sim f_n y_n$ where y_n is the normal distance from the wall and f_n is van Driest's wall damping function.

The streamlines from the intake flow case are shown in Figures 5.6 to 5.8. Here, only the k-ε model with Richardson number correction (RNC), the Smagorinsky based eddy viscosity (SEV) model solutions and the measurements of Morse et al., (1979) are presented for brevity. The standard k-ε model, low Re k-ε and the RNG k-ε model are compared to each other in Figure 5.9 only at 90° CA, as they exhibited very similar results as those of the RNC solutions at 36° CA and 144° CA. As seen from these figures the results from the RNC model compare well with the measurements in the overall sense. Whereas the SEV model is predicting slightly different results, especially the size of the recirculation region at the right corner near the piston face at 144° CA is smaller. Given the simplicity of the SEV model, the agreement between predictions and experiments is rather good.
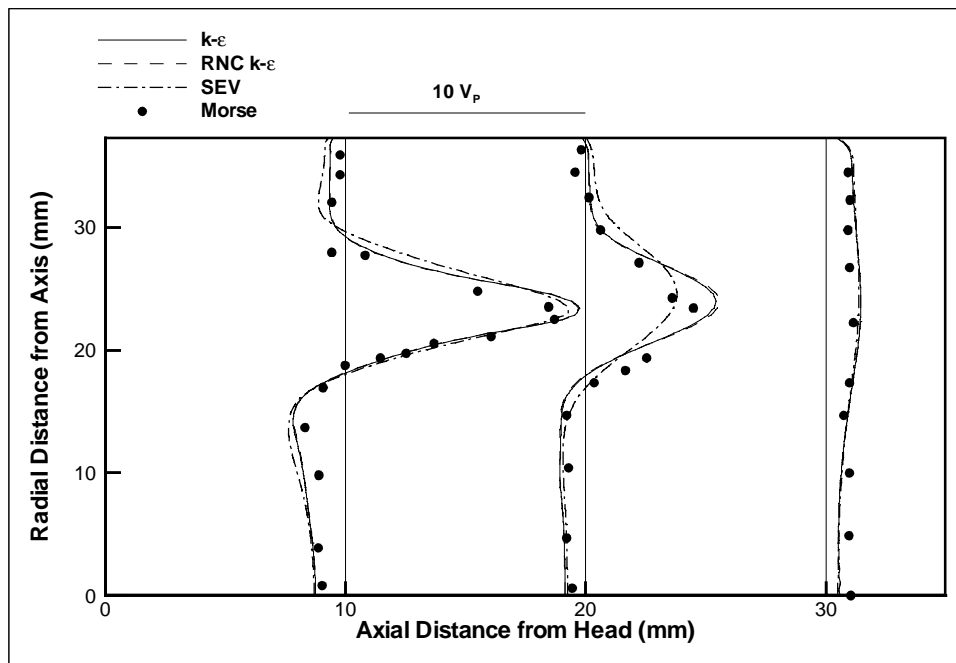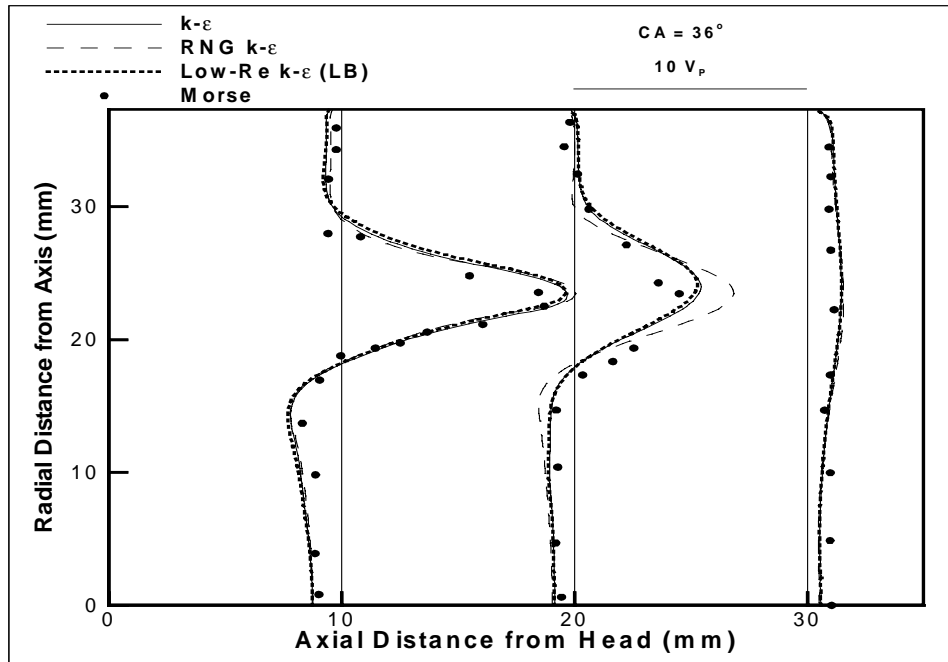
Figure 5.3 Axial velocity profiles for intake case at 36° CA ATDC
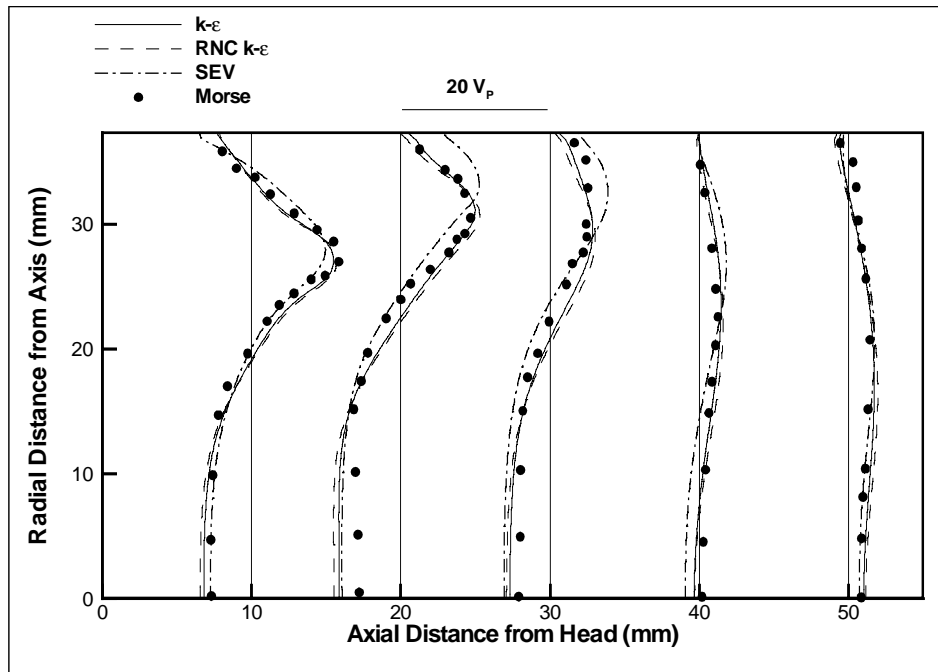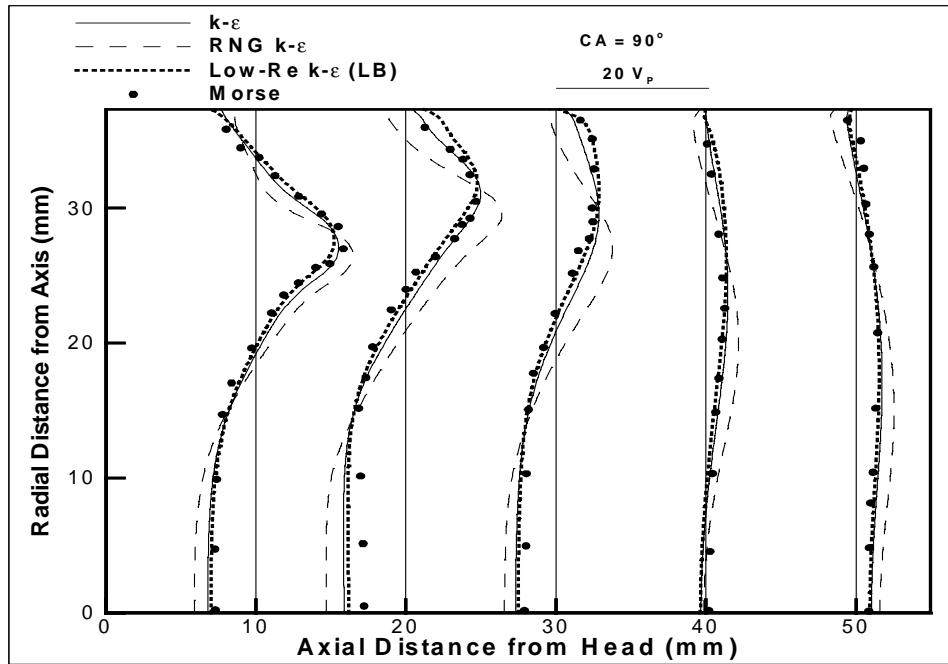
Figure 5.4 Axial velocity profiles for intake case at 90° CA ATDC
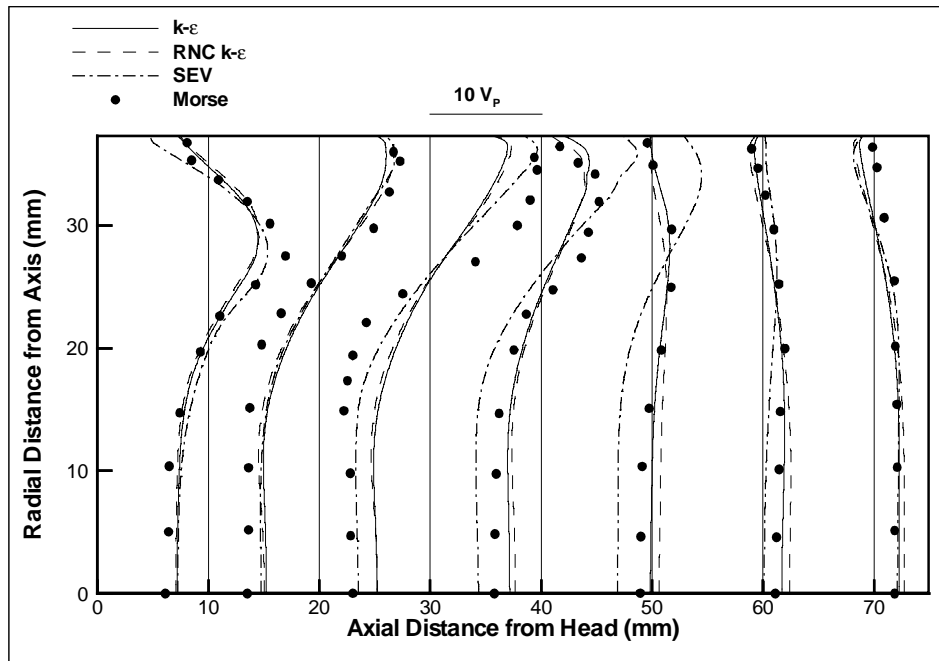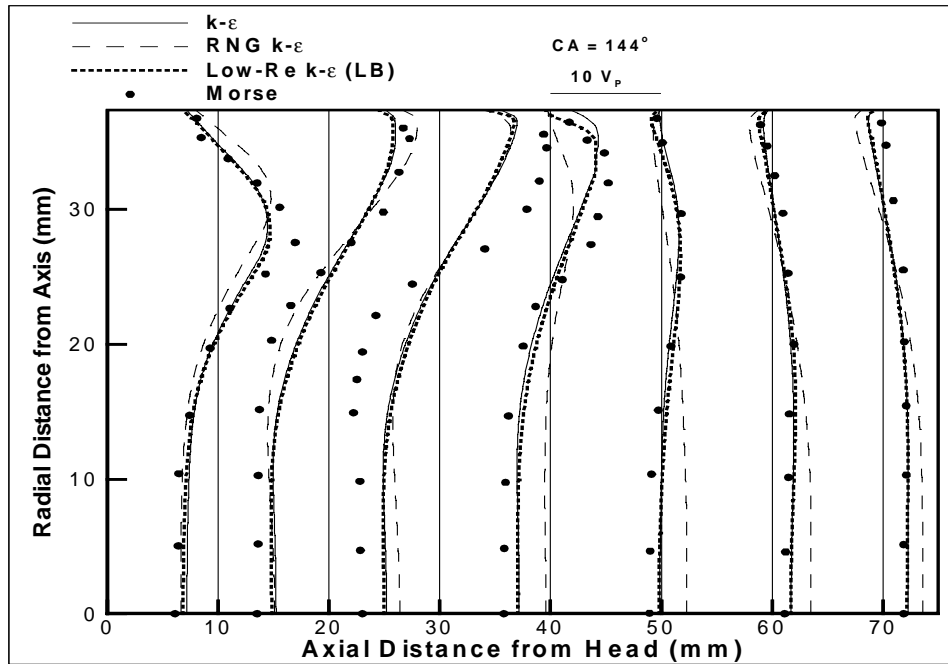
Figure 5.5 Axial velocity profiles for intake case at 144° CA ATDC
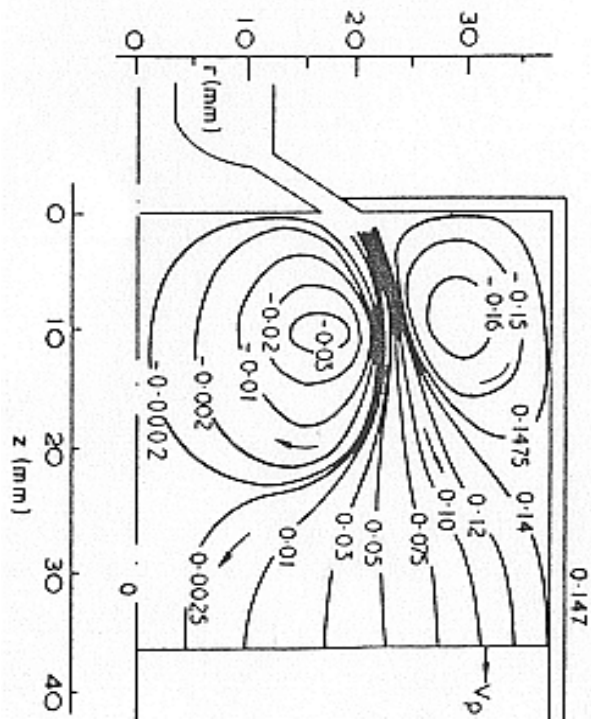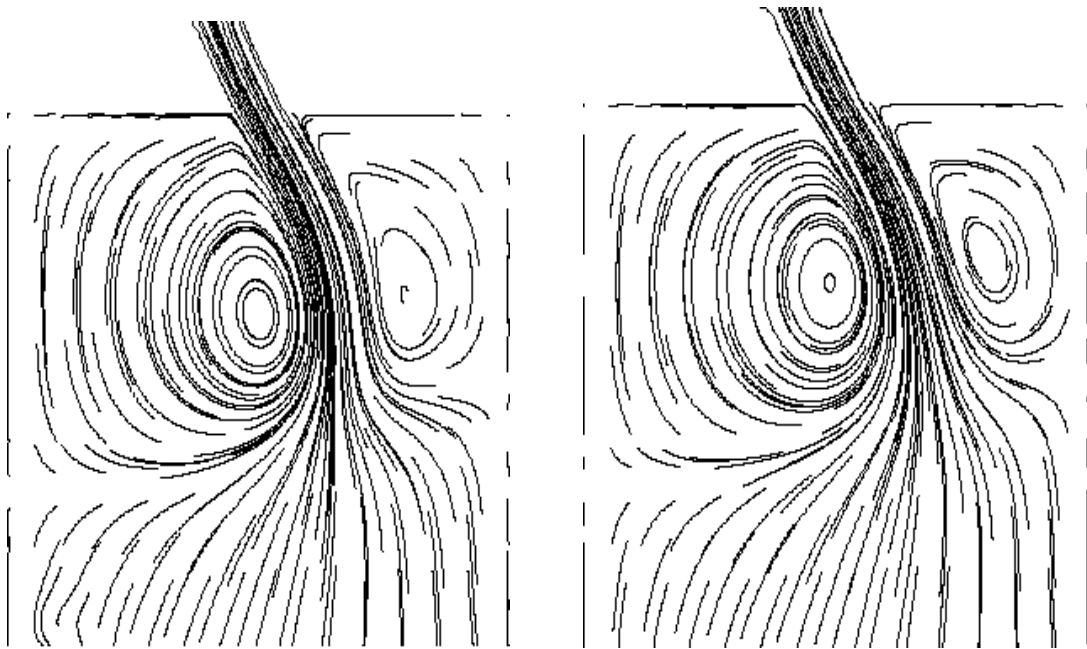
Figure 5.6 Streamlines using RNC-k-ε (left), Smagorinsky (right), and measurements (bottom) for case 1 at 36° CA
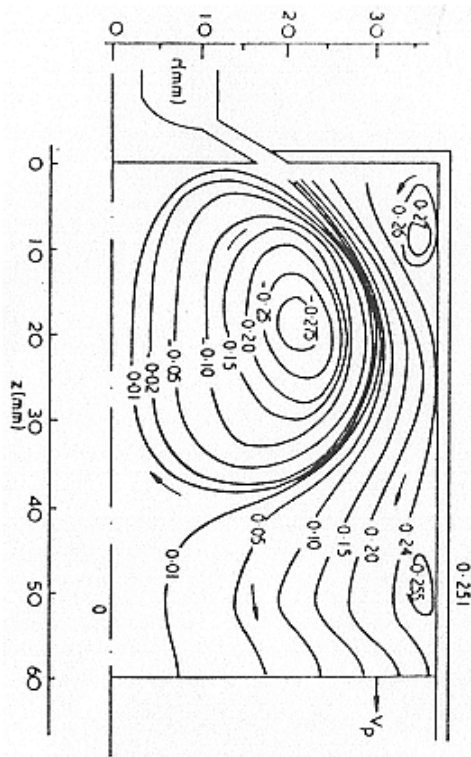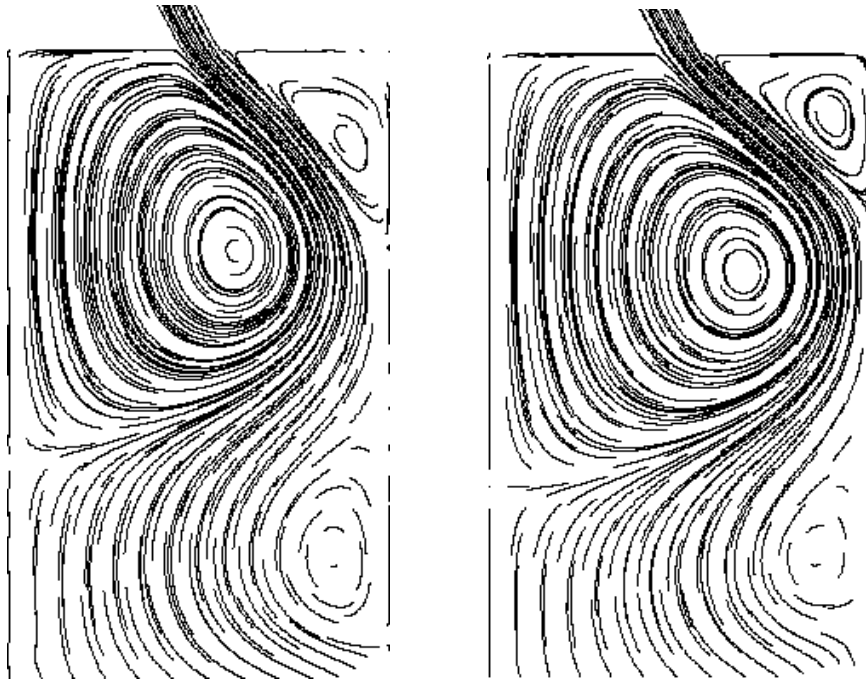
Figure 5.7 Streamlines using RNC-k-ε (left), Smagorinsky (right), and measurements (bottom) for case 1 at 90° CA

71
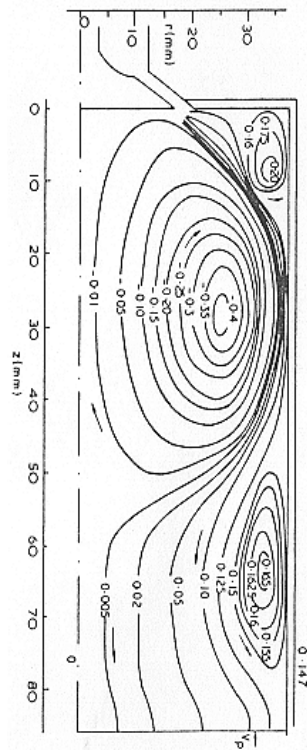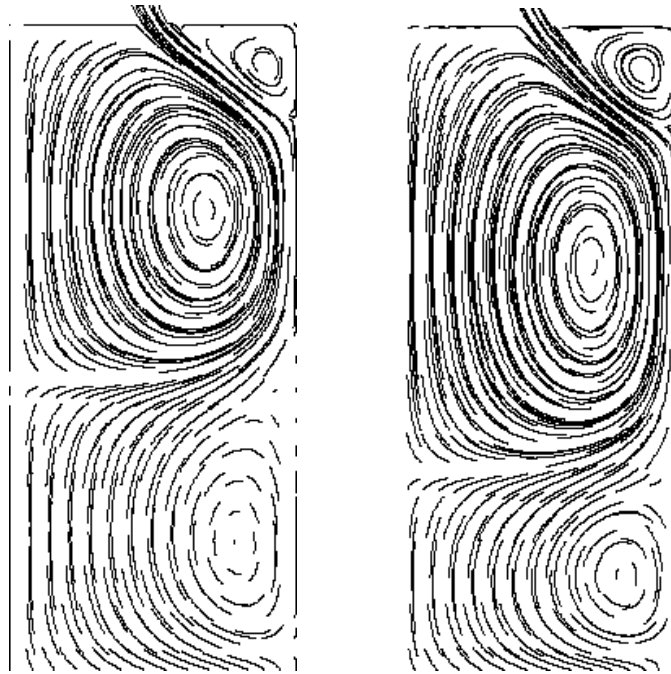
Figure 5.8 Streamlines using RNC-k-ε (left), Smagorinsky (right), and measurements (bottom) for case 1 at 144° CA

72
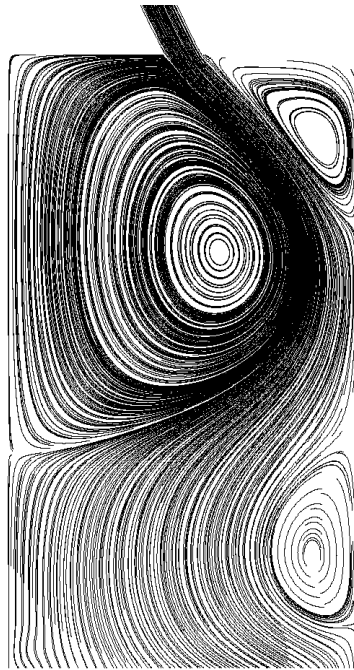
a) Standard k-ε   b) RNG k-ε
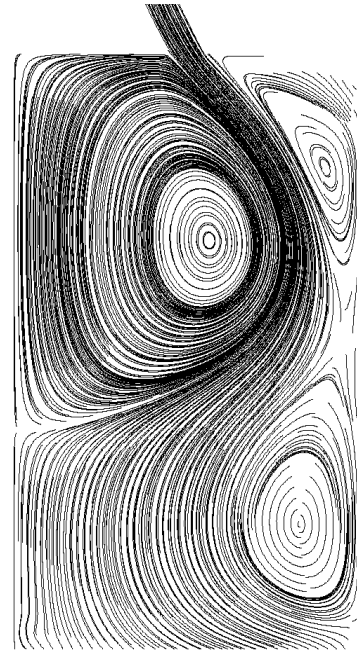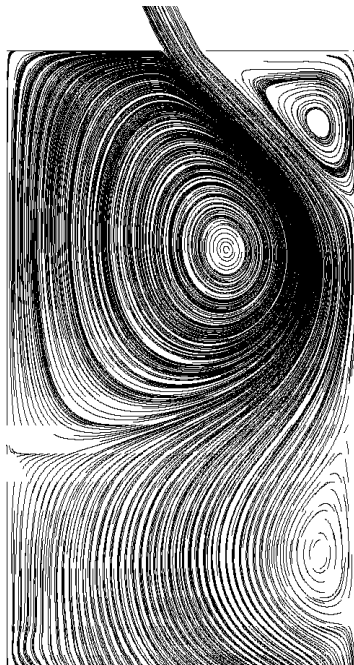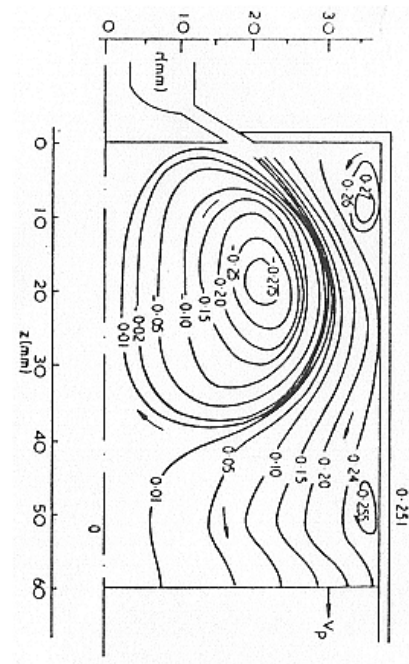
c) Low-Re k-ε (LB)   d) Measurements (Morse et al., 1979)

Figure 5.9 Streamlines of the intake case at 90° CA

The predicted streamlines from the intake flow case at 90° CA are shown in Figure 5.9 as compared to the measurements of Morse et al., (1979). The results from all three models compare well with the measurements in the overall sense. The RNG k-ε model solutions deviate more from the measurements in capturing the size of the lower wall recirculation zone. The Low-Re k-ε model performs slightly better in this regard, which is supported by the fact that the turbulent Reynolds number is low, as depicted in Figure 5.15. Moreover, the calculated turbulence intensity from the intake case was compared to the experimental data, but the agreement (not shown here) was not good for any of the models.

The axial velocity profiles obtained from the piston-bowl (case 2) predictions are presented in Figures 5.10 to 5.12 at different crank angles. Here, the most noticeable difference in the predictions of the k-ε and RNG k-ε models were the increasing divergence of the solutions from each other with increasing crank angle. The largest difference is observed at the symmetry axis. It is possible that the additional source term added to the RNG ε equation becomes singular at this boundary. It is clear that these models show significant variations in time development of the mean flow.

Finally, the predicted streamlines of the standard k-ε and RNG k-ε models are compared for the piston-bowl assembly in Figures 5.13 and 5.14. While no significant differences were observed in the intake flow case, solutions for the piston-bowl assembly are drastically different at some crank angles. This could be due to the fact that the turbulent Reynolds number is considerably higher than that of the intake flow case, as shown in Figure 5.14.
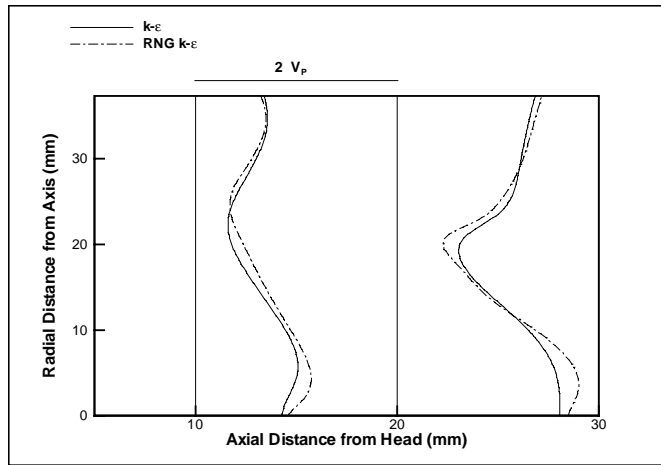
Figure 5.10 Profiles of axial velocity at 60° CA for case 2
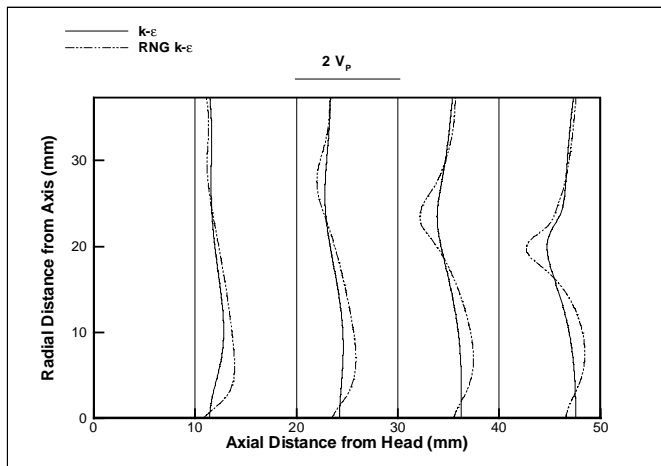
Figure 5.11 Profiles of axial velocity at 90° CA for case 2
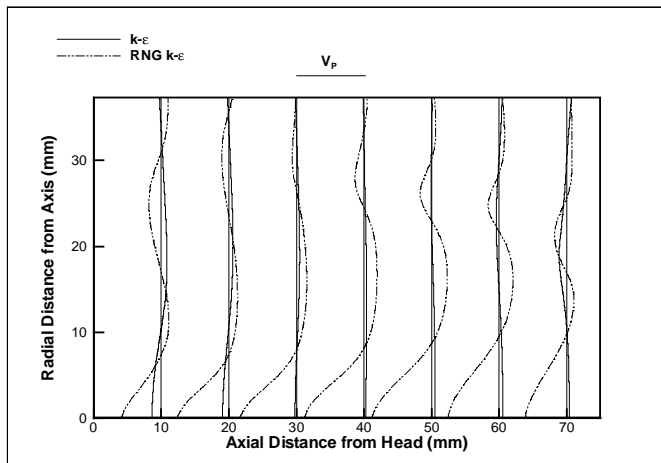
Figure 5.12 Profiles of axial velocity at 180° CA for case 2
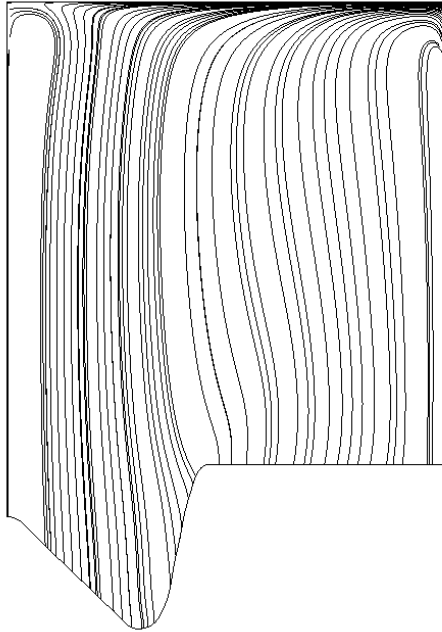
a) Standard k-ε
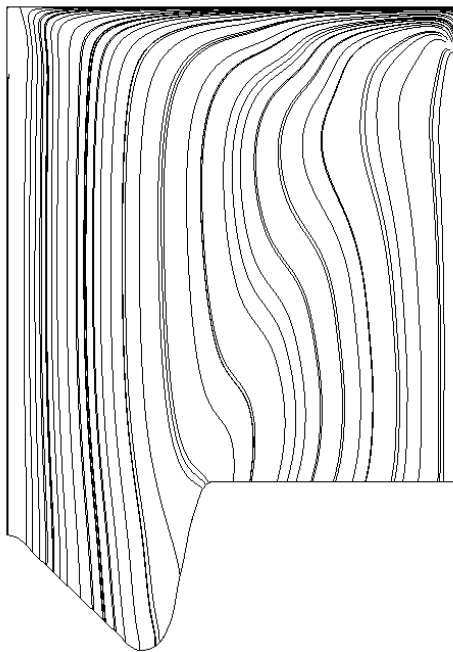
a) RNG k-ε

Figure 5.13 Streamlines of piston-bowl case at 450° CA
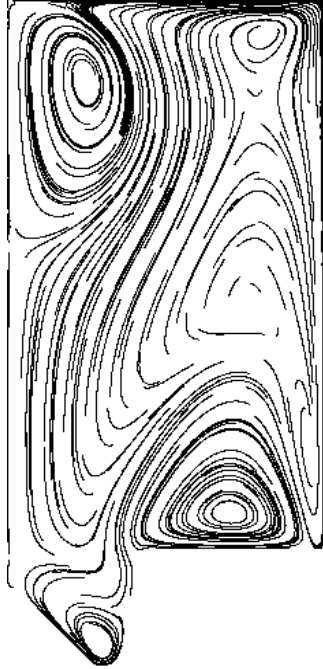
a) Standard k-ε
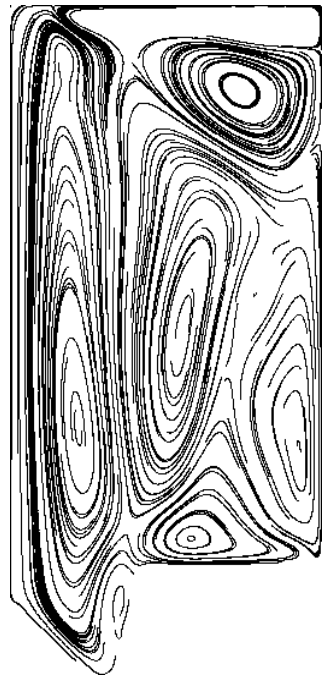
b) RNG k-ε

Figure 5.14 Streamlines of piston-bowl case at 540$^{\mathrm{o}}$ CA (BDC)
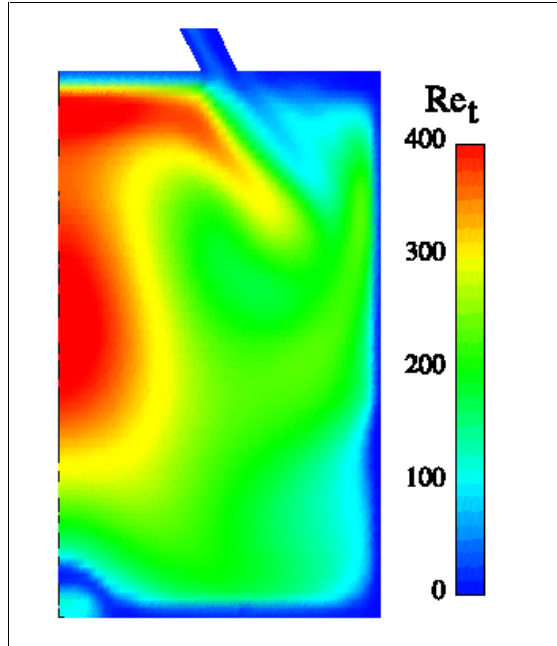
a) Intake case: Case 1
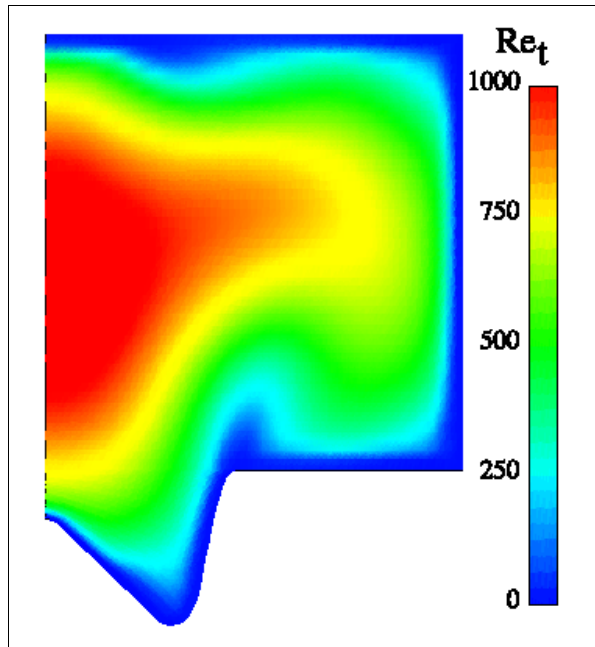
b) Piston-Bowl case: Case 2

Figure 5.15 Turbulent Reynolds number at 90° CA, as predicted by the Low-Re k-

ε model (Lam-Bremhorst)

That again raises the question, if these models are applicable to IC-engine flows at all speeds and operating conditions? Even if they both predict good results for one case, they could predict significantly different results for other cases.

For this case the influence of turbulence generated during the intake stroke was not included with the premise that it would have decayed when the BDC was reached.

5.5   Conclusions

A comparative study of the commonly used two-equation turbulence models applied to internal combustion engines was conducted. For this purpose a readily available computer code KIVA-3 was utilized, which is being widely used by the engine community for design and diagnostics. Five models were considered, namely, the standard k-ε model, the RNG-k-ε model, the Lam-Bremhorst low-Re k-ε model, a k-ε model modified for curvature effects (RNC-k-ε), and a new Smagorinsky based eddy viscosity (SEV) model. First, these models were applied to predict the turbulent flow during the intake stroke of an engine cylinder with flat piston at a low speed of 200 RPM and during the compression and expansion strokes of a piston-bowl assembly.

In general all of these models do a reasonably good job in predicting the main features of the mean flow during the intake stroke when the valve is not moving and the piston speed is low. When fine details of this flow are considered the RNC-k-ε models seems to perform slightly better, and the Low-Re model seems to perform the best, with an appreciable improvement near the walls for the case where the relatively low turbulence Reynolds numbers were observed. The SEV model has the potential to predict

the physics of this flow better, provided that the characteristic length scale is adjusted dynamically, including all the relevant scales of the engine, and the distance from the wall. In this case the RNG k-ε model performs worse than the standard k-ε model, contrary to expectations. Perhaps a low Reynolds number version of this model would perform better.

However, although the mean flow predictions are reasonably good, the turbulence intensity predictions do not compare well with the experimental data, which would show the real performance of a turbulence model.

As for the case of the piston-bowl assembly with closed valves (i.e. compression and expansion stroke) the standard k-ε model and the low-Re versions of it give essentially the same results. However, the RNG k-ε model produces drastically different results, even though their performance was very similar in the case with intake flow. Unfortunately, defining the best available RANS model for engine applications requires more validation studies at higher engine speeds and analysis of the results from several engine cycles against a reliable set of experimental data.

It seems that for IC flows transient effects are very important and the turbulence models need to be tested against a good time-dependent (in the mean) benchmark case.

Chapter 6

BOWL-INDUCED FLOW INSTABILITY IN A TYPICAL ENGINE CYLINDER

6.1   Introduction

The importance of the influence of turbulence on combustion is an undisputed fact. The current understanding of turbulence phenomenon as it relates to combustion, engine performance, and pollutant emissions, however, is far from being satisfactory. The control of the consequences of turbulence can only be possible with a clear understanding of its production and dissipation as a function of the key engine parameters. This, in turn, requires detailed quantitative study of velocity fluctuations inside the engine cylinder. Time variation of both the mean (e.g. ensemble averaged) quantities, and the statistics of their fluctuation components, such as root mean square (RMS) values, the probability density function (pdf), correlation coefficients, etc., need to be either computed or measured in such a way that a complete three dimensional mapping of the flow field can be constructed which makes the inside of the engine cylinder virtually visible to the engineers.

The RANS approach involves many modeling assumptions, (e.g., local equilibrium and isotropy in the case of k-ε model) and they are incapable of predicting

the details of turbulence statistics. A major shortcoming of these models is the assumption of a single characteristic length and time scale to represent the whole spectrum of turbulence scales. As mentioned above, a true understanding of turbulence phenomena can only be achieved by predicting the actual three-dimensional transient flow field, by minimizing the input from empirical modeling, which could be achieved via application of the LES technique.

In this chapter, a typical diesel-engine cylinder-bowl assembly is considered under motored conditions (i.e., without combustion). Only the compression and expansion strokes are simulated; hence cycle-to-cycle variations are not considered. The focus is on the prediction of flow instabilities induced by the bowl geometry and the squish flow, which may contribute significantly to the overall turbulence generation. The results are not compared with any experimental work directly because such a comparison requires strict matching of the intake flow situation, which is not part of the present study. Moreover, the experiments most of the time present ensemble averages which include cycle-to-cycle variations, and they can not be easily isolated. However, the experiments by Catania et al., (1995), and Valentino et al., (1998) are used as a guide to make qualitative assessment of the predictions. The simulations are enlightening in that they indicate that the turbulence inside an engine cylinder can potentially be predicted, and further the influence of cylinder bowl geometry can be isolated from that of the turbulence generated by other mechanisms such as shear layers and the swirl induced during the intake stroke.

6.2 Turbulence SGS Models

Favre averaging of the Navier-Stokes equations produces turbulence stresses of the form

$$\tau_R = -\rho \overline{u_i' u_j'} \tag{6.1}$$

A similar expression is obtained when the governing equations are filtered in the large eddy simulation (LES) approach (see Section 3.3.3). The Boussinesq eddy viscosity approximation is used to determine the subgrid scale stresses, which in this study refers to the difference,

$$\tau_{SGS} = \overline{\rho u_i u_j} - \overline{\rho}\, \overline{u}_i \overline{u}_j = 2\mu_t \overline{S}_{ij} - \frac{2}{3}\rho k \delta_{ij} - \frac{2}{3}\mu_t \nabla \cdot u \delta_{ij} \tag{6.2}$$

KIVA-3 allows for a SGS model, which utilizes the k equation given above along with constraining the ε values to satisfy the following inequality:

$$\varepsilon \geq \left[\frac{C_\mu}{Pr_\varepsilon (C_{\varepsilon_2} - C_{\varepsilon_1})} \right]^{\frac{1}{2}} \frac{k^{\frac{3}{2}}}{L_{SGS}} \tag{6.3}$$

L_{SGS} is an input length scale whose value is typically some measure of the computational cell dimension. In this study L_{SGS} was taken to be equal to the grid related length scale, $L_G = (\Delta x \Delta y \Delta z)^{1/3}$, and used as a constant with a typical cell size. This model will be referred to as the k-ε|$_{SGS}$ model.

The SGS turbulence model was used in conjunction with the commonly used law-of-the-wall boundary condition, which is implemented in KIVA-3. Calculations were also carried out without any SGS turbulence models.

6.3 Case Specific Numerical Issues

The flow field inside a typical piston-cylinder assembly (Figure 6.1, 2-D, axisymmetric, same as the case in Chapter 5) was simulated under motored conditions at two speeds, namely 600 RPM and 1500 RPM. The numerical mesh used in the simulations is depicted in Figure 6.2. The computations have been performed on an SGI R10000 Maximum Impact workstation.

Figure 6.1 2-D Streamlines at CA 210° ATDC (with mirror image)

Engine Data

Stroke   : 7.5 cm
Bore   : 8.6 cm
Squish   : 0.1 cm
Engine speed : 600 and 1500 RPM
No. Vertices : 20000 at BDC
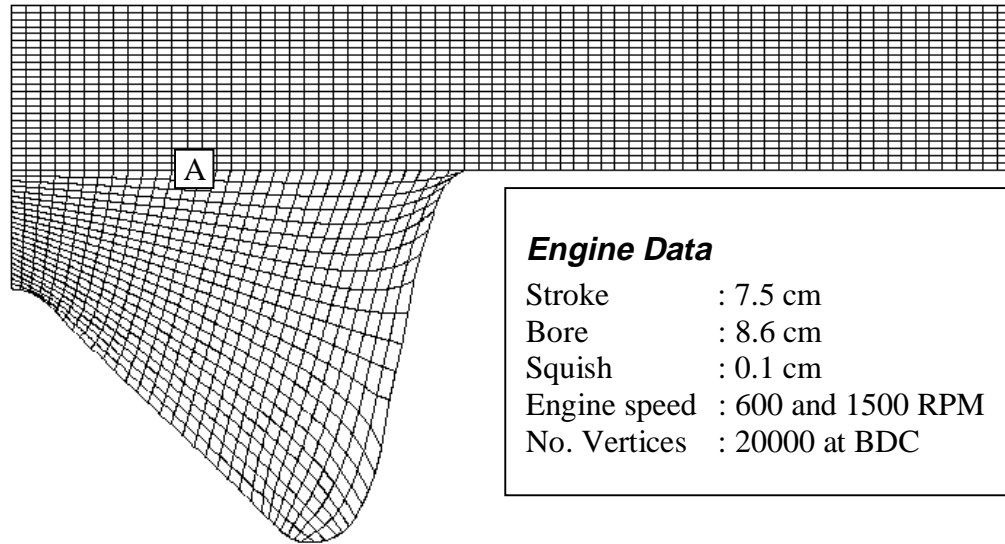
Figure 6.2 Computational mesh for 2-D simulation and specific engine data

Two numerical meshes of 20,000 and 130,000 vertices were used with a wedge angle of 0.5 and 180 degrees in the circumferential direction, respectively. Notice that the ghost-cells surrounding the computational domain were accounted in the above numbers. The maximum cell size for the wedge calculations was 0.5x0.9 mm in the radial and axial direction. The 3-D simulation with 180-degree wedge angle span was investigated with 18 cells in the circumferential direction to see the influence of the domain size. For this case the median cell size in the tangential direction was 3.0 mm. As reported by Celik and Yavuz (1997), the minimum integral length scale occurs at the end of the compression stroke and is in the order of 2-5 mm for automotive size engines.

Though the overall time accuracy in convection is only first-order accurate, the global time step is based on several considerations including stability and several accuracy constraints. The convective terms are advanced with time steps that are the same or smaller than what is used for the diffusion terms. Due to these reasons it is

believed that the time accuracy is quite good despite the formal order of accuracy. In this study the QSOU scheme was used exclusively with very small time steps to assure time accuracy.

Early calculations have revealed that it was possible to capture flow instability with the present grid resolution even at the lower engine speed of 600 RPM. However, the selection of the time step played a crucial role in the resulting amplitude and the frequency of oscillations. It was possible to totally destroy the flow instability (most probably induced by the flow separation at the corner where the bowl meets the piston head) either by increasing the time step, or by simply using the standard k-ε turbulence model, which is known to be overly diffusive. The time steps used in the results presented here were selected carefully after much experimentation.

Several other problems are worth mentioning. One is a rezoning problem that happens near the TDC. If a large grid cell expansion ratio is encountered as a result of rezoning (deleting or adding cells as the piston moves) there appears to be some local discontinuity, restricted to one grid line in the radial direction, in the velocity field, which does not spread to the rest of the field but remains for a short time as a local disturbance. Some of the instabilities observed might have been initiated by these local disturbances. However, the overall frequency spectrum does not seem to be correlated with the frequency of rezoning.

As was mentioned above the quasi-second order upwind (QSOU) scheme was used for the convective terms, and central differencing for the diffusion terms. Normally the central differencing (CD) scheme should be used for the momentum equations. However, CD is usually an unstable scheme when used for convection. The stability can

be secured by adding some diffusion, via either SGS model or artificially. Therefore, prediction of turbulent fluctuations via the QSOU scheme, which is strictly monotonic, was preferred at the expense of some loss of formal accuracy near sharp gradients that may be present in the flow field.

The simulations were started at CA 90° BTDC. As an initial condition the radial velocity was taken as zero and the axial velocity varied linearly from piston velocity at the piston face to zero at the cylinder head. The tangential velocity was defined by the Bessel function dependent on engine speed as provided in the code. Moreover, periodic boundary conditions were applied on the front and back face of the wedge, whereas the law of the wall was applied on the walls. Also, in the case the SGS model was applied, an initial turbulence intensity of 10% and $L_{SGS} = 0.4$ cm was used, whereas without the SGS model no turbulence quantities were initiated at all.

Time averaging was applied to the calculated data to separate the mean and fluctuating components of the instantaneous velocity, as follows

$$\bar{u}(t) = \frac{1}{\Delta t_{int}} \int\limits_{t-0.5\Delta t_{int}}^{t+0.5\Delta t_{int}} u(t')dt' \tag{6.4}$$

$$u'(t) = u(t) - \bar{u}(t) \tag{6.5}$$

and

$$u_{rms}^2(t) = \frac{1}{\Delta t_{int}} \int\limits_{t-0.5\Delta t_{int}}^{t+0.5\Delta t_{int}} u'(t')u'(t')dt' \tag{6.6}$$

For non-stationary turbulence, as in the case of IC engines, the selection of Δt_{int} is an important step. Here Δt_{int} = 0.75 ms (6.75° CA) was used, but its effect was investigated by also using 1.5 ms (13.5° CA).

6.4   Results and Discussion

To have the proper perspective about results presented in this section it should be noted that, the predictions do not include any turbulence induced by the intake stroke. The residual turbulence generated during the intake stroke is believed to be important (Hessel and Ruthland, 1995) regarding its contribution to the turbulence generated during the compression/expansion stroke. Unfortunately, this could not be included in the present simulations due to limitations in computational resources.

An example of the complexity of the flow field is shown in Figure 6.1 as predicted with the present model. This figure is indicative of the level of details, that can be captured by the present simulations. The predicted, instantaneous velocity components at location A (see Fig. 6.2), which is fixed with respect to the bowl, 1.0 mm below the piston face and 10.6 mm from the axis, are depicted along with the time averaged values in Figures 6.3 to 6.5 for the compression-expansion stroke. Here, the two indicated TDC's (Figures 6.3 to 6.5) are repetitions of the compression/expansion stroke.

As it was expected, the fluctuations in the tangential direction are much smaller compared to the other two directions. This is a direct consequence of the pseudo two-dimensional nature of the present calculations with 0.5 deg. angle in the tangential direction. Both the large scale time variation of the velocity components induced by the

88

piston motion, as well as the random "turbulent" fluctuations are captured. Figures 6.6 to 6.8 show these random velocity fluctuations as a function of the crank angle. It is seen that the turbulence intensity is somewhat reduced during the second compression/expansion stroke; however, it persists at a considerable level indicating that the numerical diffusion in the code is sufficiently small not to damp the turbulent dynamics of the flow. Whether these fluctuations will continue to persist over several cycles remains to be seen. Although it can not be seen in Figures 6.3 to 6.5, there are small fluctuations in the tangential direction, especially near the TDC.

Figure 6.3 Instantaneous radial velocity at point A (without SGS model) : pseudo
2-D calculations

Figure 6.4 Instantaneous axial velocity at point A (without SGS model) : pseudo

2-D calculations

Figure 6.5 Instantaneous tangential velocity at point A (without SGS model):

pseudo 2-D calculations

Figures 6.6 to 6.11 indicate that there are significant changes occurring near the TDC both in the magnitude and frequency of the velocity fluctuations. It is premature at this stage to make a conclusion as to whether the fluctuations increase or decrease as TDC is approached. As is shown in Figures 6.9 to 6.14 the time averaging interval, as well as the time step used for the numerical simulation has significant influence on the intensity of the fluctuations.

The predicted "turbulent" fluctuations are anisotropic (Figs. 6.12 to 6.14) even very near the TDC. The magnitudes of the fluctuations are in the range 0.5-1.0 m/sec in radial, 1.0-2.0 m/sec in the axial and 0.5-1.5 m/sec in the tangential directions, respectively. For a similar engine configuration, Catania and Spessa (1996) measured velocity fluctuations in the order of 10 m/s for the cycle-resolved turbulence intensities, and about 5m/s for the RMS fluctuations of the in-cycle mean velocity. According to Catania (1998), the present computations should be compared to their cycle-resolved turbulence intensities. In another experimental study Auriemma et al., (1998) reported measured RMS velocity fluctuations during the compression/expansion stroke of a motored engine at 1500 RPM. These indicated maximum values of 2 m/s for the radial and 3.5 m/s for the tangential directions respectively. The measured values included both cycle-to-cycle fluctuations and in-cycle fluctuations. Valentino et al., (1998) presented a method to reduce the effect of cycle-to-cycle variations of mean motion on turbulence. Their results seem to indicate that the cycle-resolved turbulence can be augmented by as much as 30% due to cycle-to-cycle-variations. In any case, the experimental data indicate that the predicted turbulence intensities are much lower compared to those measured,

although direct comparison is not possible at this stage. This may be mainly due to the fact that the large-scale turbulence generated during the intake stroke was not included.

It should be pointed out that the predicted "turbulent" fluctuations are significantly affected by the time step (Figure 6.12). The smaller the time steps, the better is the resolution of turbulence scale, and the higher is the turbulent RMS intensities. Figure 6.13 shows the influence of SGS turbulence model, which essentially has a damping effect. At this grid resolution, which is relatively coarse for LES simulations it is believed that the results without the SGS model should be better than the ones with a SGS model.
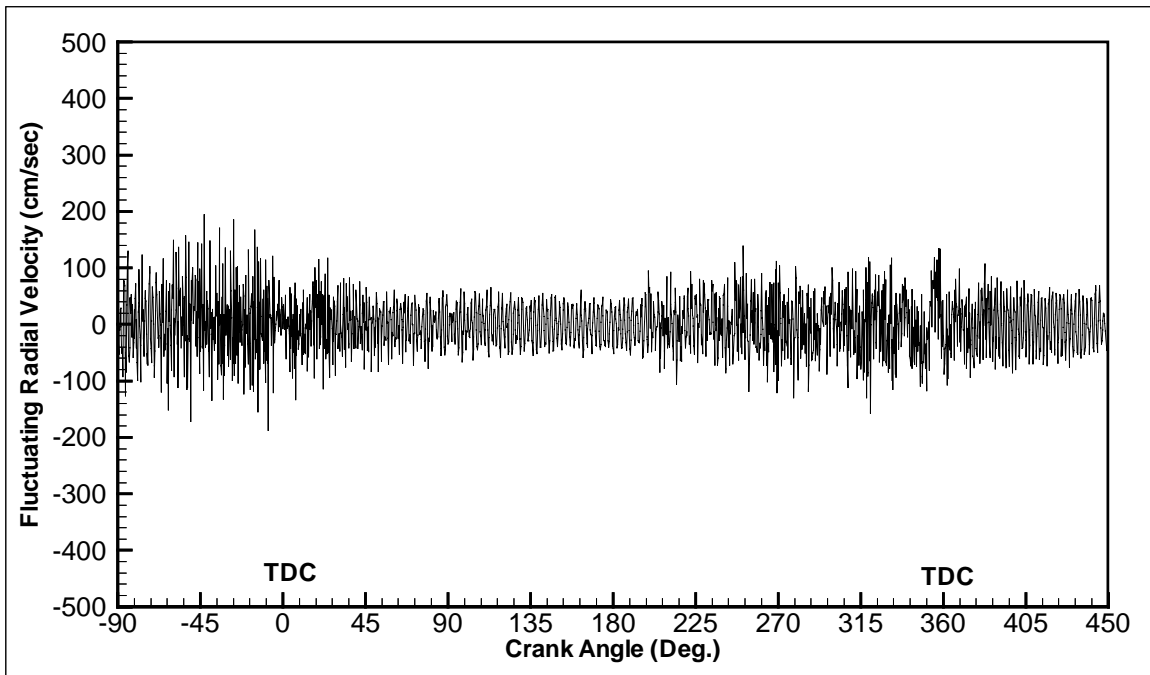
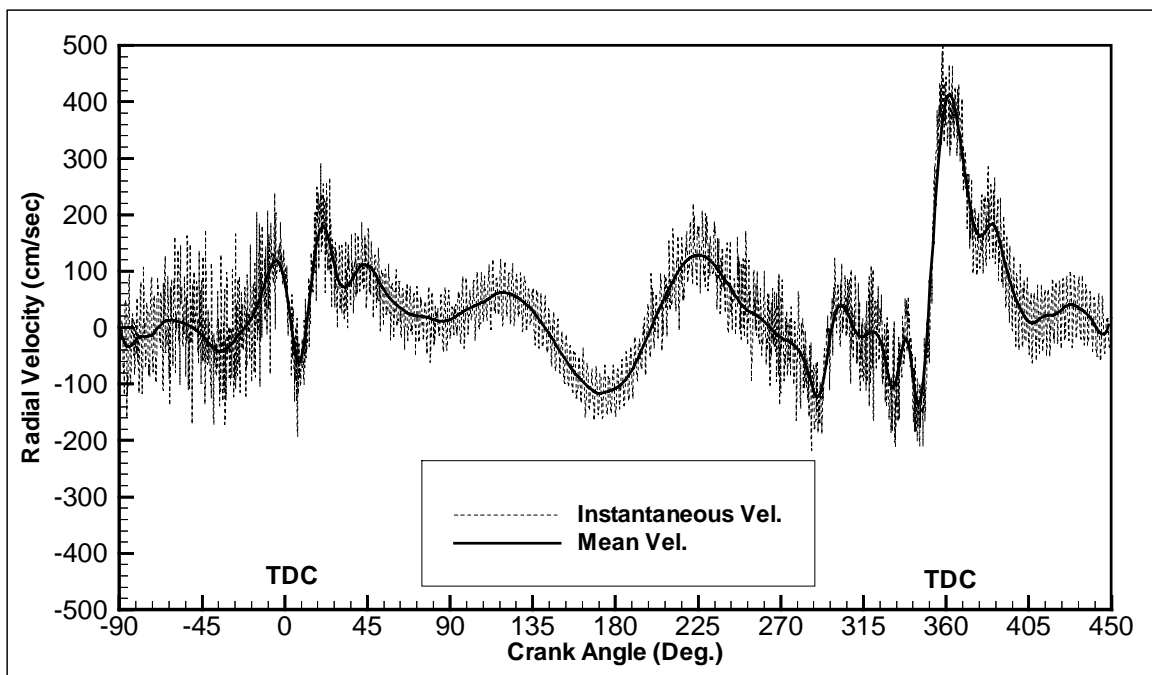Figure 6.6 Instantaneous fluctuating radial velocity at point A (without SGS model): pseudo 2-D calculations
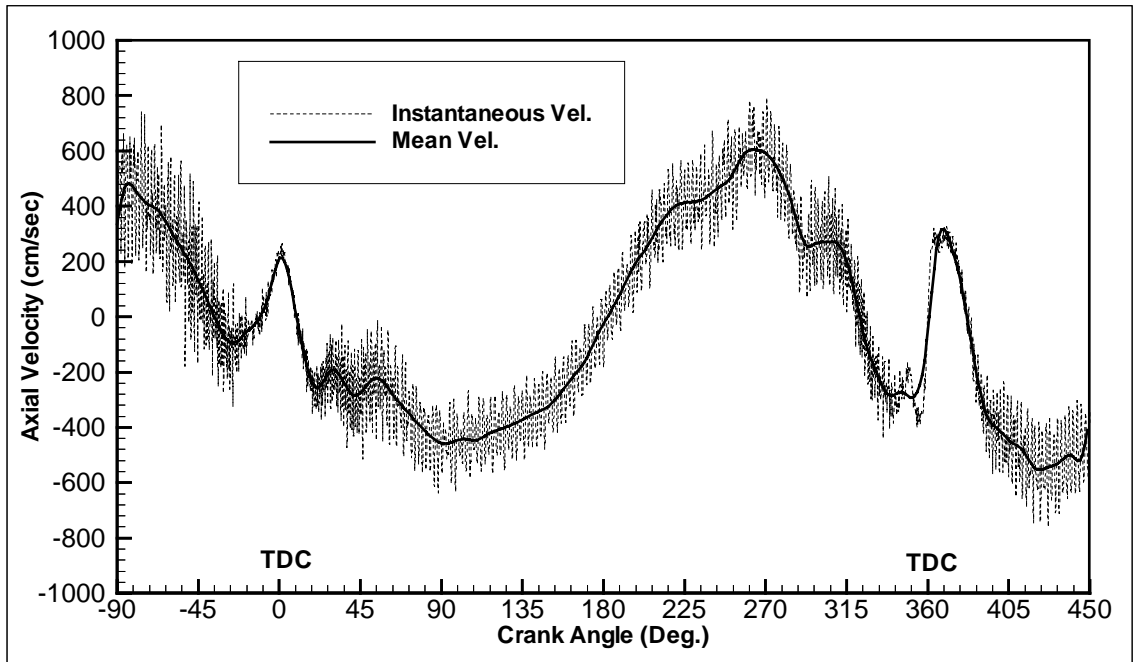
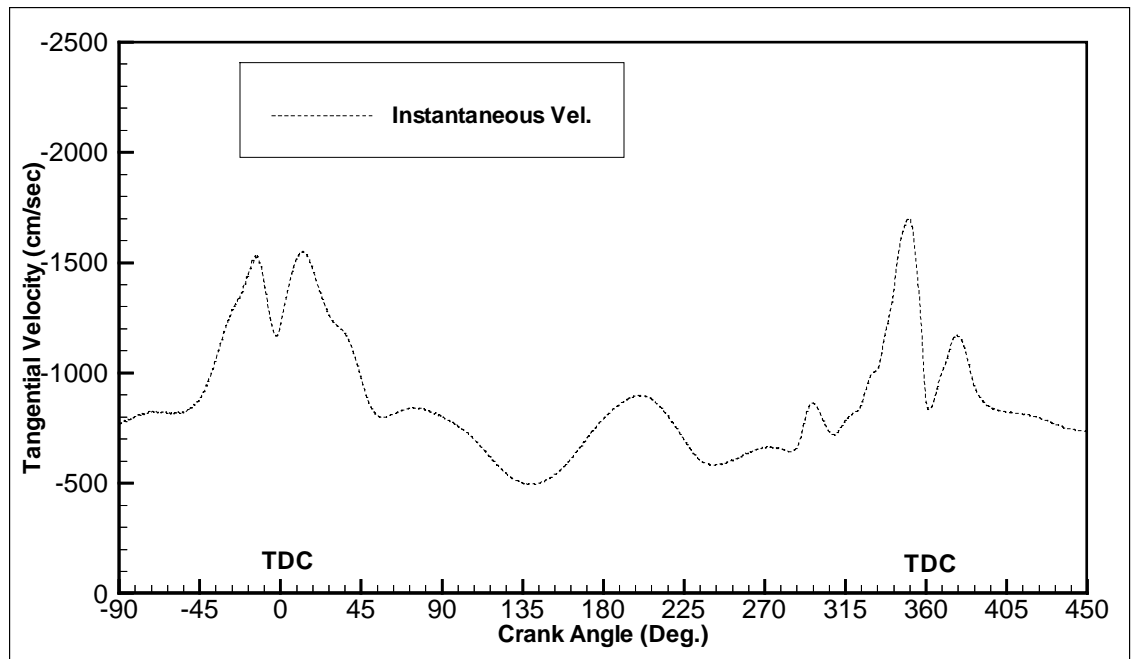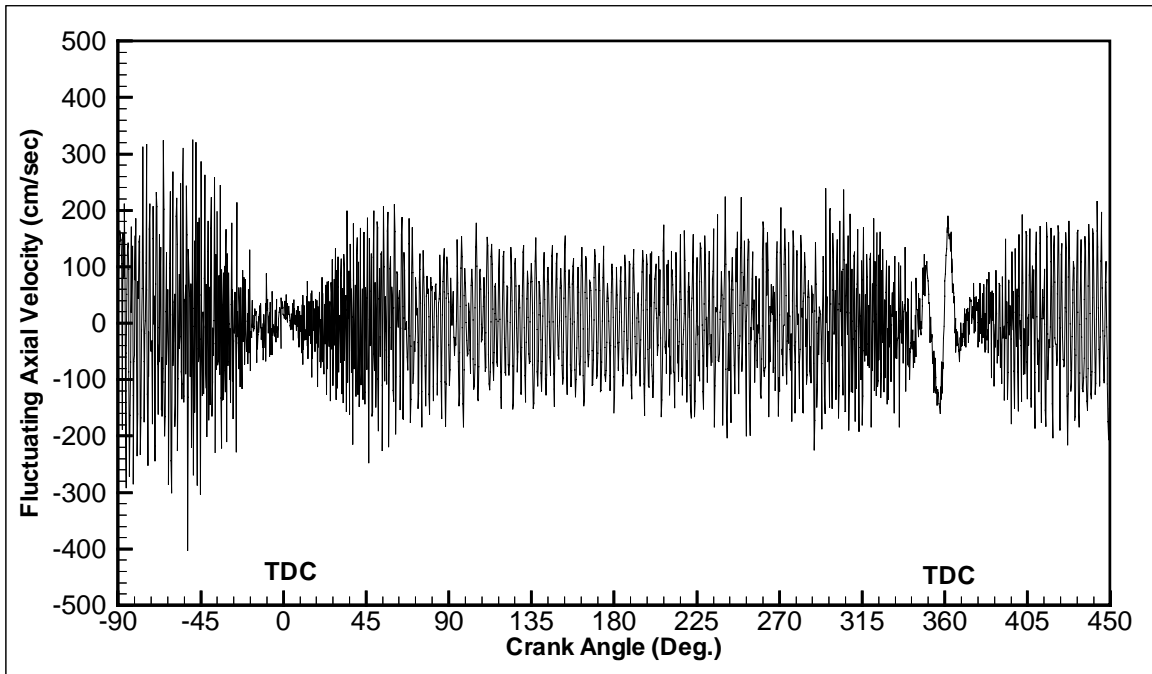Figure 6.7 Instantaneous fluctuating axial velocity at point A (without SGS model): pseudo 2-D calculations
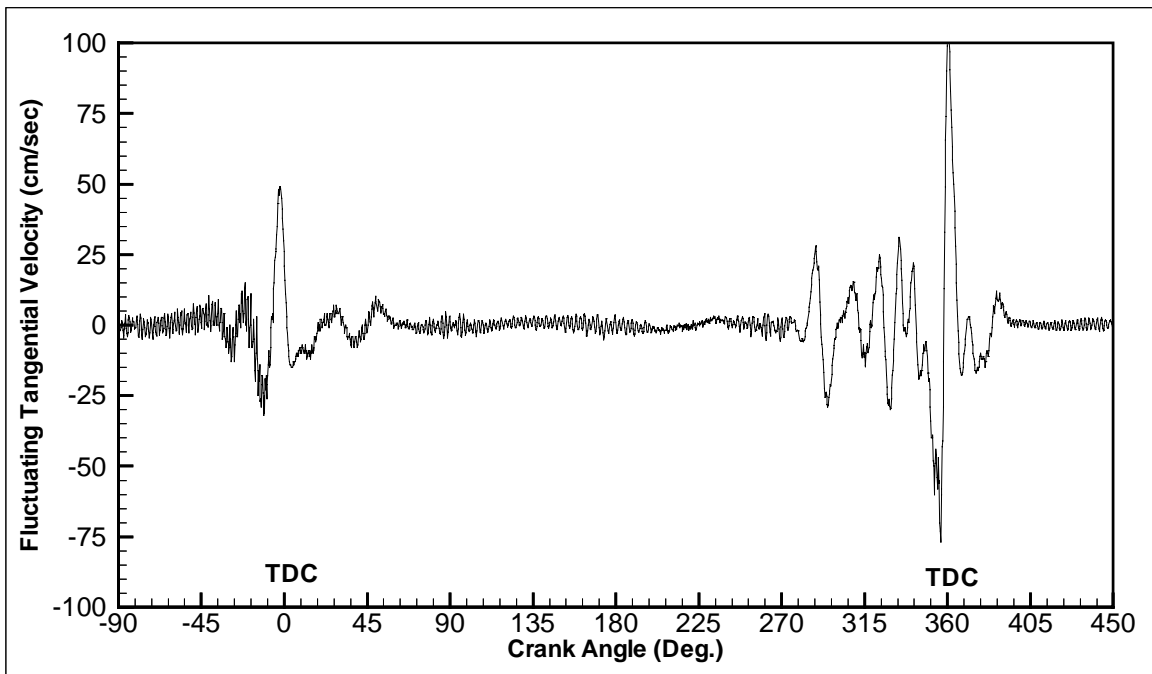
Figure 6.8 Instantaneous fluctuating tangential velocity at point A (without SGS model): pseudo 2-D calculations
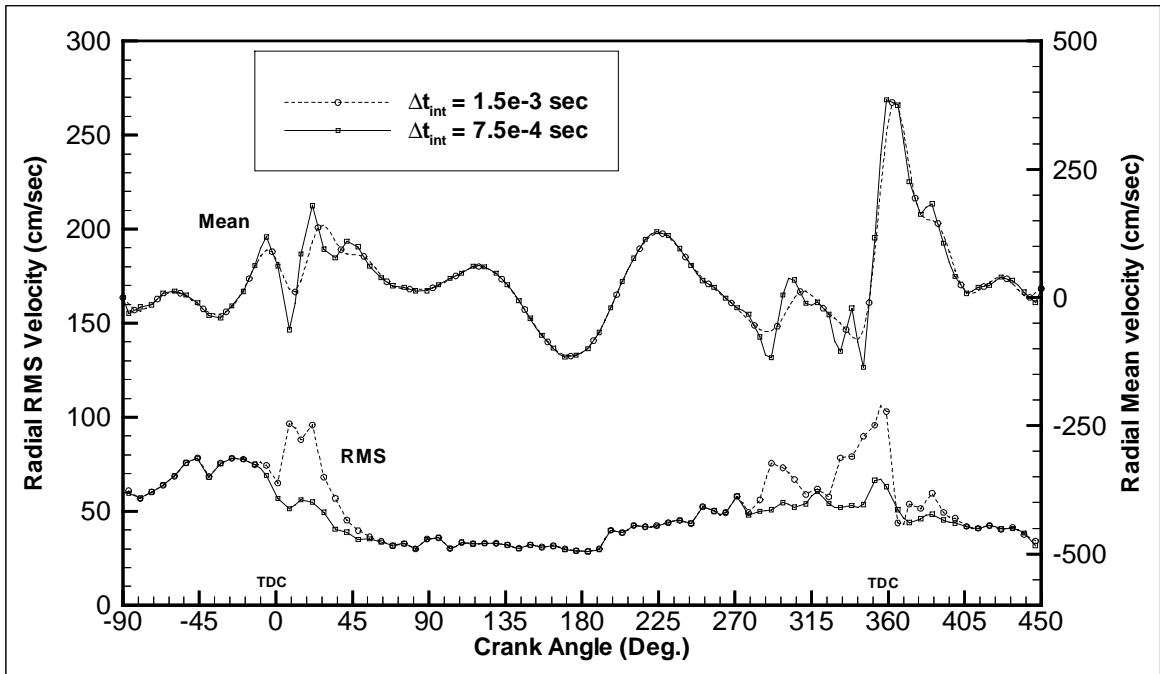
Figure 6.9 Influence of time averaging interval on radial velocity quantities:

pseudo 2-D calculations
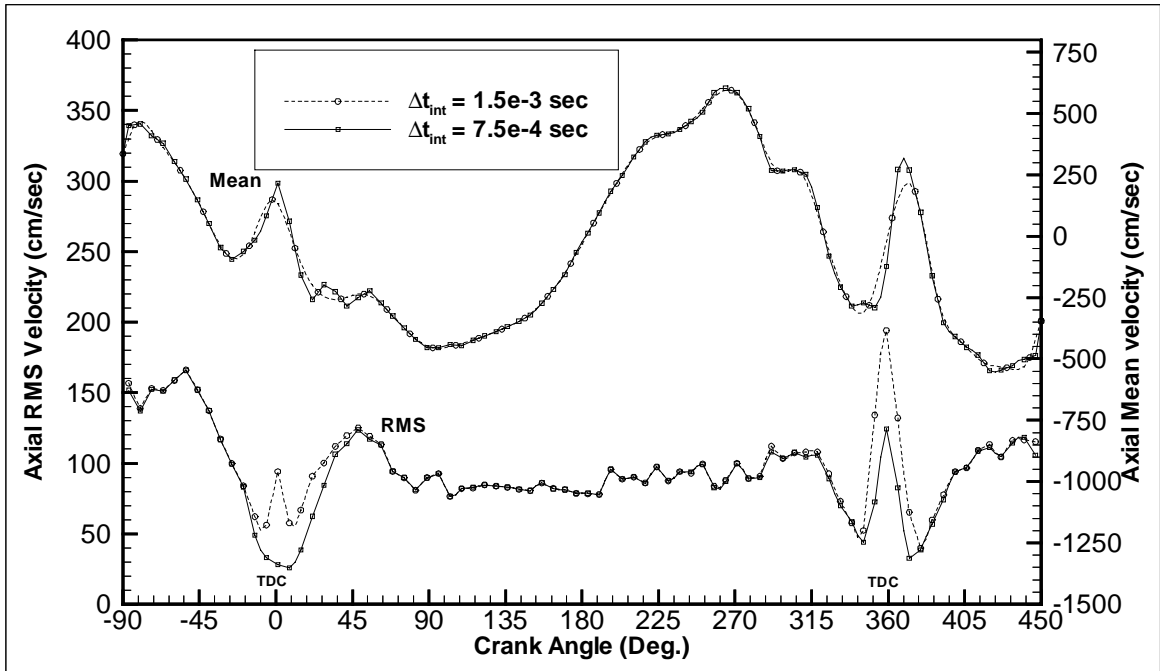
Figure 6.10 Influence of time averaging interval on axial velocity quantities:

pseudo 2-D calculations

94
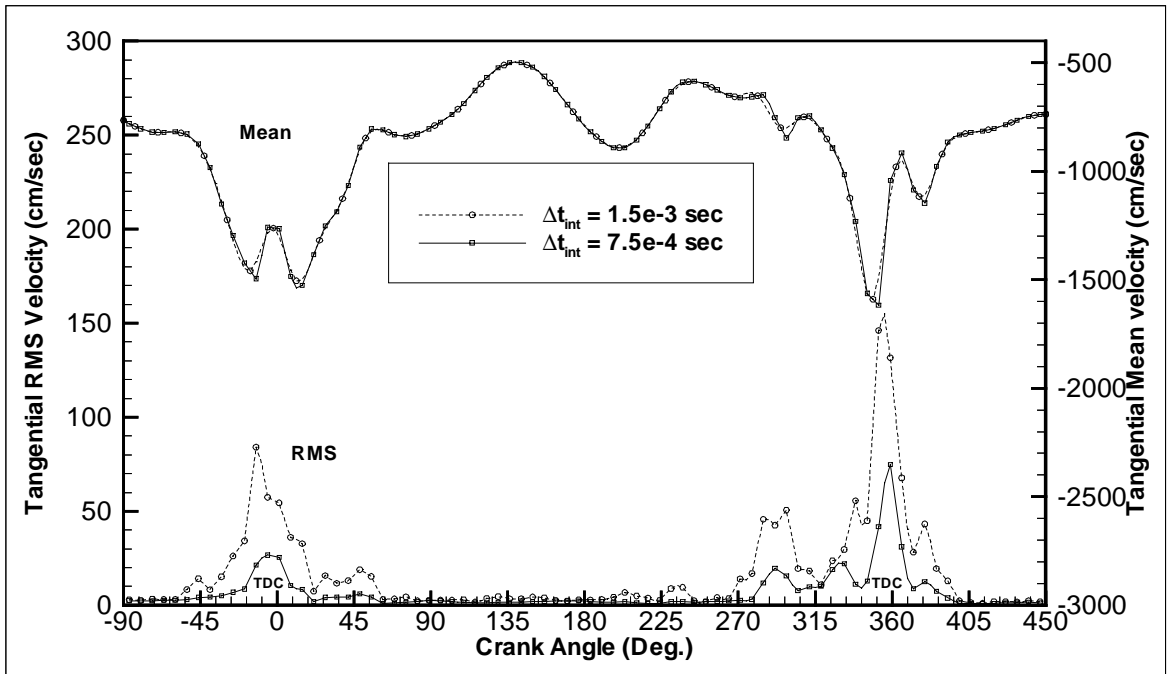
Figure 6.11 Influence of time averaging interval on tangential velocity quantities:

pseudo 2-D calculations
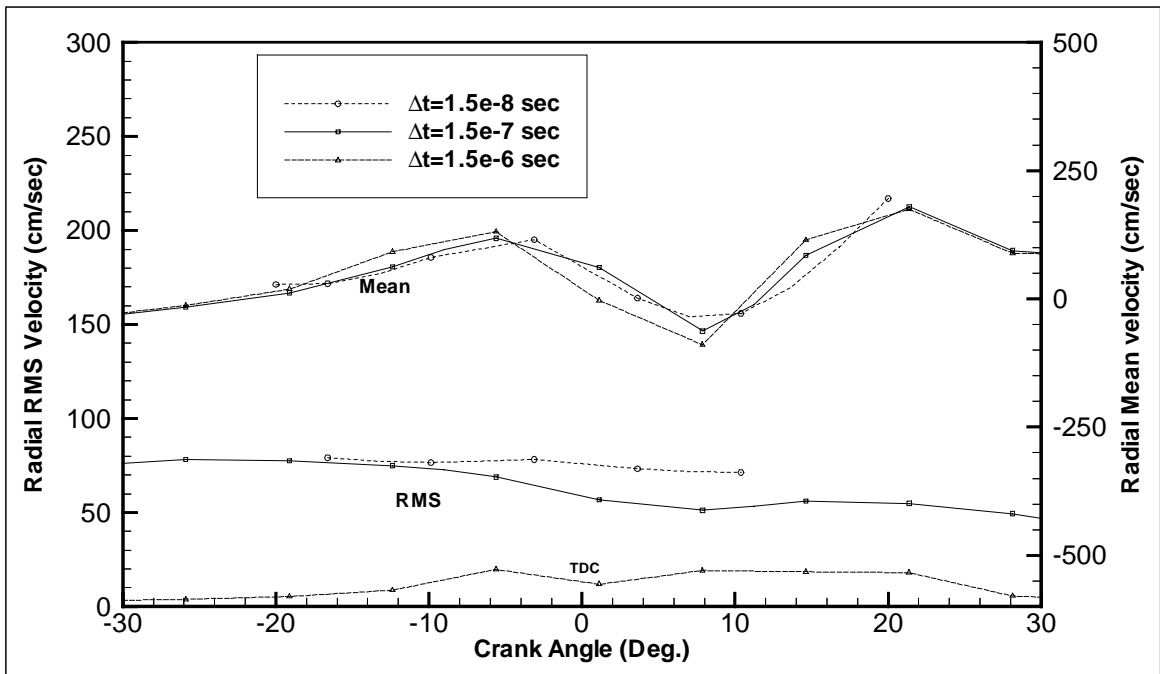
Figure 6.12 Influence of timestep on radial velocity quantities: pseudo 2-D
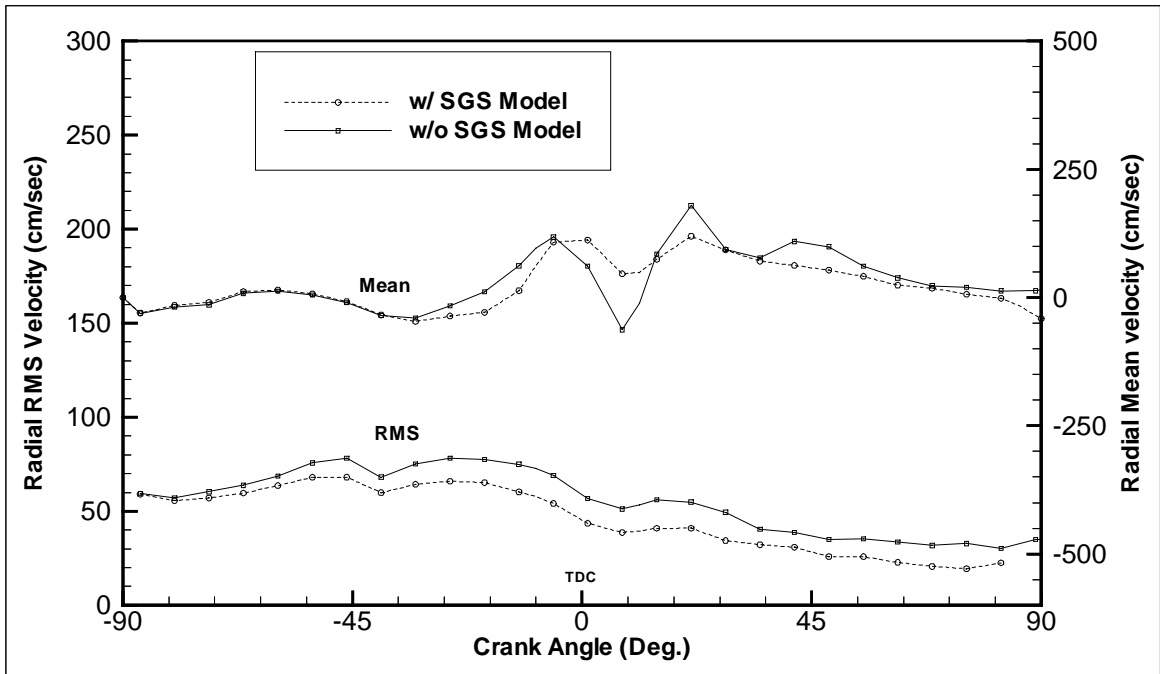
calculations

Figure 6.13 Influence of SGS model on radial velocity quantities: pseudo 2-D
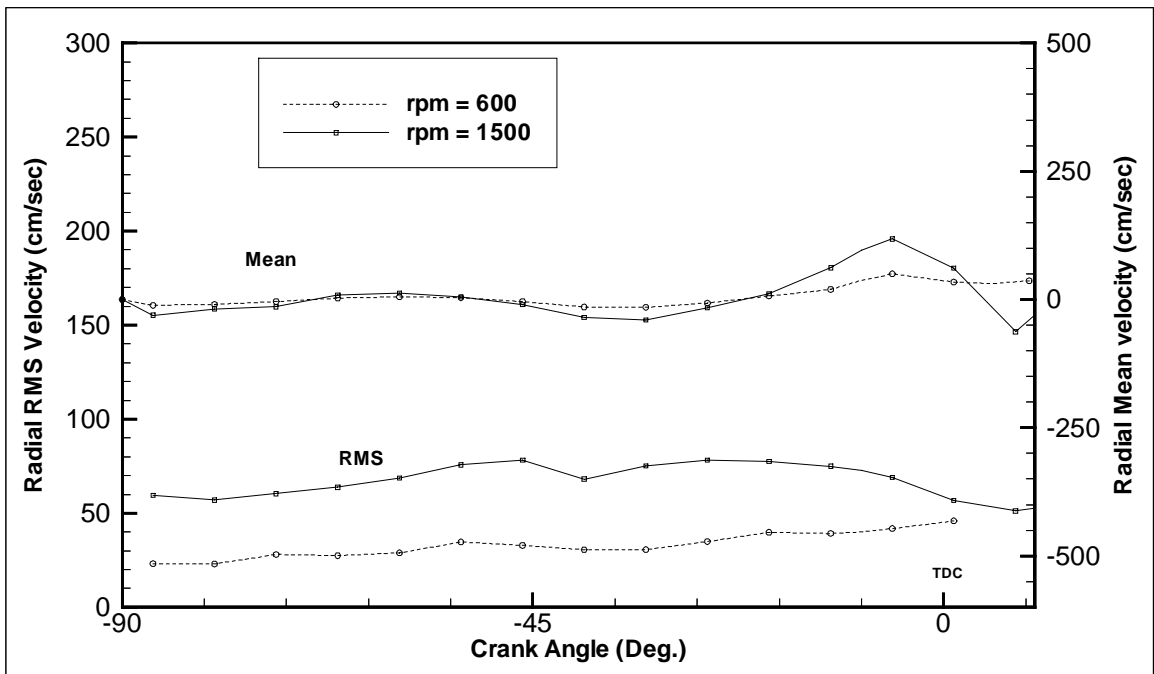
calculations

Figure 6.14 Influence of engine speed on radial velocity quantities: pseudo 2-D

calculations

a)

b)
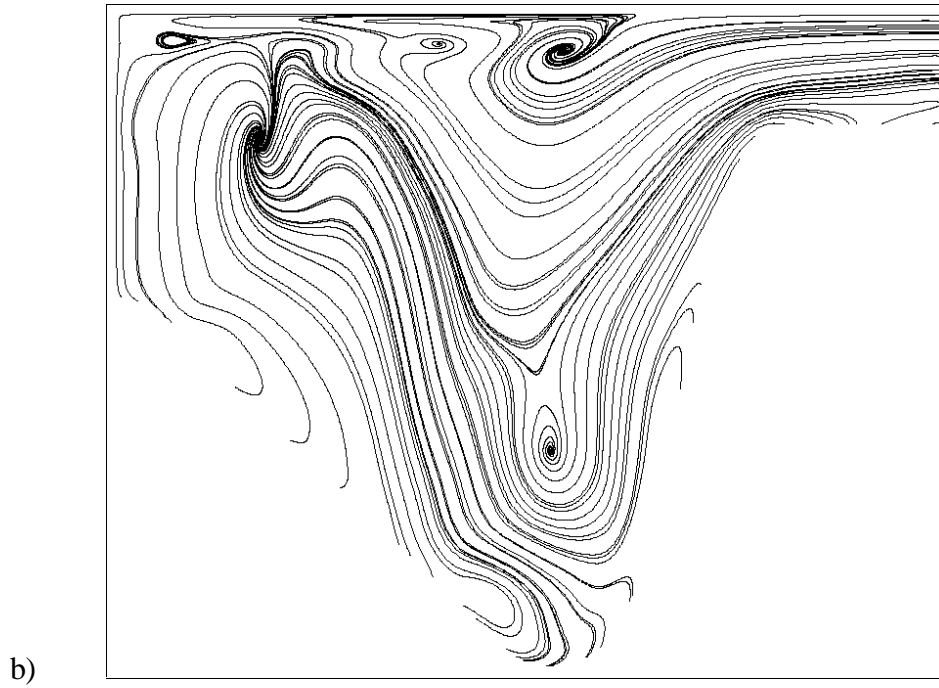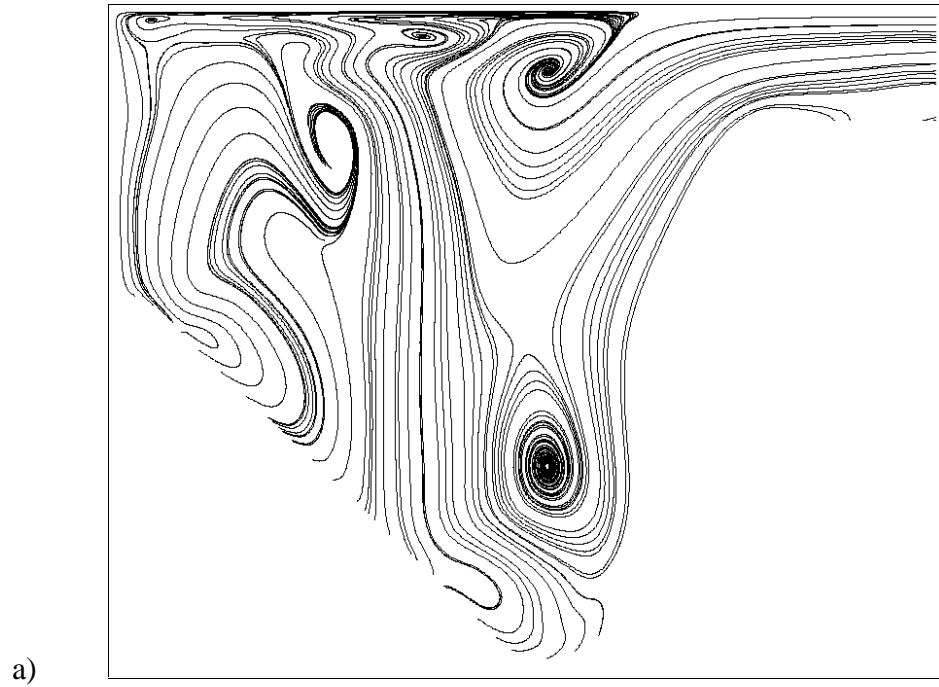
Figure 6.15 Streamlines to show the influence of three-dimesionality on the flow

field at CA 18° ATDC at a) 0° and b) 90° wedge angles

In Figure 6.14, the influence of engine speed is depicted. There is a significant increase in predicted turbulent intensity with increasing engine speed as has been observed in experiments (see e.g., Corcione and Valentino, 1994; Catania and Spessa, 1996).

The 3-D, 180° wedge calculations with 130000 vertices did not show any significant change in the predicted RMS fluctuations. This could be due to the stabilizing effect of the arbitrarily imposed swirl velocity profile in addition to the coarse grid used in the tangential direction. However, investigating streamlines on two perpendicular planes of the 3-D geometry (Figs. 6.15a and 6.15b), revealed some expected 3-D effects.

6.5   Conclusions

Three dimensional, and pseudo-two dimensional (i.e., a small wedge angle), time accurate calculations have been performed to predict the flow field inside a typical diesel engine piston-bowl assembly. The first stage of these calculations is for motored conditions at 600 and 1500 RPM, spanning only the compression and expansion strokes. The objective was to capture the flow instabilities, and maybe turbulence induced by the bowl geometry alone, i.e. without the influence of residual turbulence generated during the intake stroke. It was shown that this was possible by using the KIVA-3 code with a fine grid resolution and relatively small time steps. The bowl induced "turbulence" appears to be persistent over a few cycles without recharging induced by the intake stroke. The small scale flow instabilities and unsteadiness observed in the computer simulations seem to be the results of unsteady flow separation that occurs at the sharp corner of the piston bowl and the flat piston head. This is in accordance with the

combustion improvements that are observed experimentally when re-entrant type bowl geometry is used. The magnitude of the calculated RMS velocity fluctuations seem to be much lower than measured ones under similar geometry and operating conditions. However, the calculations do not include the significant contribution that arises from the turbulence generated during the intake stroke, nor do they include the significant cycle-to-cycle variations. Although the grid resolution used in the present study may be considered as coarse for LES, this study is unique in that, for the first time (to the best of knowledge gained from the literature in the public domain) it was demonstrated that there is a potential to predict in-cylinder turbulence for IC engines using large eddy simulations with relatively modest computational resources at the workstation level.

Chapter 7

A NEW APPROACH IN SMAGORINSKY-BASED EDDY VISCOSITY MODELING

7.1   Introduction

The previously developed SEV (Smagorinsky based eddy viscosity) model presented in Chapter 5 has been improved and implemented in the KIVA-3 code together with a wall damping function, (e.g. van Driest) and tested against experimental benchmarks. Results are compared with the standard k-ε model and the basic Smagorinsky model, which was implemented in KIVA-3 during this study. In addition, a smooth transition from RANS calculations to LES or vice versa is established so that for coarse grids RANS, for sufficiently small grids LES and eventually DNS can be obtained in the limit of very fine grid size, i.e. in the order of Kolmogorov scales.

7.2   Formulation

Following the suggestion by Speziale (1998), a computational procedure is formulated such that the sub-grid scale (SGS) turbulence model utilized in large eddy simulations (LES) is consistent with the RANS (Reynolds Averaged Navier-Stokes)

simulations in the limit of coarse grid mesh. The need for a universal turbulence model that transitions continuously from RANS to LES as the grid is refined led to the following formulation. The compressible subgrid scale stresses are written as follows

$$-\overline{u_i' u_j'} = \nu_t \left(2\overline{S}_{ij} - \frac{2}{3} \nabla \cdot u \delta_{ij} \right) - \frac{2}{3} k \delta_{ij} = \nu_t \left(\frac{\partial \overline{U}_i}{\partial x_j} + \frac{\partial \overline{U}_j}{\partial x_i} - \frac{2}{3} \nabla \cdot U \delta_{ij} \right) - \frac{2}{3} k \delta_{ij} \quad (7.1)$$

This equation satisfies the identity

$$-\overline{u_i' u_i'} = 2\nu_t \left(\frac{\partial \overline{U}_i}{\partial x_i} - \nabla \cdot U \right) - \frac{2}{3} k \delta_{ij} = 0 - 2k \quad (7.2)$$

The eddy viscosity in the Smagorinsky model is usually defined as

$$\nu_t^{(LES)} = C_s \Delta^2 \left(\overline{S}_{ij} \overline{S}_{ij} \right)^{\frac{1}{2}} \quad (7.3)$$

An equivalent RANS model can be formulated as

$$\nu_t^R = C_R \, \ell_{ch}^2 \left(\overline{S}_{ij} \overline{S}_{ij} \right)^{\frac{1}{2}} \quad (7.4)$$

where the characteristic length scale, ℓ_{ch} can be obtained for IC-engine flows from Eqn. (7.5). Here, κ, γ_1, and γ_2 are model constants, y_w is the wall distance, ℓ_c the clearance height and B is the bore diameter. An application of this model has been presented by Yavuz and Celik (1999), where they suggested that

$$\ell_{ch} = \min \left(\kappa y_w, \gamma_1 \ell_c, \gamma_2 \frac{B}{2} \right) \quad (7.5)$$

The following model is proposed to provide a continuous transitioning from LES to RANS.

$$\nu_t = \left(1 - e^{-\alpha^2 \Delta^2 / \ell_k^2}\right) \nu_t^R \qquad (7.6)$$

This equation ensures that as the filter width Δ ($\sim$ grid size) gets close to Kolmogorov scale ℓ_k $\nu_t \to \nu_t^R$. To find a value for α in the LES range, the truncated Taylor series is utilized as

$$e^{-x^2} = 1 - x^2 + \frac{x^4}{2!} - \dots \qquad (7.7)$$

upon which the following approximation is obtained for small $x = \alpha \Delta / \ell_k$

$$\left(1 - e^{-\alpha^2 \Delta^2 / \ell_k^2}\right) \cong \alpha^2 \Delta^2 / \ell_k^2 \qquad (7.8)$$

Using this approximation, Equation 7.6 can be written as

$$\nu_t = \alpha^2 \Delta^2 / \ell_k^2 \, C_R \ell_{ch}^2 \left(\overline{S}_{ij} \overline{S}_{ij}\right)^{1/2} \qquad (7.9)$$

Comparing this equation to the Smagorinsky model (Eqn. 7.3) gives a dynamically changing Smagorinsky constant C_s,

$$\frac{\alpha^2 C_R \ell_{ch}^2}{\ell_k^2} \approx C_s \qquad (7.10)$$

If the RANS model constant C_R is approximated as having an order of magnitude one and assuming that $\ell_{ch} \cong 100 \, \ell_k$ holds for IC-engine flows, it follows that

$$\alpha^2 = 10^{-4} C_s = 2 \cdot 10^{-5} \qquad (7.11)$$

where a typical value of $C_s = 0.2$ is utilized for the Smagorinsky constant.

$$F = 1 - e^{-\alpha \, (\Delta / l_k)^2}$$
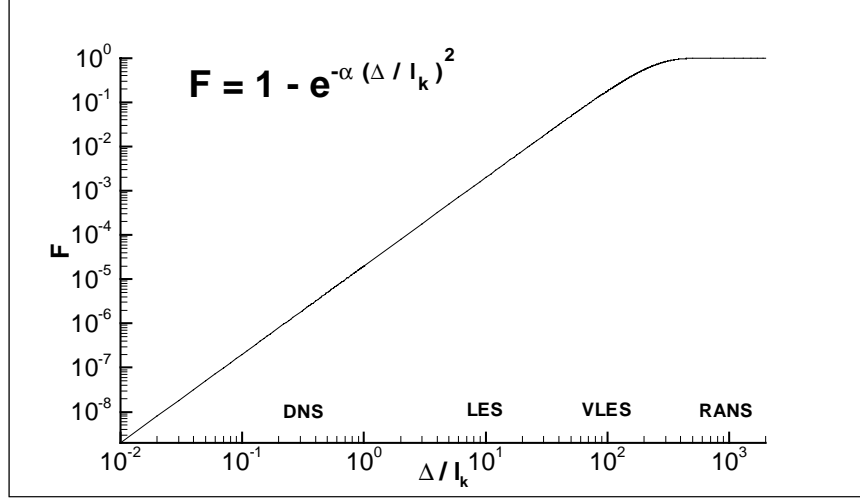
Figure 7.1 Variation of F with Δ / l_k

The function $F = 1 - e^{-\alpha^2 \Delta^2 / \ell_k^2}$ is depicted in Figure 7.1 using Δ/ℓ_k as the independent variable. It is seen that, in the limit as $\Delta/\ell_k \to 0$ $F \to 0$ all relevant scales are resolved, i.e. DNS; as $\Delta/\ell_k \to \infty$ $F \to 1$ the mesh becomes coarse, which leads to a RANS, i.e., $\nu_t = \nu_t^R$. In between one has LES or VLES (very large eddy simulation, that is, a significant portion of the turbulent kinetic energy is not resolved). In the range $\Delta/\ell_k \cong 10$ this model reduces to the Smagorinsky model with $F = 2 \cdot 10^{-3}$, $C_R = 1$, and $\ell_{ch}/\Delta \cong 10$ Equation 7.6 yields

$$\nu_t = \left(1 - e^{-\alpha^2 \Delta^2 / \ell_k^2}\right) C_R \frac{\ell_{ch}^2}{\Delta^2} \Delta^2 \left(\overline{S}_{ij} \overline{S}_{ij}\right)^{1/2} = 0.2 \Delta^2 \left(\overline{S}_{ij} \overline{S}_{ij}\right)^{1/2} \tag{7.12}$$

If C_s and C_R are tuned for specific problems (e.g. wall layers), α has to be changed according to Equation 7.10. One more advantage of this model is that C_s will go to zero, as ℓ_{ch} will go to zero while approaching the wall. However, this model is still

103

isotropic, and if anisotropy has to be taken into account, a better alternative would be to apply a non-linear eddy viscosity model.

Furthermore, Equation 7.6 is modified to account for the dependency of engine turbulence on piston speed as follows

$$\nu_t = \left(1 - e^{-y_w^{+2}\big/C_w}\right)\left(1 - e^{-C_1\left(C_2\left(\frac{|v_p|}{V_p}\right)^2 + C_3\left(\frac{\nu_t^R}{\nu}\right)^{0.5}\right)}\right)\left(1 - e^{-\alpha^2\Delta^2\big/\ell_k^2}\right)\nu_t^R \tag{7.13}$$

where C_w is a wall damping coefficient to imply an exponential decrease of ν_t instead of a linear decrease implied by ν_t^R. In the second exponential term C_1, C_2 and C_3 are model parameters and V_p and v_p are the mean speed and instantaneous piston speed, respectively. The term with C_2 is a low (turbulence) Reynolds number correction. In this study, $C_1 = 5.0$, $C_2 = 0.1$ and $C_3 = 0.03$ were found to provide a good combination to improve IC-engine flow predictions. Strictly speaking, there are only two model constants to include the low Reynolds number effect (ν_t^R/ν) and the effect of piston speed (v_p/V_p); these are $C_2^* = C_1 C_2 = 0.5$, $C_3^* = C_1 C_3 = 0.15$.

7.3   Applications

The same case as in Chapter 6, an isothermal, incompressible flow within a piston-cylinder arrangement (Morse et al., 1979; Haworth, 1998) motored without compression at 200 RPM is investigated. The mean piston speed V_p was 40 cm/sec in these calculations. There was no swirl imposed. The computational meshes used in the 2-D axisymmetric simulations are shown in Figure 7.2. The seat angle was 60° with the

horizontal axis. A time step of 1×10^{-6} seconds was used for time marching. Numerical meshes of 2,700 and 40,000 vertices were employed with a wedge angle of 0.5 degrees in the circumferential direction. The maximum cell size was 1.6x3.0 mm for the coarse grid calculations and 0.3x0.9 mm for the fine grid calculations in the radial and axial directions, respectively. The inlet pressure was atmospheric and the initial flow was at rest until the piston started to move away from TDC (0° CA). In this study QSOU scheme was used exclusively.
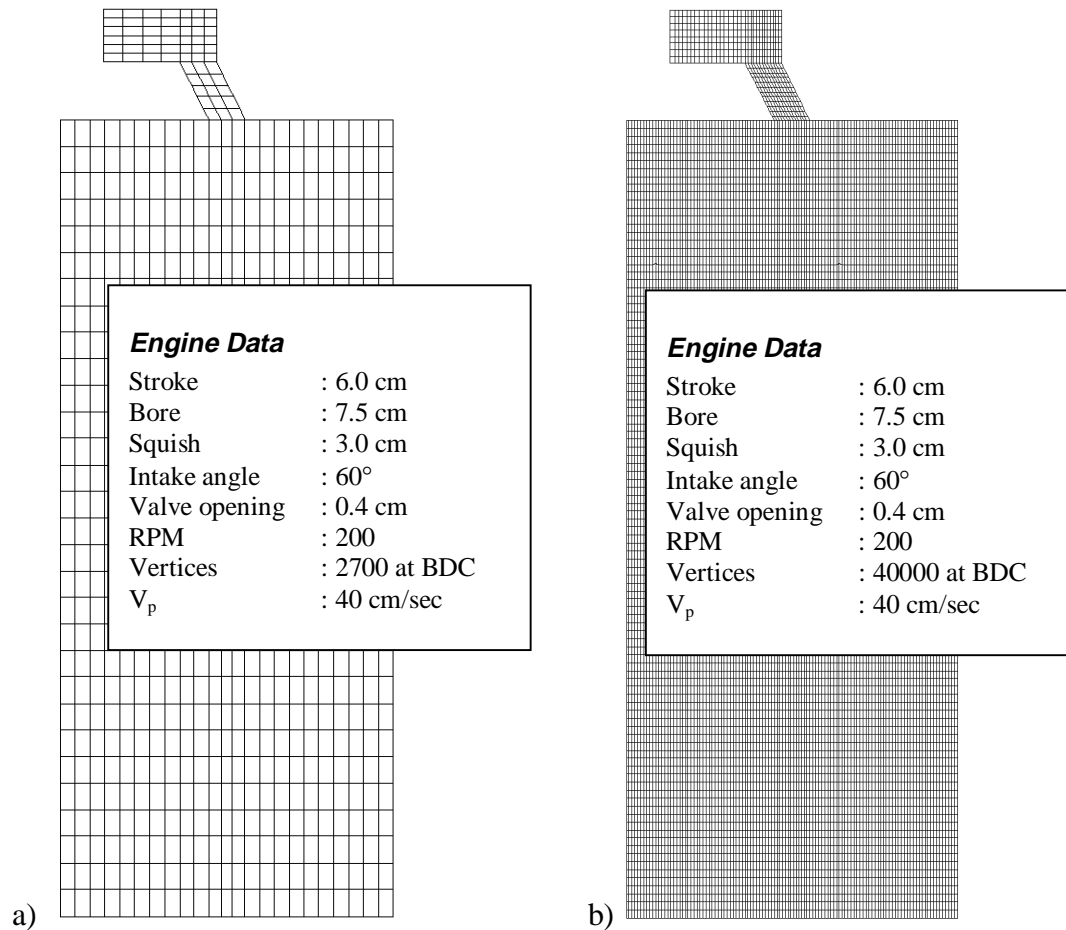
Figure 7.2 Computational mesh and specific engine data (left edge is the symmetry line) for a) RANS simulations, b) pseudo LES simulations

7.4   Results and Discussion

First, the RANS predictions of this simulation are investigated. In Figures 7.3 to
7.5 the axial velocity profiles are compared at various stations inside the cylinder. The
standard k-ε model and the SEV model results are compared to each other and with the
measurements. The SEV model is deviating from the k-ε model predictions in some
regions favorably and in others not so favorably. It should be noted that the SEV model
usually overpredicts the lower recirculation region near the cylinder wall.

In Figures 7.6 to 7.8 the predicted root mean square velocites of each case are
compared to experiments. As seen from these figures the SEV model is almost as good as
the standard k-ε model, except near the wall where it usually underpredicts the calculated
root mean square velocity.
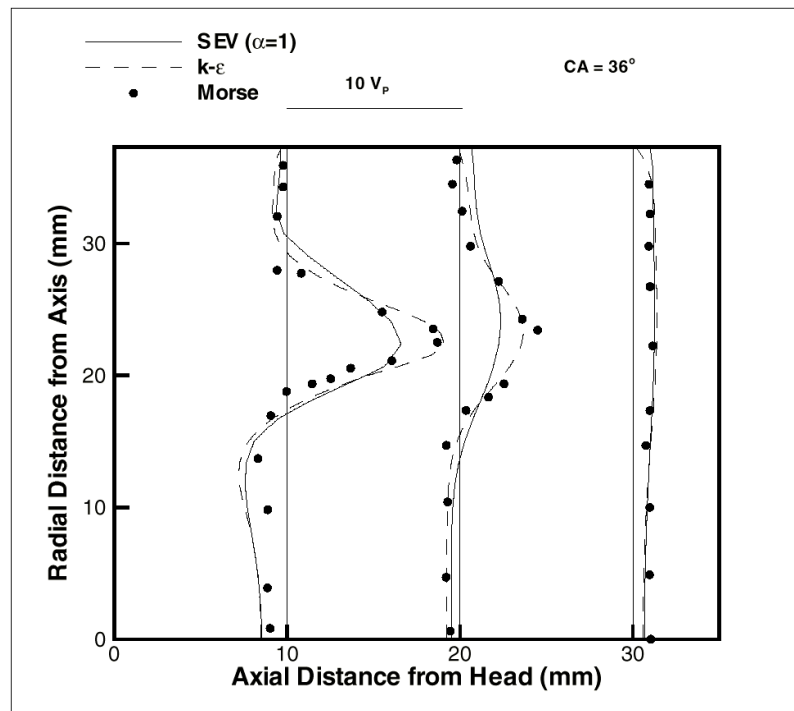
Figure 7.3 Axial velocity profiles at 36° CA ATDC
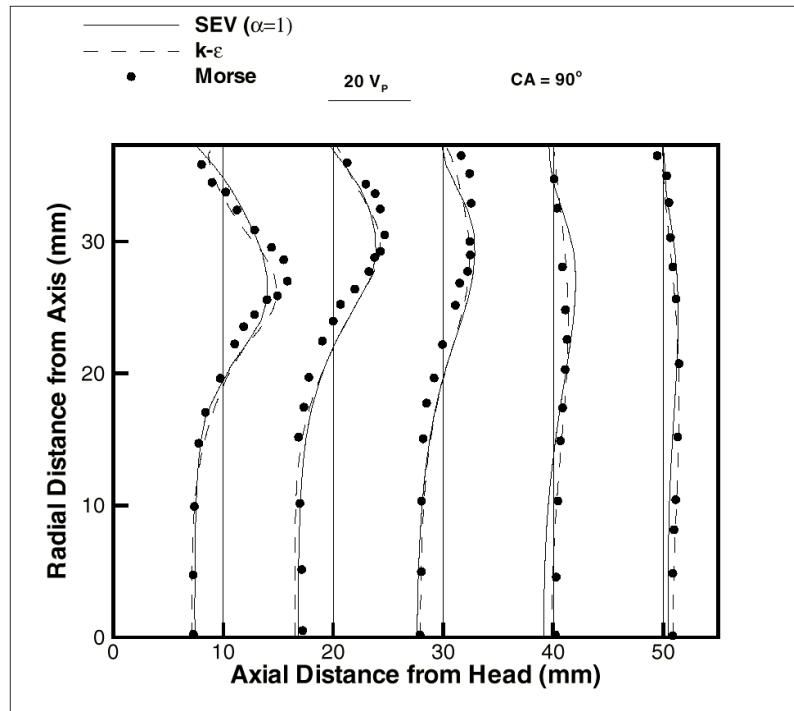
Figure 7.4 Axial velocity profiles at 90° CA ATDC
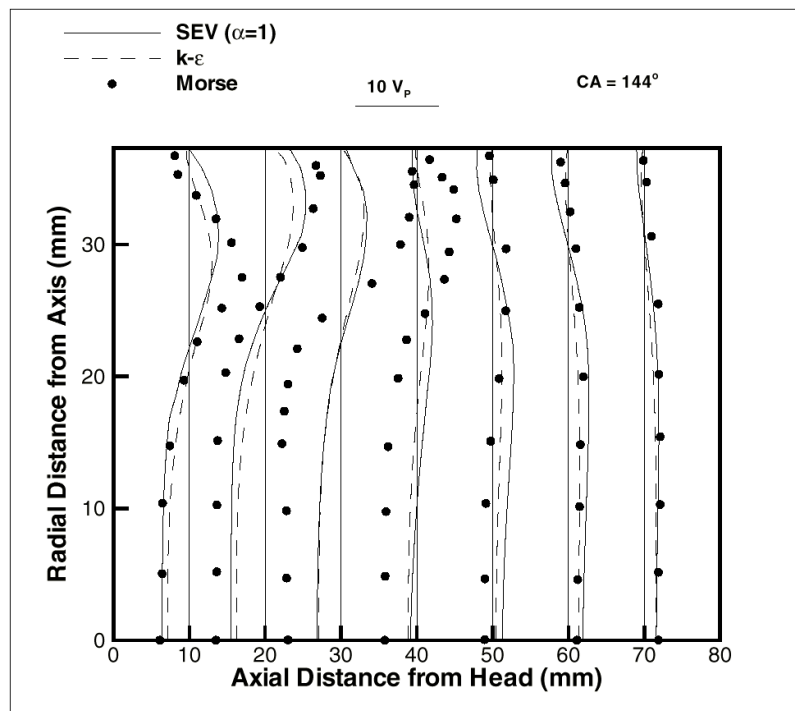
Figure 7.5 Axial velocity profiles for at 144° CA ATDC
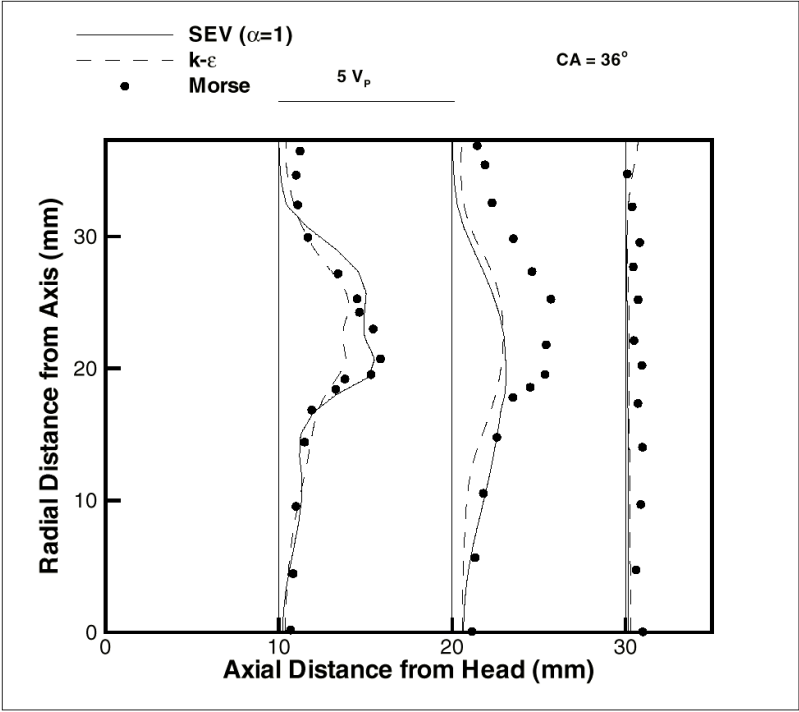
Figure 7.6 u_{rms} profiles at 36° CA ATDC
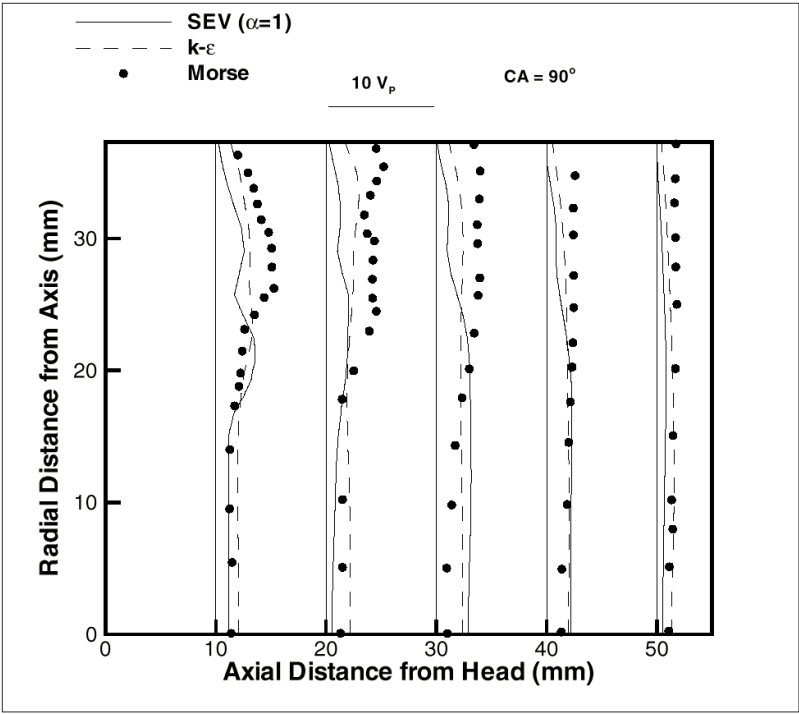
Figure 7.7 u_{rms} profiles at 90° CA ATDC
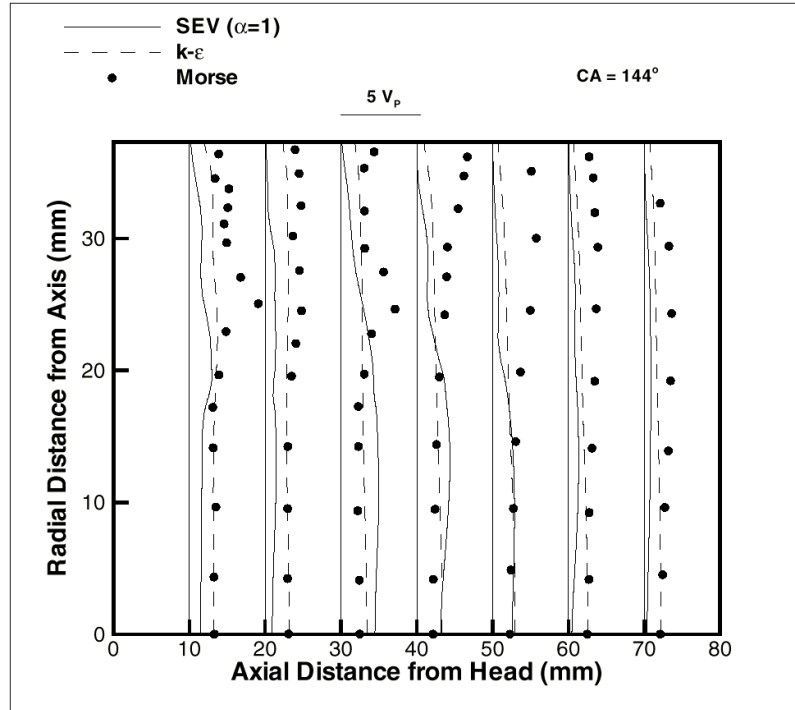
Figure 7.8 u_{rms} profiles at 144° CA ATDC

The streamlines from the intake flow case are shown in Figures 7.9 to 711. Here, again the standard k-ε model and the Smagorinsky based eddy viscosity (SEV) model solutions and the measurements of Morse et al., (1979) are presented. As seen from these figures the results from both models compare well with the measurements in the overall sense. The SEV model predicts slightly different results, especially the size of the recirculation region at the right corner near the piston face at 90° CA and 144° CA is smaller in favor with experiments. However, the lower recirculation region is slightly overpredicted. Given the simplicity of the SEV model, the agreement between predictions and experiments is rather good.
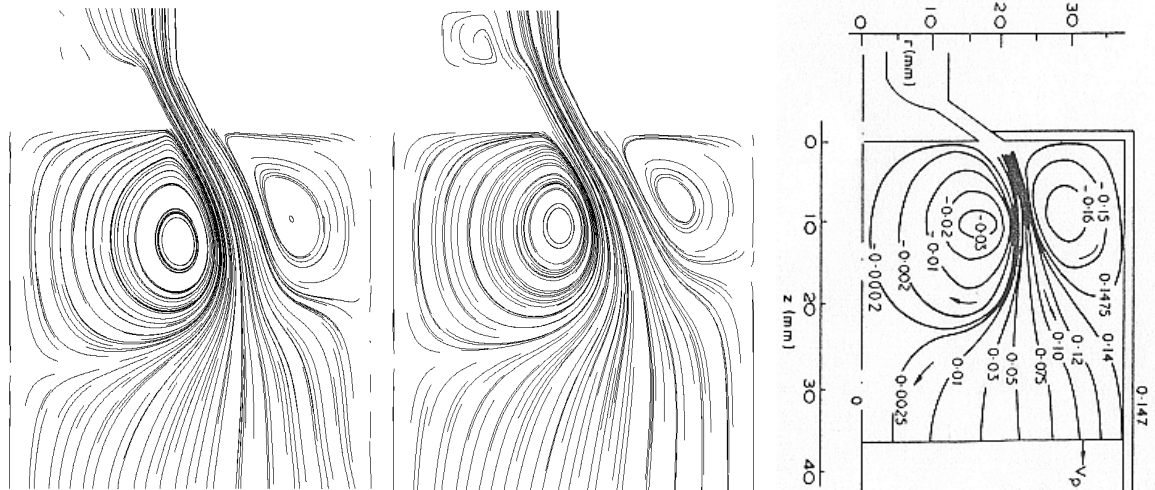
Figure 7.9 Streamlines of predictions of the k-ε model (left) and SEV model

(middle) at 36° CA compared with Morse et al. (1979) (right)
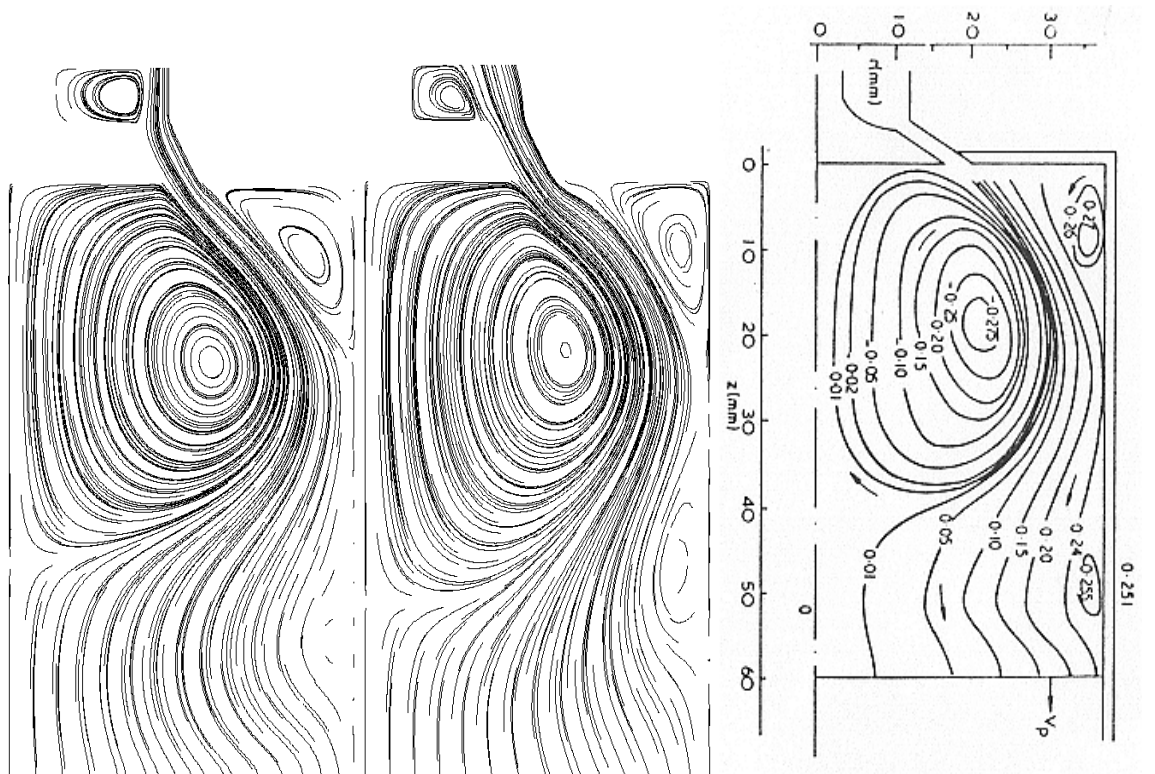
Figure 7.10 Streamlines of predictions of the k-ε model (left) and SEV model

(middle) at 90° CA compared with Morse et al. (1979) (right)

110
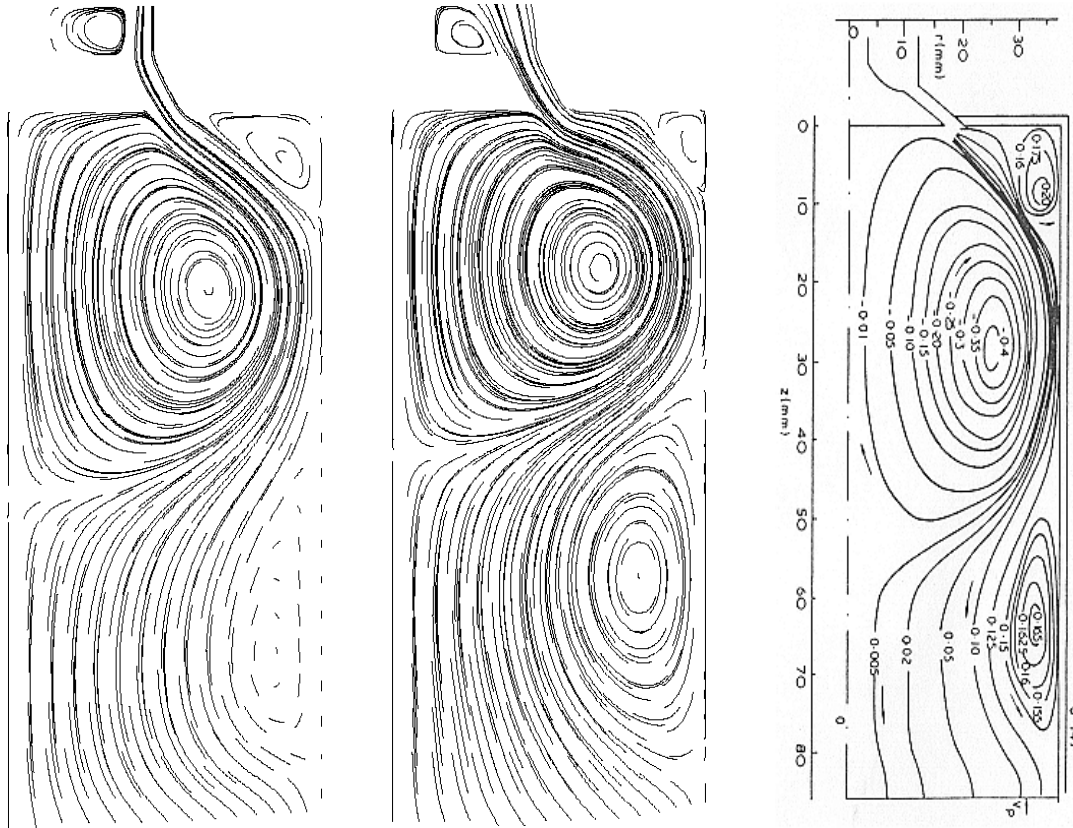
Figure 7.11 Streamlines of predictions of the k-ε model (left) and SEV model (middle) at 90° CA compared with Morse et al. (1979) (right)

Second, the pseudo LES part of the SEV model is investigated. The grid properties used are shown in Figure 7.2b. First of all, it has to be pointed out, that these simulations were calculated for one stroke. Therefore, a meaningful mean flow field could not be predicted, unless a sufficient amount of cycles had been simulated. In this case, the simulations were requiring a CPU time of approximately 150 hours per stroke on a DEC Alpha 21164 workstation, which made running more cycles for this case not so practical. Also, the inlet flow was not perturbed, instability has developed during the flow without interference.
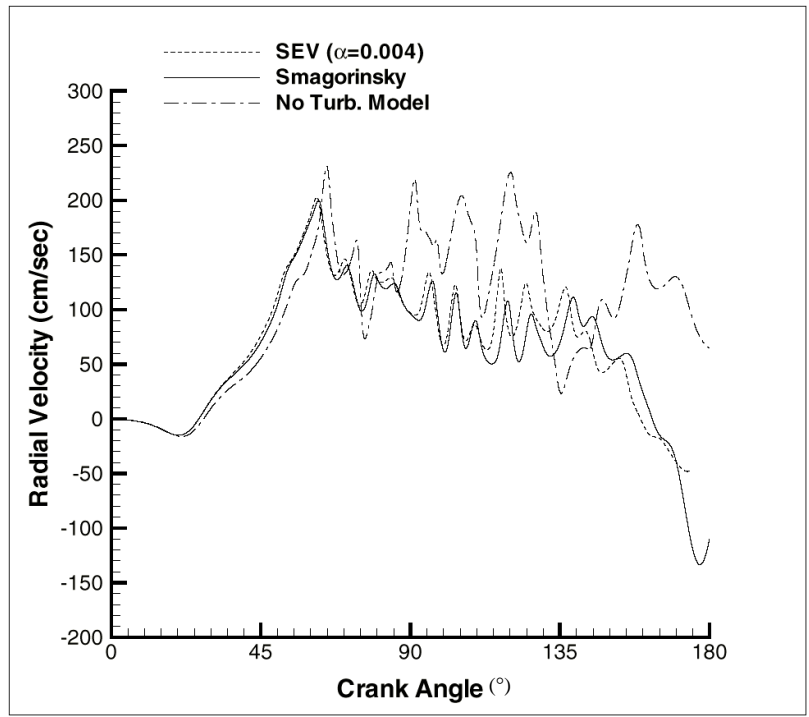
Figure 7.12 Radial velocity predictions for pseudo LES (QSOU)
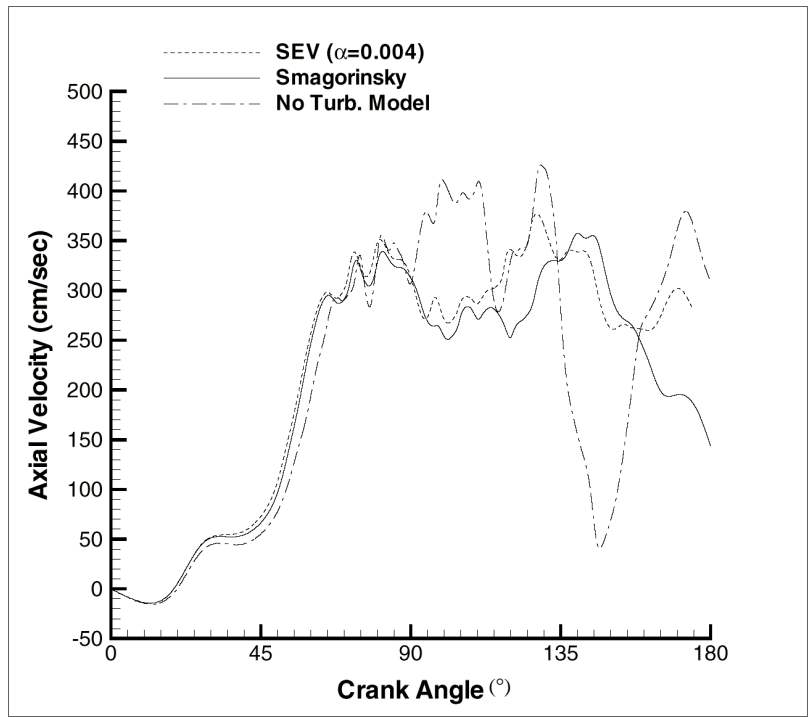
Figure 7.13 Axial velocity predictions for pseudo LES (QSOU)

112
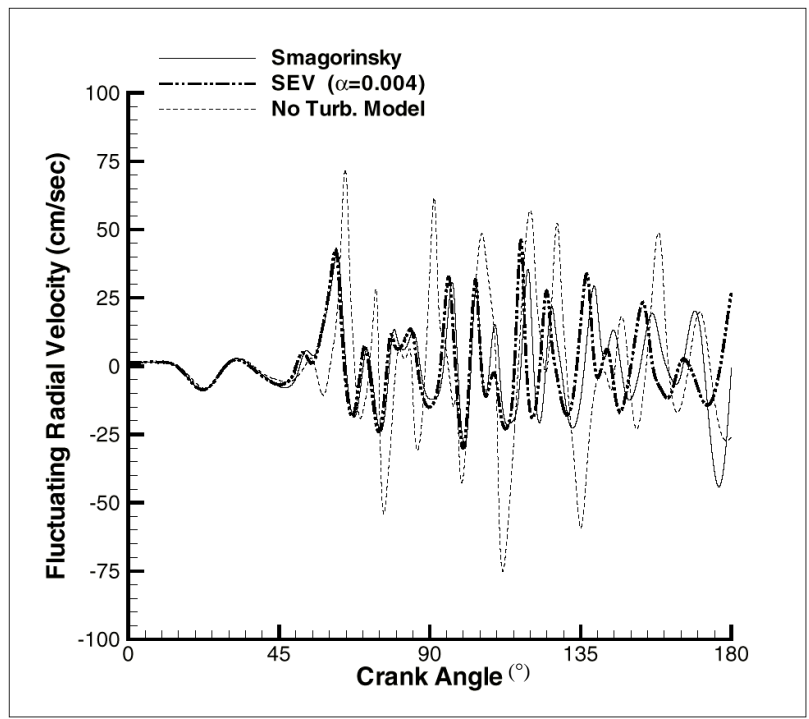
Figure 7.14 Fluctuating axial velocity predictions for pseudo LES (QSOU)
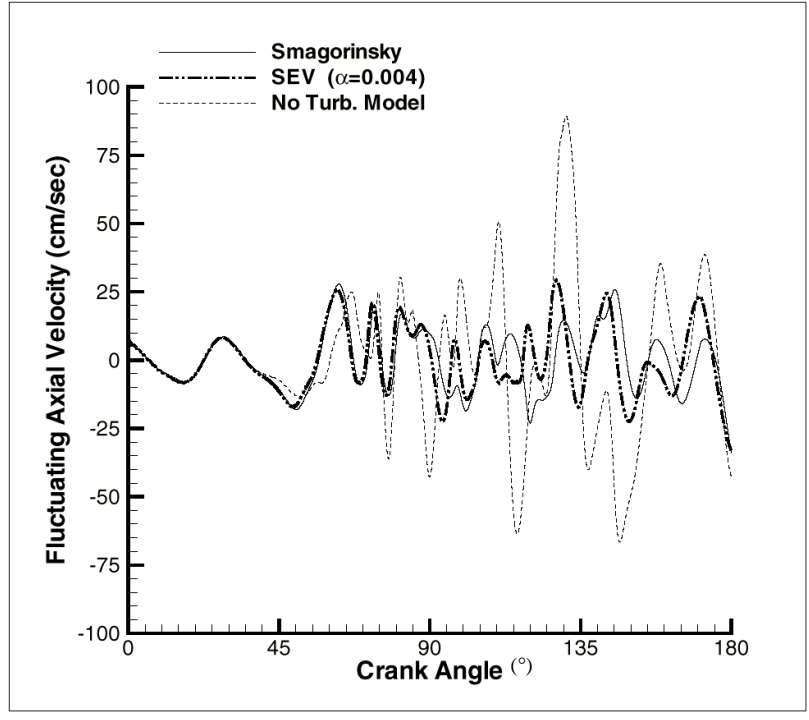
Figure 7.15 Fluctuating axial velocity predictions for pseudo LES (QSOU)

113

In Figures 7.12 and 7.13 the radial and axial velocity variations at a point fixed at 1.0 cm below the cylinder head and 1.0 cm from the axis are compared. As seen in these figures the SEV model, which has been adjusted for LES simulations, and the Smagorinsky model results are predicting essentially the same variations. Notice that these simulations are called pseudo LES, since they are 2-D axisymmtric simulations. The results from a case without a SGS-turbulence model was included here to point out that it is not the same as the SEV model. The same trend is seen in Figures 7.14 and 7.15 where the velocity fluctuations of the SEV model and Smagorinsky model are essentially the same, but the fluctuations predicted without a turbulence model have a much higher amplitude. This is a direct result of the lack of the sub grid viscosity in this model.
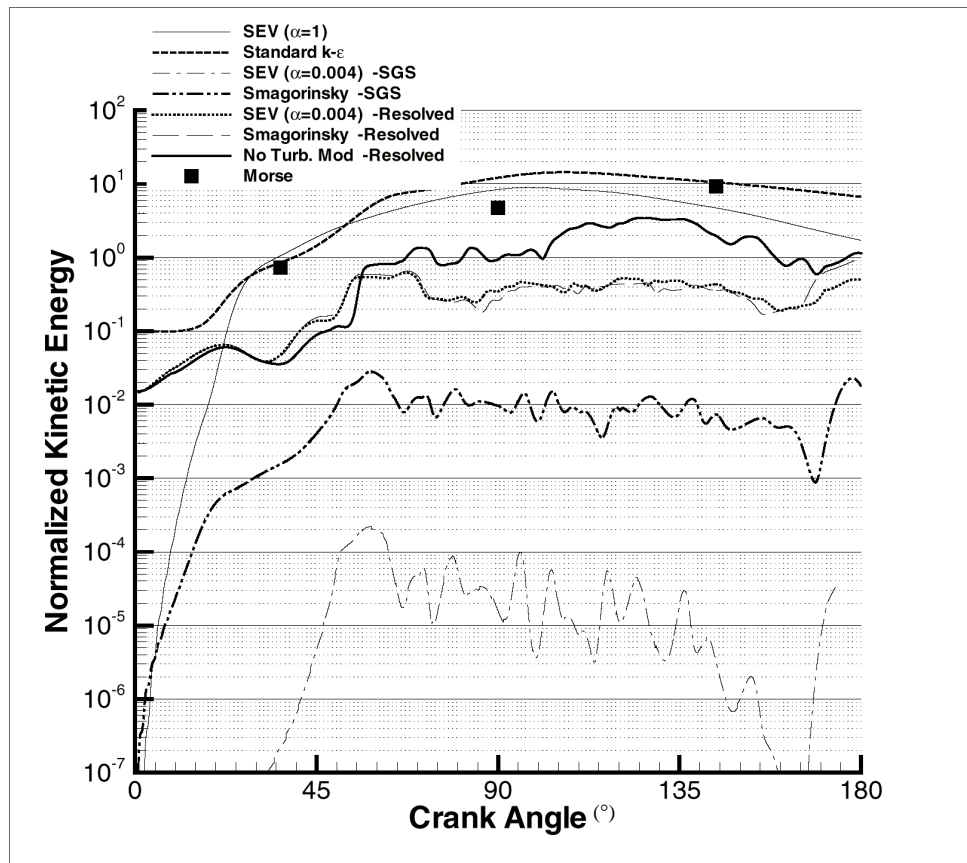
Figure 7.16 Normalized kinetic energy variations for pseudo LES (QSOU)

In Figure 7.16 the normalized kinetic energy of several models are compared. Here the kinetic energy was divided by the mean piston kinetic energy $V_p^2/2$, where V_p is the mean piston speed. As seen from this figure the predicted SGS kinetic energy of the SEV model adjusted for pseudo LES and Smagorinsky model are low when compared to the prediction of the k-ε model. But the resolved kinetic energy of these models is comparable in magnitude. Here, it has to be pointed out that all these simulations were done using the QSOU scheme, which is too dissipative for LES applications. In the next chapter central differencing is used in the simulations, which resulted in a considerable increase in magnitude and frequency of the fluctuations. The predictions without a turbulence model show again a higher resolved kinetic energy than the SEV model adjusted for LES or Smagorinsky model which predict almost the same trend.
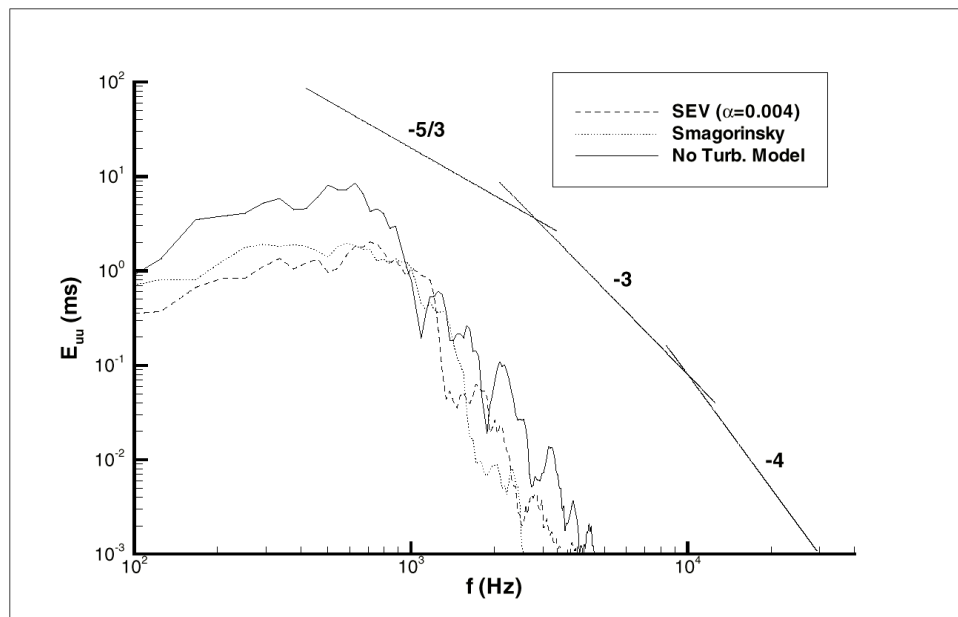
Figure 7.17 Energy Spectra for pseudo LES (QSOU)

115
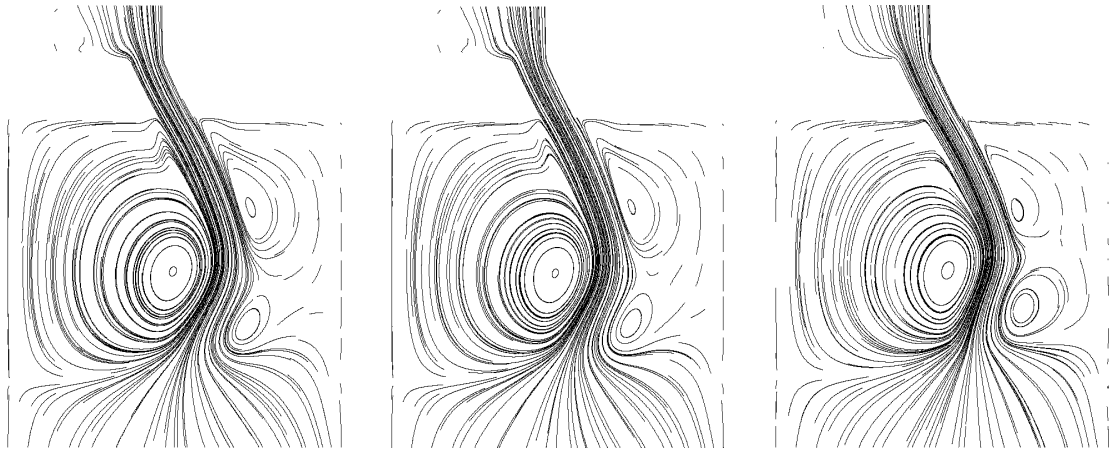
Figure 7.18 Instantaneous streamlines of flow predictions of the Smagorinsky model (left), SEV (α = 0.004) model (middle) and w/o a turbulence model (right) at 36° CA

Figure 7.19 Instantaneous streamlines of flow predictions of the Smagorinsky model (left), SEV (α = 0.004) model (middle) and w/o a turbulence model (right) at 90° CA
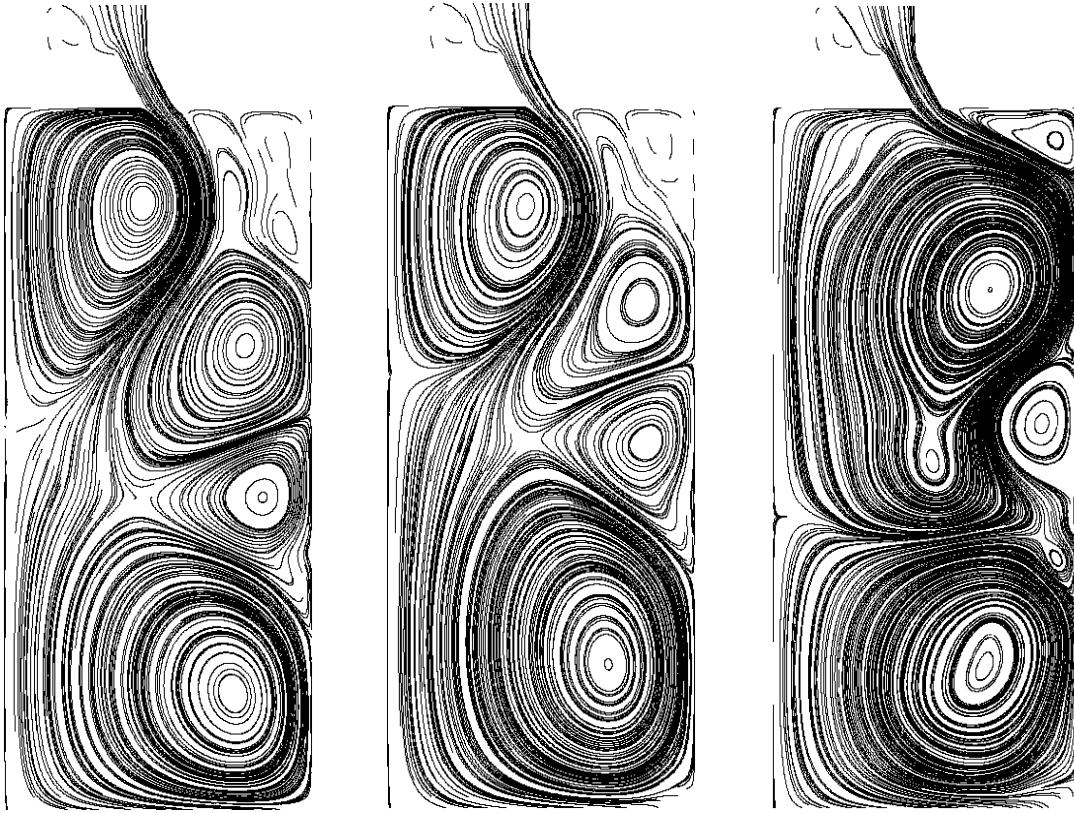
Figure 7.20 Instantaneous streamlines of flow predictions of the Smagorinsky model (left), SEV ($\alpha = 0.004$) model (middle) and w/o a turbulence model (right) at 36° CA

Figure 7.17 presents the energy spectra corresponding to the axial velocity fluctuations for the three models considered. As expected the predictions show a lower frequency range than experiments. Finally, the streamlines of the predicted flowfield of these simulations are presented in figures 7.18 to 7.20. Here, the SEV model and Smagorinsky model predict almost the same flowfield while without a turbulence model the flowfield is considerably different especially at 144° CA, which exhibit a lot more flow structures in the form of thoroidal eddies.

7.5   Conclusions

A first attempt to develop a turbulence model which provides a smooth transition from RANS calculations to LES or vice versa is established so that for coarse grids RANS, for sufficiently small grids LES, and eventually DNS can be obtained in the limit of very fine grid size. For this purpose the SEV model presented in Chapter 5 has been improved and tested against experimental benchmarks. Simulations for RANS are compared with the standard k-ε, and simulations for pseudo LES are compared with the Smagorinsky model and a case without turbulence model. These models were applied to predict the turbulent flow during the intake stroke of an engine cylinder with flat piston at a low speed of 200 RPM.

The results indicate that the SEV model provides an alternative in predicting the mean flow field in IC engines without solving the kinetic energy and dissipation rate equations. In addition, it has the potential to predict some physical flow aspects better than the k-ε model. On the other hand, it can also be used as a SGS model for LES in case of a sufficiently small grid size.

Chapter 8

ANALYSIS OF LES OF INTAKE FLOW INDUCED TURBULENCE

8.1   Introduction

In this section important findings from application of the LES technique to typical engine cylinder geometries are presented. First, the flow dynamics due to piston motion without valve movement during the intake stroke is studied for different engine speeds and the effects of the discretization scheme on the flow solutions are presented. Next, the flow inside the cylinder during the intake stroke and compression strokes without combustion was simulated including the valve dynamics. Here, the objective was to investigate the generation of turbulence during the intake and subsequently its decay during compression stroke and demonstrate the predictive capability of the LES technique when applied to in-cylinder turbulence.

8.2   Methodology

Modifications were made to the KIVA code to allow a fairly simple Smagorinsky SGS model where the eddy viscosity is calculated from the algebraic relation (Equation

7.3). The model constant C_s was set equal to 0.2, a typical value used in the literature (see e.g. Rodi et al., 1997). The sub-grid length-scale was estimated as an average computational cell dimension (see Smith et al., 1998 and 1999).

In some of the cases presented "no SGS turbulence model" was used. This requires, in most instances, some numerical diffusion for stability, which is accomplished via the use of QSOU (Quasi Second Order Upwind) scheme instead of the central differencing (CD) which has no diffusion error, or by using a combination of CD and upwind differencing heavily biased towards CD.

The above turbulence models were employed in conjunction with the commonly used law-of-the-wall boundary condition which is implemented in KIVA-3. The basic assumption here is that the interaction between the modeled near wall region and the outer region is weak as observed experimentally by Brooke and Hanratty, (1993).

Convective terms are advanced explicitly in time and the diffusion terms are advanced explicitly, implicitly, or semi-implicitly. The degree to which the diffusion terms are implicitly discretized is based on a combination of stability and efficiency considerations. Sub-time steps (referred to as sub-cycles) are taken to advance the convective terms. The time step in each sub-cycle is based on Courant stability considerations. The convective terms are advanced with time steps that are the same or smaller than what is used for the diffusion terms. Though the overall time accuracy for convection terms is only of the first-order, the global time step is based on several considerations including stability and several accuracy constraints. To increase the time accuracy even further the time step was confined to $1 \cdot 10^{-6}$ sec for axisymmetric simulations and $5 \cdot 10^{-7}$ sec for 3-D simulations far below the Kolmogorov time scale,

which is in the order of 10^{-4} -10^{-5} seconds for a typical automotive size engine (Celik and Yavuz, 1997). It is believed that this precaution compensates for the first order time accuracy of convective terms and guarantees the time resolution required for LES.

8.3   The Effects of Engine Speed on Intake Flow Induced Turbulence

An isothermal, incompressible flow within a piston-cylinder arrangement (Morse et al., 1979; Haworth, 1998) motored without compression at 200 RPM to 2000 RPM is investigated. The mean piston speed V_p was 40 cm/sec to 400 cm/sec in these calculations. There was no swirl imposed. The computational mesh used in the 2-D axisymmetric simulations has been shown in Fig.7.2b. The seat angle was 60° with the horizontal axis. A time step of $1x10^{-6}$ seconds was used for time marching. A numerical mesh of 40,000 vertices was employed with a wedge angle of 0.5 degrees in the circumferential direction. The maximum cell size was 0.3x0.9 mm for these calculations in the radial and axial direction inside the cylinder. The inlet pressure was atmospheric and the initial flow was at rest till the piston started to move away from TDC (0° CA). In this study QSOU and CD (central differencing) schemes were utilized.

In Figures 8.1 and 8.2 the non-dimensional axial and radial velocity variations with crank angle are compared for a range of engine speed at a point 10 mm from the axis and 10 mm below the cylinder head inside the cylinder. These results were normalized by dividing the velocities by the corresponding mean piston speed V_p. As seen from these figures the normalized radial velocity variations almost coincide with each other. The same behavior is displayed in figures 8.3 and 8.4 where the calculated RMS (root mean

square) variations are presented. This indicates that turbulent fluctuations scale with engine speed.

The energy spectrum is shown in Figure 8.5, which was simply calculated according to Hayasa (1999) as

$$E_{uu}(f) = \frac{1}{V_p^2} \frac{\Delta t}{2\pi N} \left[\sum_{n=1}^{N} u'(t_n) \exp(-i\omega t_n) \right]^2 \qquad (8.1)$$

where $\omega = 2\pi n / (N\Delta t)$ is the non-dimensional circular frequency. As seen from this figure the spectrum does not change very much with engine speed for this case. And the resolved frequency range is in the lower LES range, which is due to the fact that these simulations are done using the QSOU scheme and they are two-dimensional.
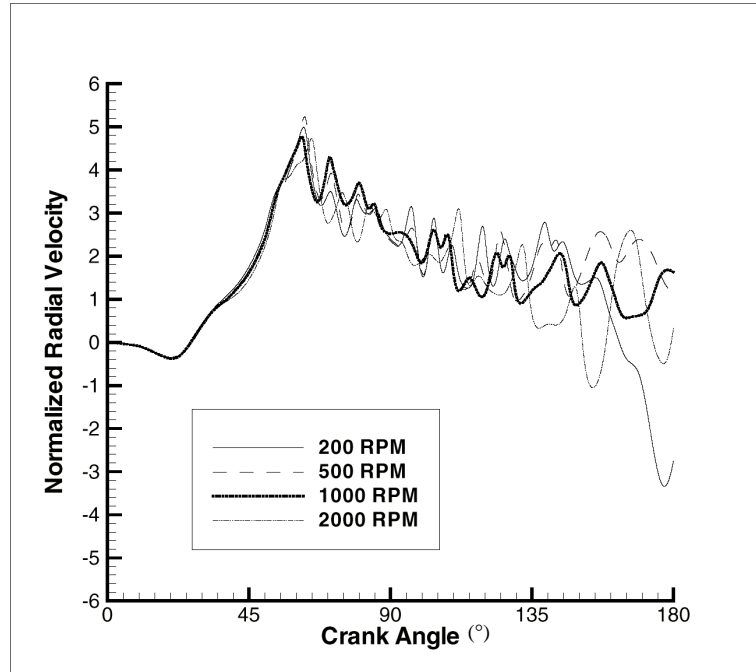
Figure 8.1 Normalized radial velocity (u/V$_p$) variations with crank angle at different engine speeds
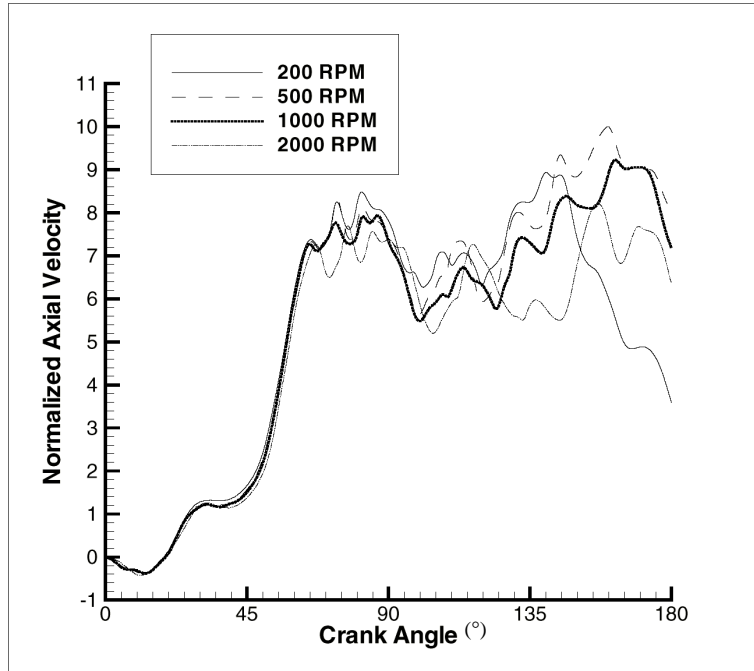
Figure 8.2 Normalized axial velocity (w/V_p) variations with crank angle at different engine speeds
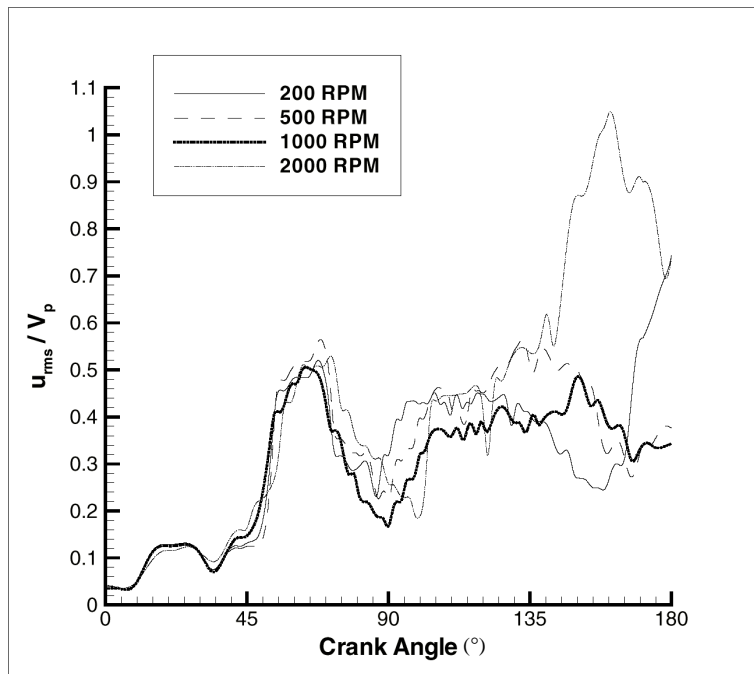
Figure 8.3 Normalized radial RMS velocity variations with crank angle at different engine speeds

123
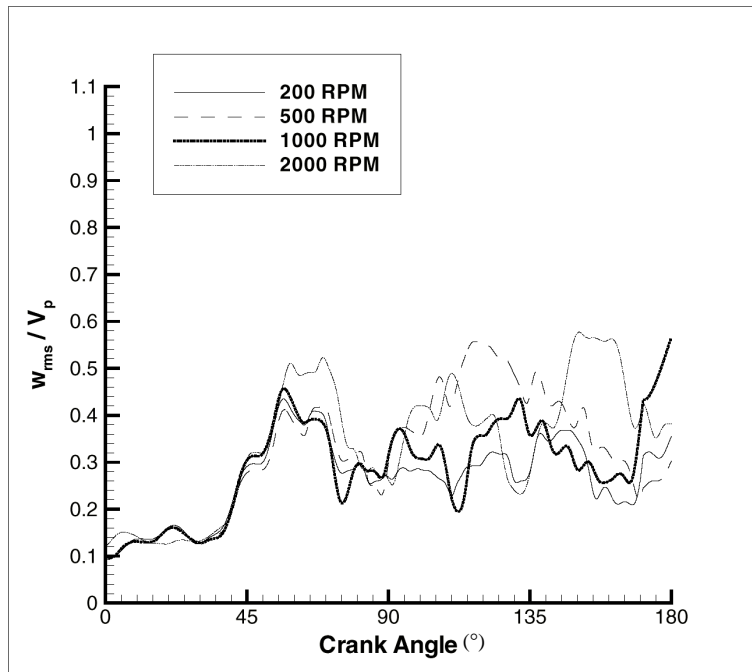
Figure 8.4 Normalized axial RMS velocity variations with crank angle at different
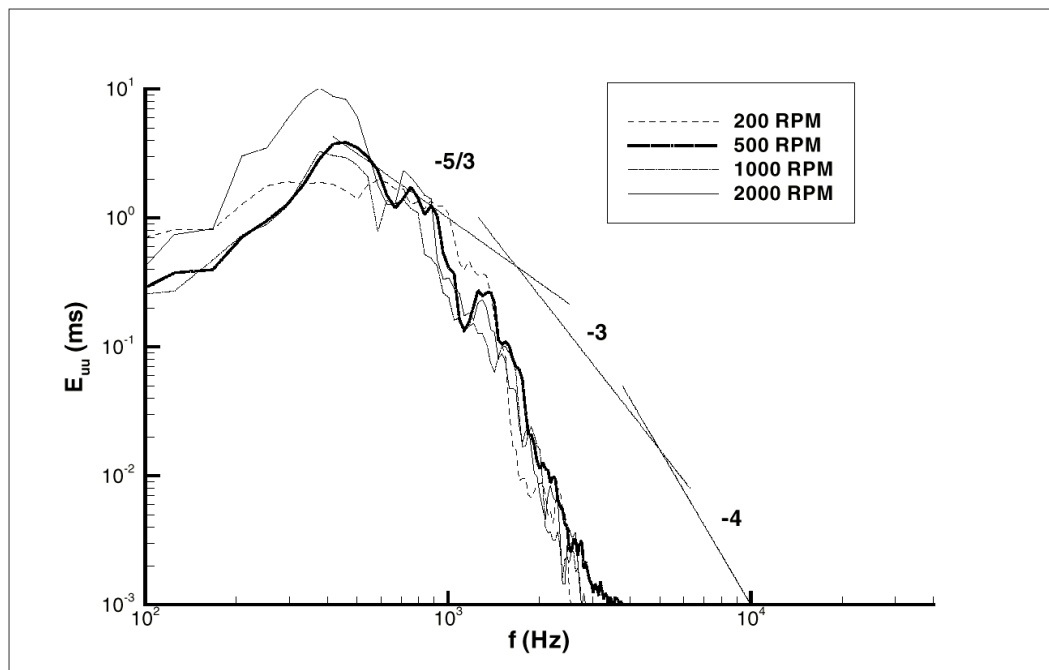
engine speeds

Figure 8.5 Energy spectra at different engine speeds

Figure 8.6 shows the normalized axial RMS velocity variation with engine speed. Data was calculated at a point 10-mm from the axis and 10-mm below the cylinder head inside the cylinder. It can be noted that the normalized velocity is almost constant with changing engine speed, which reveals that the fluctuations increase almost linearly with mean piston speed. This was also pointed out by the simulations of Naitoh et al. (1992). The total kinetic energy variation with engine spped is shown in Figure 8.7 which was calculated from

$$k_T = k_{resolved} + k_{sgs} = 3/2\left(u_{rms}^2 + w_{rms}^2\right) + k_{sgs} \tag{8.2}$$

Here , it should be noted that k_T first increases than decreases as the piston moves from 36° CA to 144° CA. It has to be also noted that these are axisymmetric calculations and v_{rms} (the turbulent fluctuations in the aximuthal direction) is filtered out by imposing a very large filter width in this direction. Figure 8.8 exhibits again the same linear behavior noticed in Figure 8.6. Here, the total kinetic energy was normalized by $1/2\,V_p^2$.
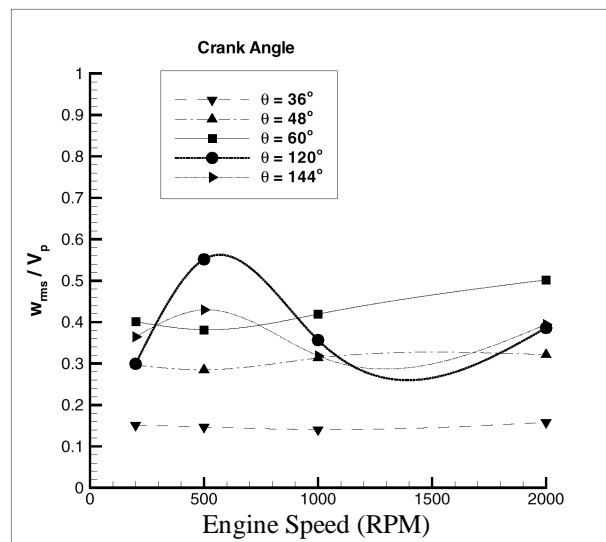
Figure 8.6 Normalized axial RMS velocity variation with engine speed at a fixed point inside the cylinder at different crank angles
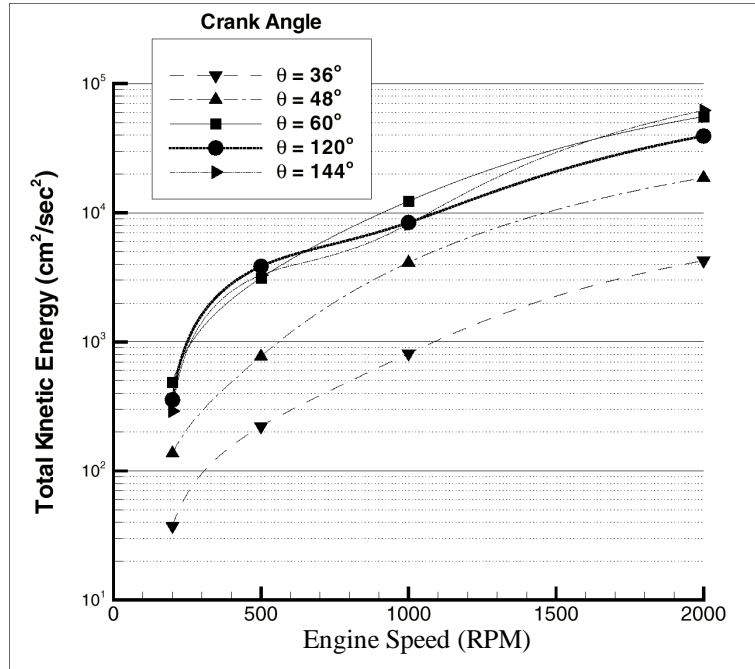
Figure 8.7 Total kinetic energy variation with engine speed at a fixed point inside

the cylinder at different crank angles
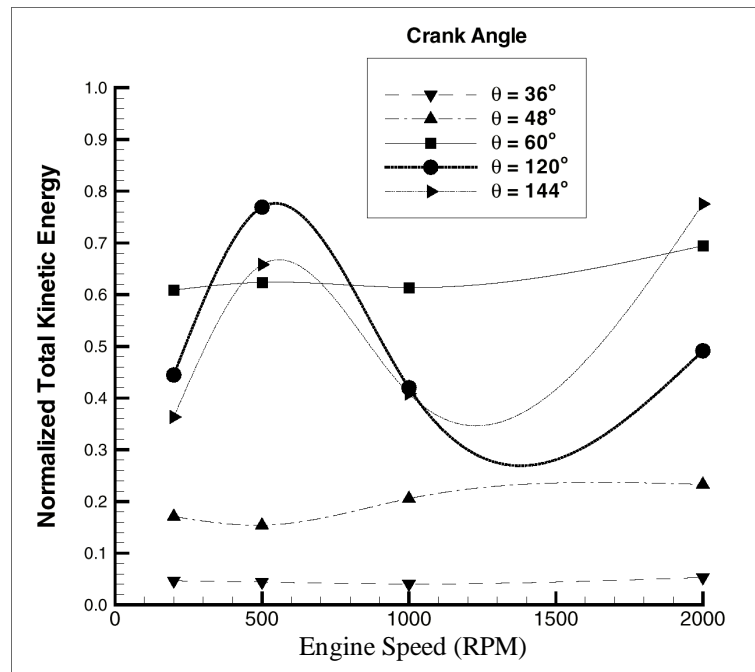
Figure 8.8 Normalized total kinetic energy variation with RPM at a fixed point

inside the cylinder at different crank angles

8.4   The Effects of the Differencing Scheme on Intake Flow Induced Turbulence

The same configuration in Section 8.3 was investigated using the central differencing scheme with the Smagorinsky model. Results are compared with preditions using the Smagorinsky model and a case without a SGS turbulence model, which utilize the QSOU (Quasi Second Order Upwind) scheme. Note that, whenever CD is used for the convective terms in the momentum equation, QSOU is used for all scalar variables.

Figure 8.9 and 8.10 present the axial velocity and axial fluctuating velocity variations with crank angle, respectively. The simulation using central differencing scheme preditcs much larger velocity fluctuations at a higher frequency.
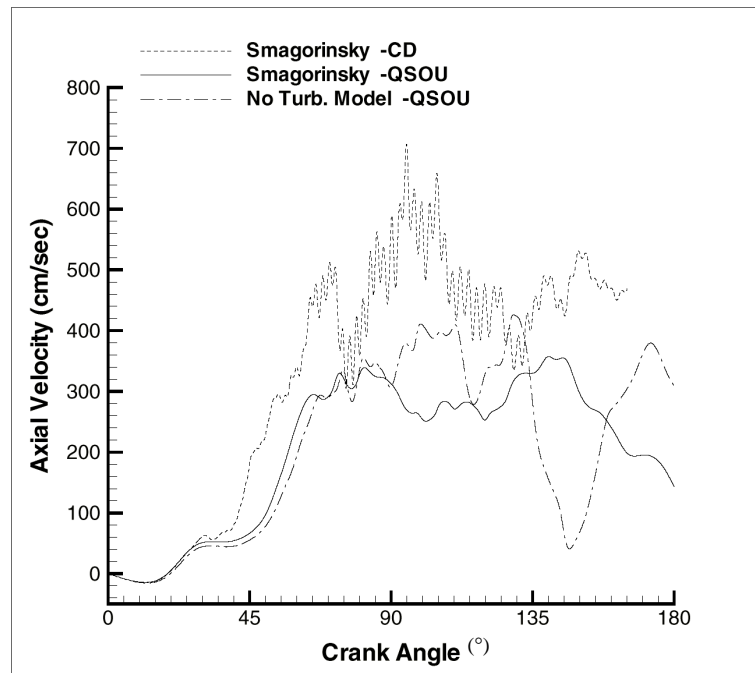
Figure 8.9 Axial velocity variations with crank angle for simulations with different discretization schemes

127
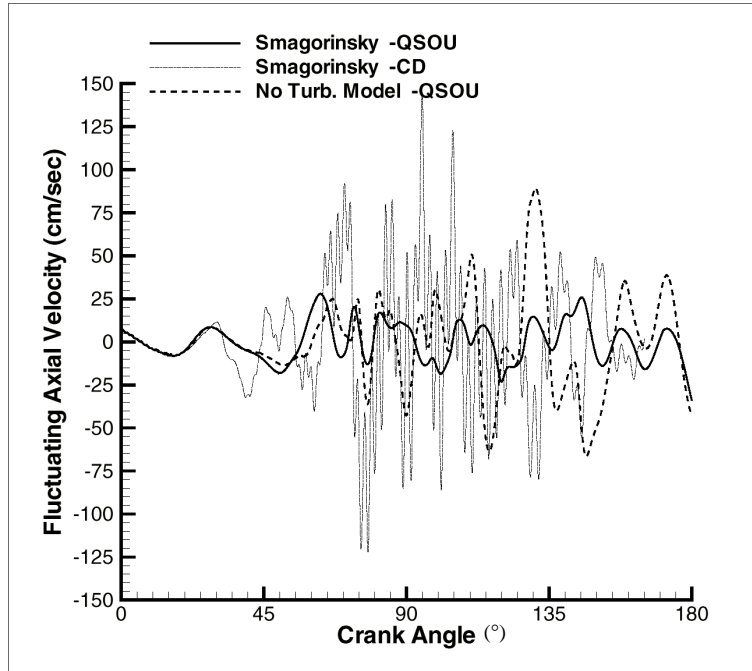
Figure 8.10 Axial fluctuating velocity variations with crank angle for simulations

with different discretization schemes
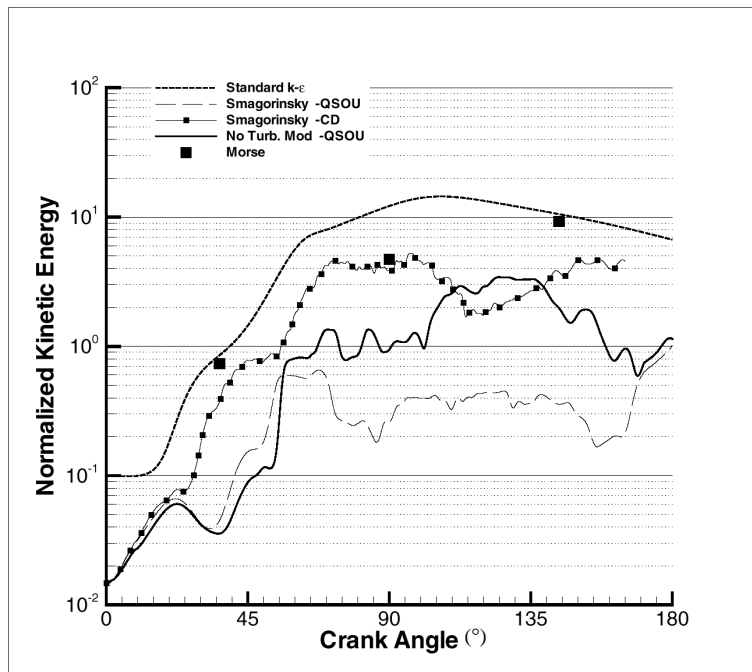
Figure 8.11 Normalized resolved kinetic energy variations with crank angle for

simulations with different discretization schemes
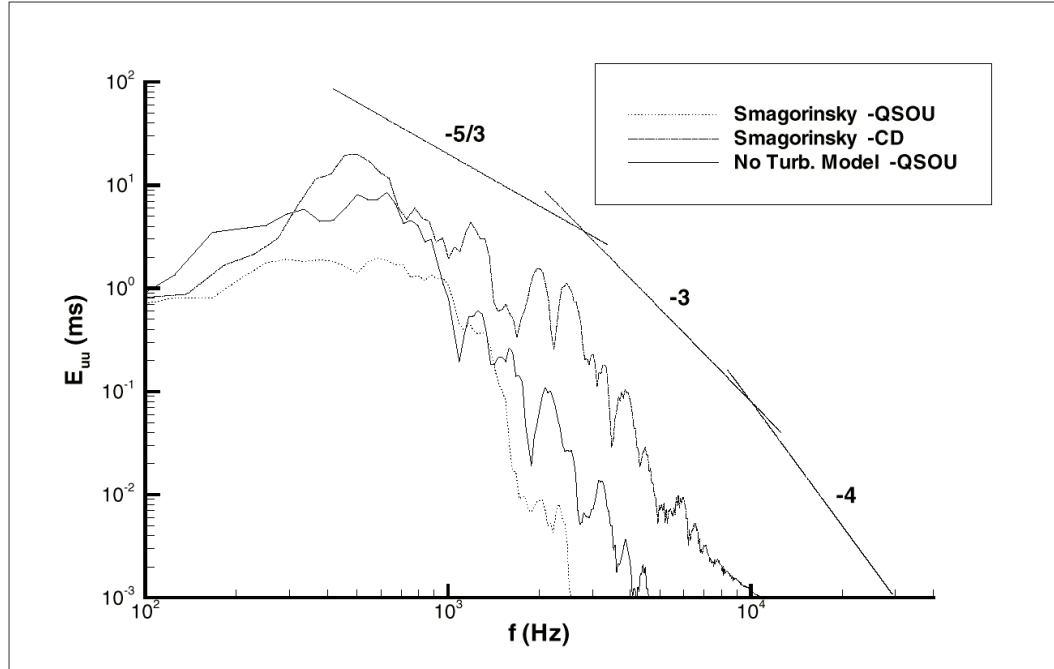
Figure 8.12 Energy spectrum for simulations with different discretization schemes

The normalized resolved kinetic energy variation with crank angle is shown in Figure 8.11. Here the simulations using central differencing predict almost an order of magnitude higher resolved kinetic energy when compared to the simulations with the Smagorinsky model using the QSOU scheme. The same behavior is interpreted in Figure 8.12 where the CD solutions show a much higher frequency content than the QSOU predictions. It has to be noted that the results without a SGS turbulence model are between the two Smagorinsky model results. This indicates that simulations could be performed without a turbulence model, solely relying on the numerical diffusion of the QSOU scheme. However, the pseudo LES predictions presented in Figure 8.11 show that simulations with the CD scheme are well in the range of predictions using the k-ε model and experiments, although these simulations are axisymmetric and much higher values

are anticipated in three-dimensional simulations with fine grid resolution. This leads to the conclusion that CD is the logical scheme to use for attempting LES utilizing the KIVA code.

8.5 Prediction of Turbulence Induced by Intake Flow

The computational procedure described in Section 8.4 was applied to a typical engine geometry for full 3-D calculations. The cylinder assembly was taken as generic IC engine with a Mexican hat shaped bowl. The cylinder geometry, the three-dimensional numerical grid and engine parameters are depicted in Figure 8.13. Some additional parameters are as follows: the compression ratio is ~11, inlet valve opening is at 15° BTDC, inlet valve closure is at 25° ABDC, exhaust valve opening is at 40° BBDC, exhaust valve closure 10° ATDC. Piston speed was set to 1600 rpm. A valve geometry with the swirling intake configuration was used (Figure 8.13). The computations were performed on a grid consisting of 300,000 nodes including the intake/exhaust ducts. The average grid size was in the order of 1-1.5 millimeter. A curvilinear block-structured coordinate system was used in preference to the cylindrical coordinate system because the former avoids high grid distortions at the cylinder axis. The computations were carried out with the standard k-ε model and without any turbulence model using the QSOU numerical scheme. The same computations were repeated with the Smagorinsky sub-grid-scale turbulence model and the second order discretization scheme for the convective terms (as described by Smith et al., 1999).
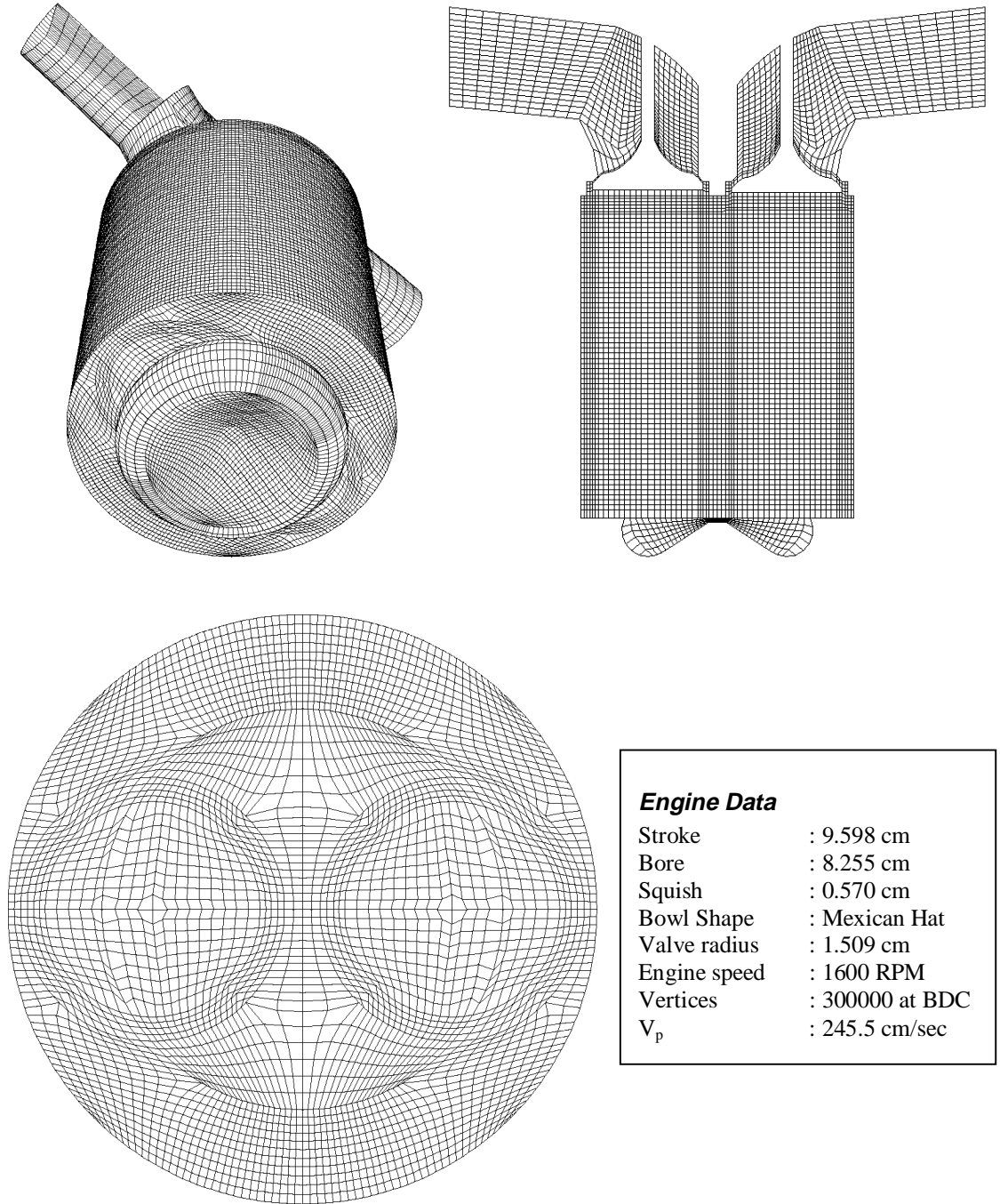
Figure 8.13 Computational mesh (top-left) and vertical (top-right) and horizontal

(bottom-left) section views and specific engine data

Engine Data

Stroke	: 9.598 cm
Bore	: 8.255 cm
Squish	: 0.570 cm
Bowl Shape	: Mexican Hat
Valve radius	: 1.509 cm
Engine speed	: 1600 RPM
Vertices	: 300000 at BDC
V_p	: 245.5 cm/sec

The exhaust and inlet duct pressure was set equal to the atmospheric pressure. It should be noted that the simulated engine configuration and the one studied experimentally by Catania et al. (1997) are not exactly the same, though some qualitative comparison is made. The intake valve geometry and movement were not modeled in accordance with the actual engine parameters, but a generic profile was used to describe the shape of the upper portions of the valves (Figure 8.13).

Figure 8.14 and Figure 8.15 show the instantaneous radial velocity and its fluctuating part located at a point approximately 5 mm below the cylinder head and 10 mm to the left of the cylinder centerline towards the intake duct centerline. As such this particular point can be compared with one measurement point of Catania and Spessa (1996) which is 5 mm below the cylinder head, and close to the cylinder axis. The RMS velocity fluctuations are also depicted in Figure 8.15 which shows that the turbulence intensity may become an order magnitude larger than the value of the mean piston speed (V_p=245.5 cm/sec). The reader is reminded that the geometry of Catania's experiment is different from the computational model and comparisons are on a qualitative base. However, the main concern was to reproduce the trend in the fluctuating component, which is seen to agree well with experimental data (Figure 8.16). It is noteworthy to see that the velocity fluctuation decrease significantly towards the BDC and during the compression phase as observed in the measurements. It is also important to note that these particular measurements (Catania and Spessa, 1996) show cycle-resolved turbulence rather than ensemble averages.

In Figure 8.17 and Figure 8.18 the normalized autospectral density function (i.e. energy spectra) is presented to compare with experiments at a representative point which

roughly corresponds to the measurement point. The agreement of both the energy content and the frequency ranges captured in the present simulations are good in spite of the differences in the cylinder configurations as explained above.

Figure 8.17 is seen as a confirmation of the fact that the present methodology is capable of resolving a significant portion of the inertial sub-range in the energy spectra. Here it has to be noted that the grid density is only moderately fine and with a much higher grid density higher fluctuations both in magnitude and frequency could be predicted.
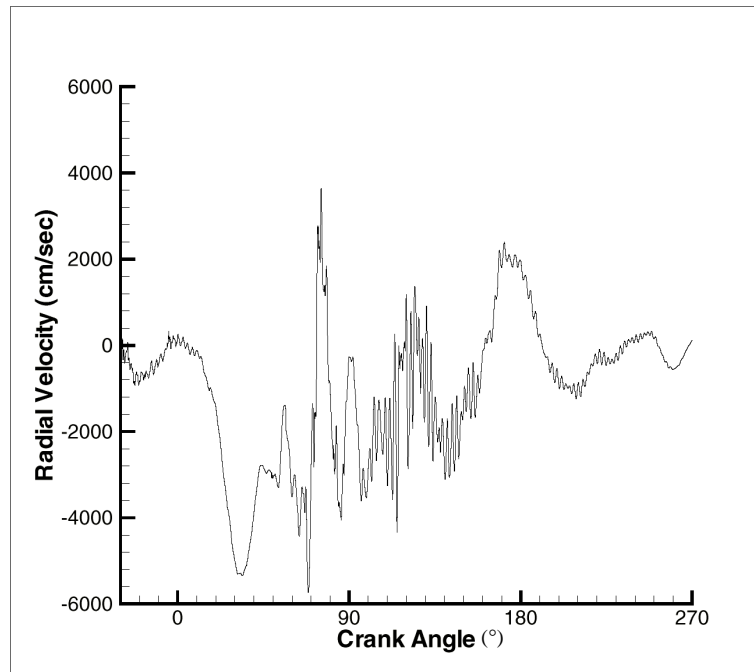
Figure 8.14 Instantaneous radial velocity at a fixed point 5 mm below the cylinder
head
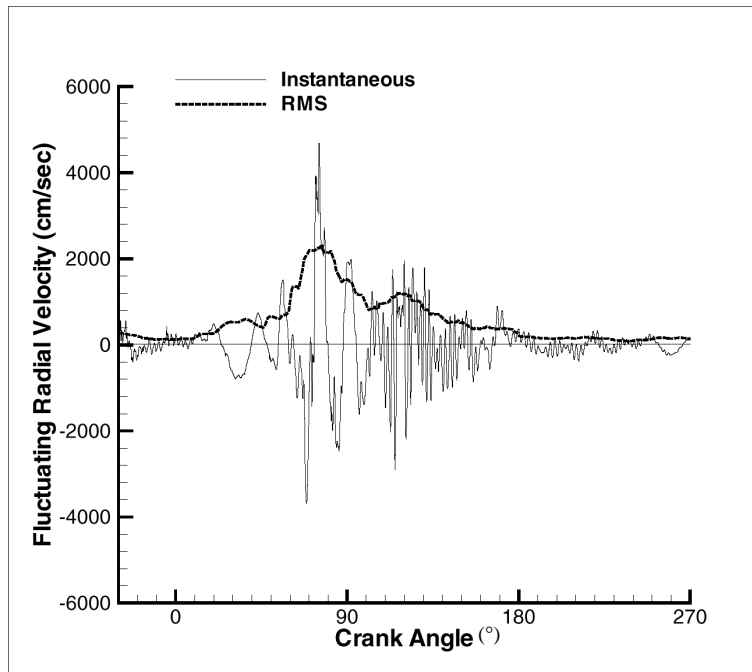
Figure 8.15 Instantaneous radial velocity fluctuations and radial RMS velocity

(u_{rms}) at a fixed point 5 mm below the cylinder head
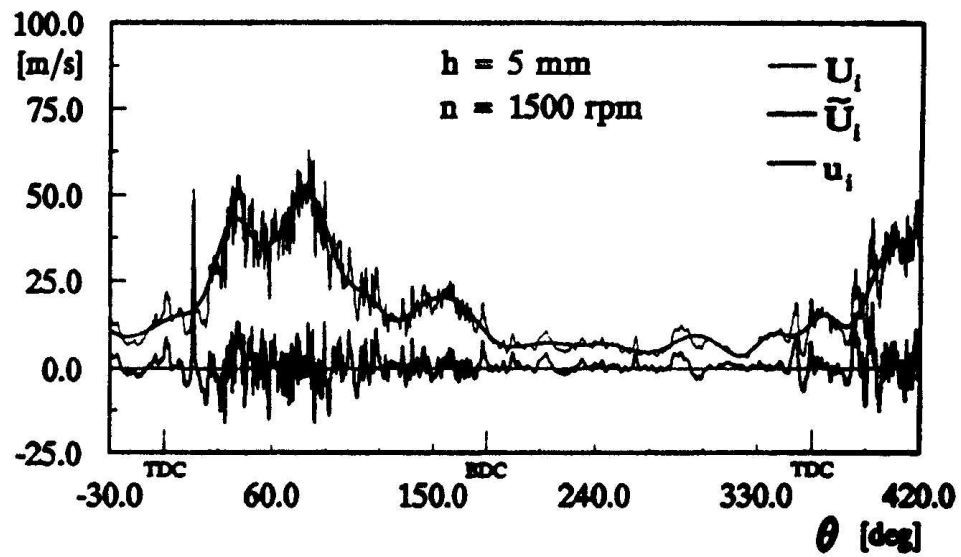
Figure 8.16 Measured instantaneous radial velocity components at a fixed point 5

mm below the cylinder head by Catania and Spessa (1996)
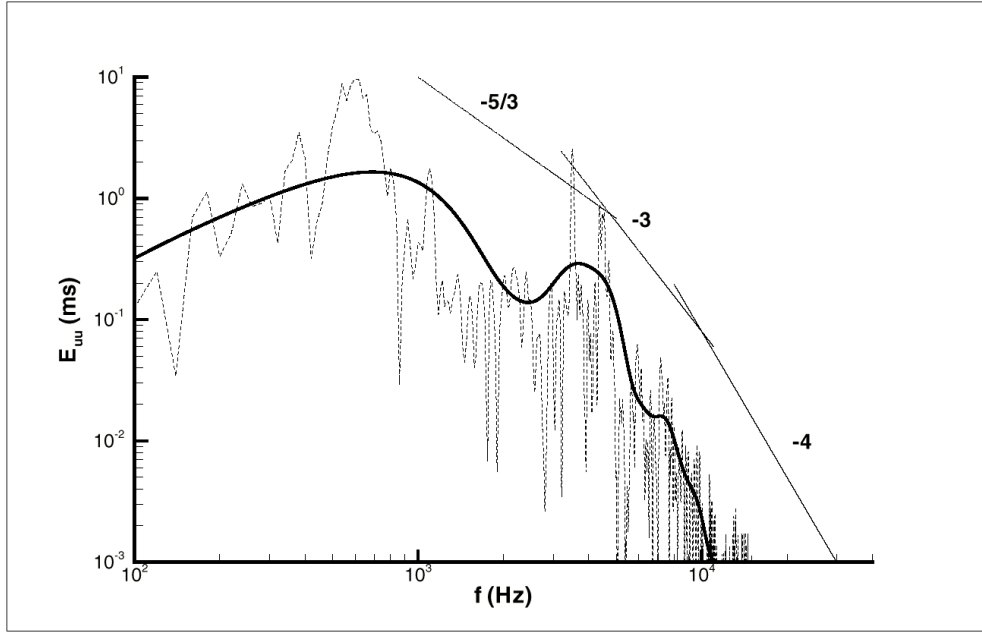
Figure 8.17 Energy spectrum of instantaneous radial velocity fluctuations and RMS velocity at a fixed point 5 mm below the cylinder head
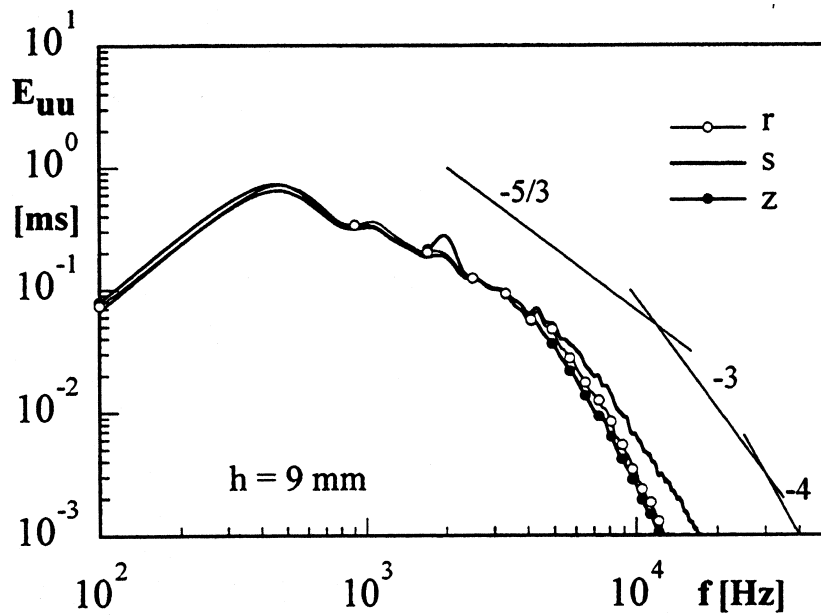
Figure 8.18 Energy spectrum of the measured instantaneous velocity fluctuations at a fixed point 9 mm below the cylinder head by Catania and Spessa (1996)

135
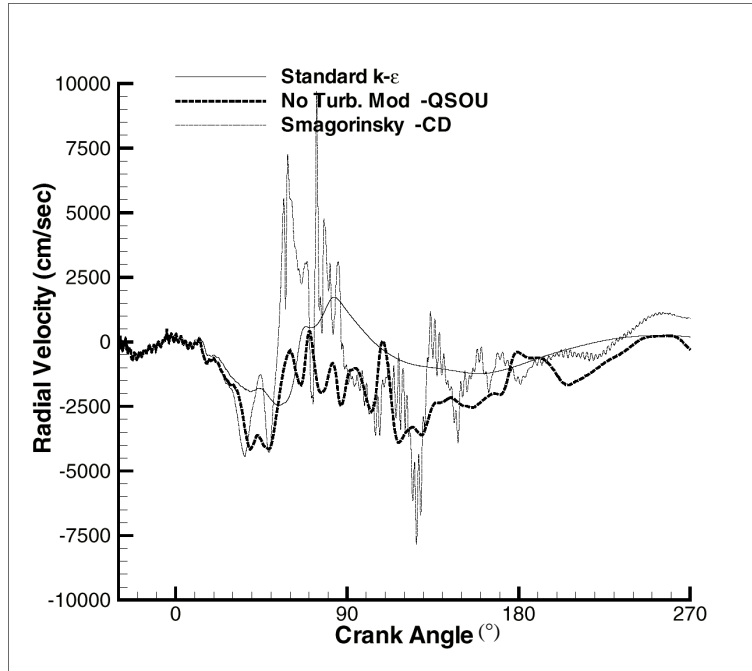
Figure 8.19 Instantaneous radial velocity at a fixed point relative to the piston
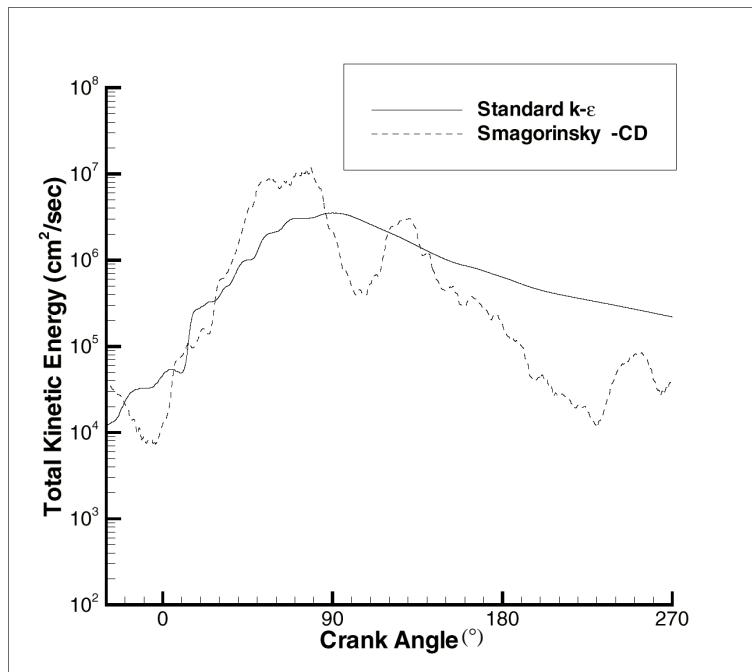
bowl

Figure 8.20 Total kinetic energy at a fixed point relative to the piston bowl

predicted by the Smagorinsky model with CD

Figure 8.19 shows the instantaneous radial velocity located at a fixed point relative to the piston-bowl, approximately 10-mm to the left of the cylinder centerline towards the intake duct centerline and flush with the piston-face. The simulations without a turbulence model using QSOU and the ones with the Smagorinsky model using CD are compared to the predictions of the simulations with the standard k-ε model. Here, all models have been used with the same time step of $5 \cdot 10^{-7}$ sec for consistency. They all seem to follow the same trend in the mean flow predictions. The total kinetic energy of the Smagorinsky simulation is well in the range of the k-ε model as seen in Figure 8.20. It has to be kept in mind that the turbulence intensity was calculated using an individual cycle mean, and a ensemble averaged mean may show a considerable difference in the calculated magnitude of the fluctuations as shown in Figure 8.21 (Lumley, 1999).
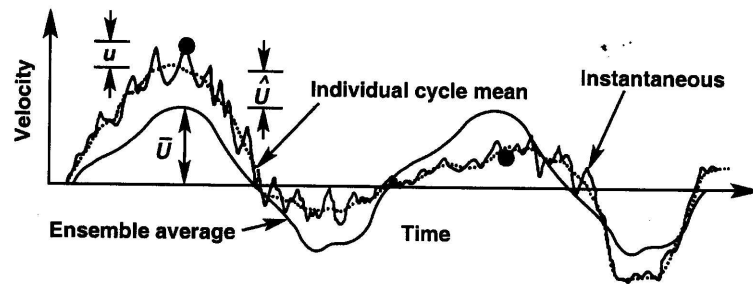
Figure 8.21 Velocity variation with crank angle at a fixed location in the cylinder during two consecutive cycles of an engine (Lumley, 1999)

The velocity vectors at 150° CA during the intake stroke are shown in Figures 8.22 to 8.24. The k-ε model and Smagorinsky model solutions show highly different predictions of the velocity distribution. As seen from these figures both models predict the same locations of the strongest circulation regions. However, as expected the Smagorinsky model resolves much smaller structures.

137
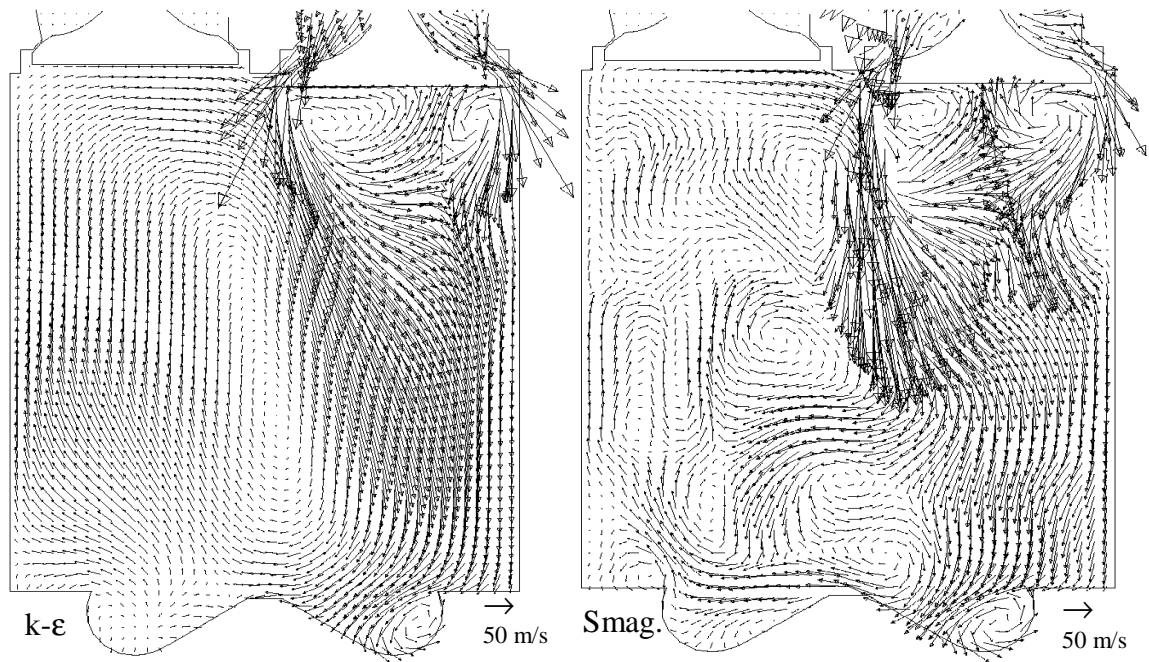
Figure 8.22 Velocity vectors at a vertical cross-section through the centerline at 150° CA

during the intake stroke for the k-ε model and Smagorinsky model predictions
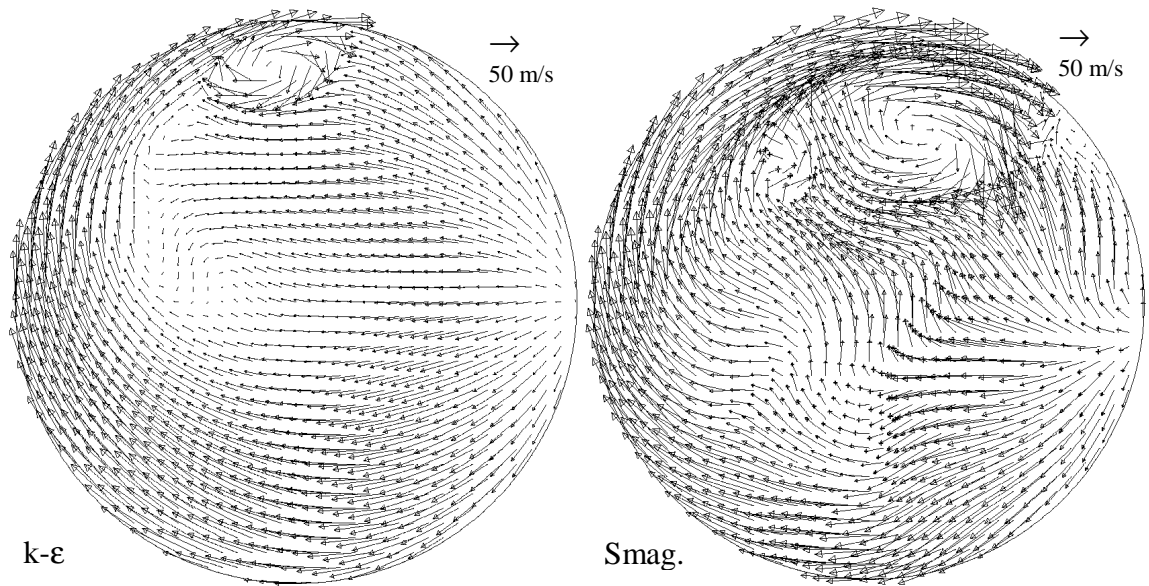
Figure 8.23 Velocity vectors at a horizontal section 6 cm below the cylinder head at 150°

CA during the intake for the k-ε model and Smagorinsky model predictions
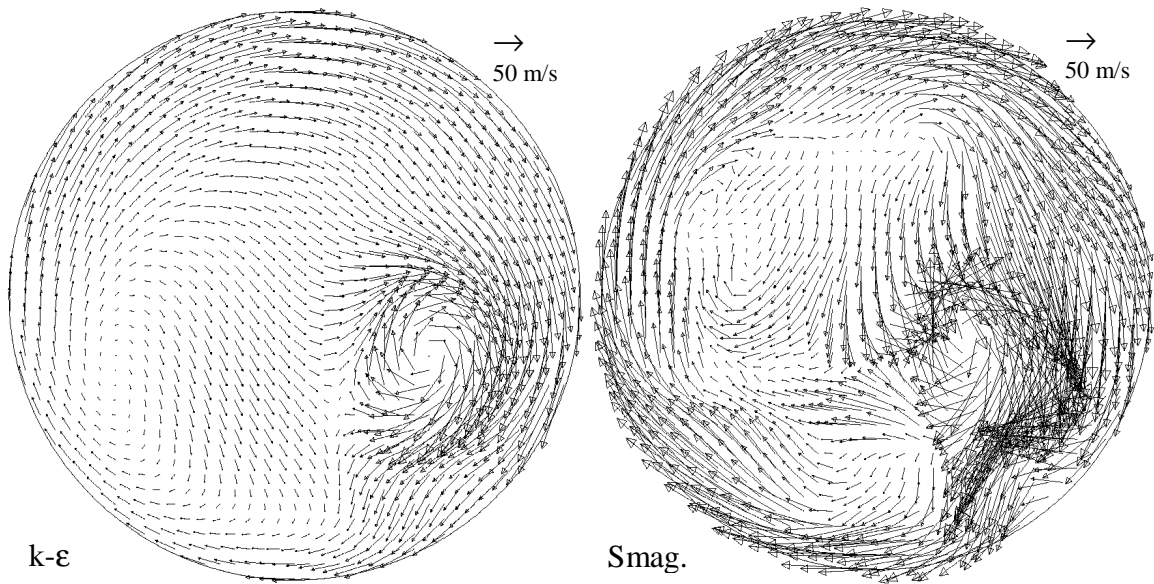
Figure 8.24 Velocity vectors at a horizontal section 2.5 cm below the cylinder head at 150° CA during the intake stroke for the k-ε model and Smagorinsky model predictions
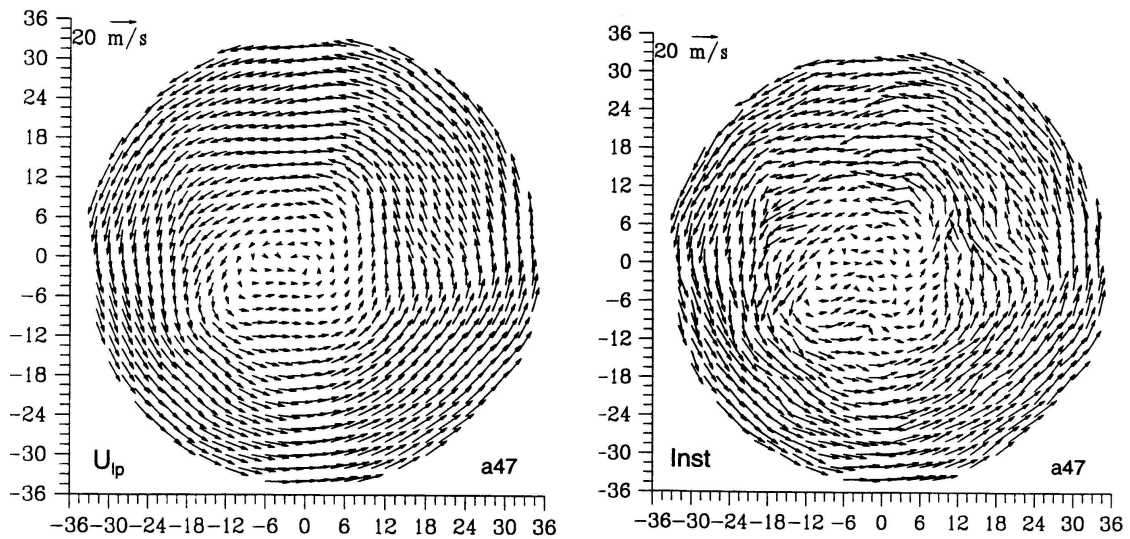
Figure 8.25 PIV measurements (Reuss, 2000) a) Low-pass filtered velocity vectors, b) Instantaneous velocity vectors (axis show coordinates of the domain)
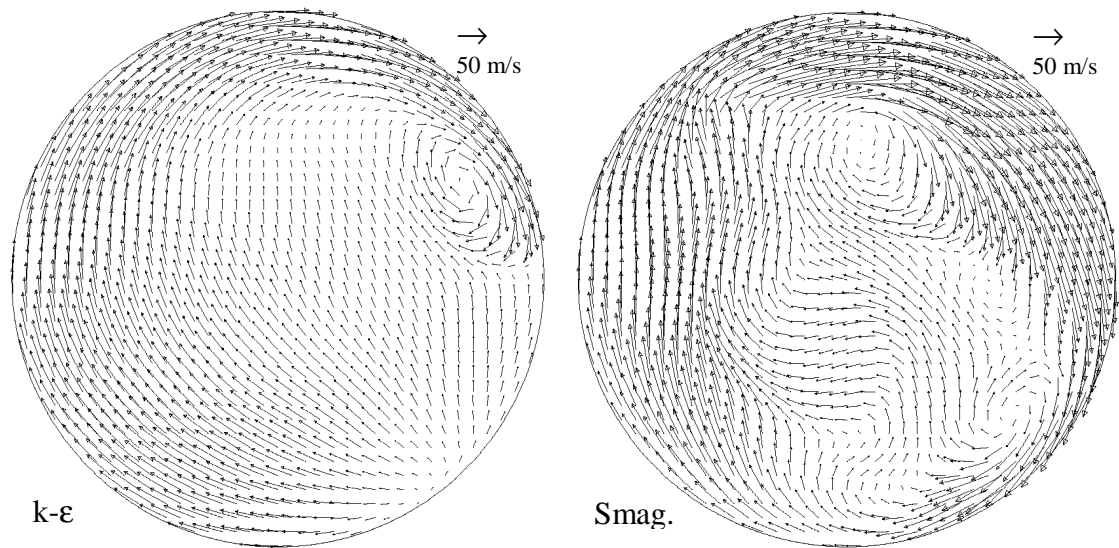
Figure 8.26 Velocity vectors at a horizontal cross-section 9 cm below the cylinder

head at 210° CA during the compression stroke for the k-ε model and

Smagorinsky model predictions

PIV measurements conducted by Reuss (2000) are shown in Figure 8.25. These figures are shown for a qualitative comparison of the predicted velocity distributions. However, as expected, measurements seem to capture even smaller structures than the Smagorinsky model predictions. This refers to the fact that the numerical grid size used in this simulation is still not adequate and a smaller grid size has to be employed. However, the current simulations would last for 30 days on a DecAlpha 21164 workstation. Due to limitations in resources only a few simulations could be performed.

In Figure 8.26 the velocity vectors at 210° CA during the compression stroke are shown. The effect of the induced swirl via a swirling intake flow is presented in these figures. Here the k-ε model exhibits already a uniform velocity field, which refers to the dissipative nature of this model, whereas some secondary vortices are still surviving in the Smagorinsky predictions.
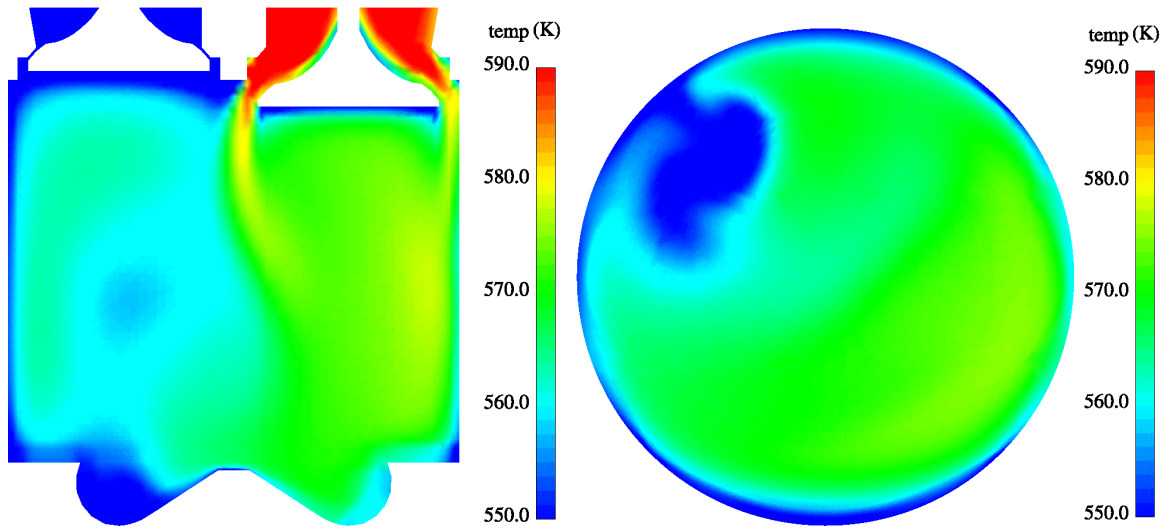
Figure 8.27 Temperature contours at a vertical cross-section through the centerline and at a horizontal cross-section 6 cm below the cylinder head at 105° CA during the intake stroke for the k-ε model predictions
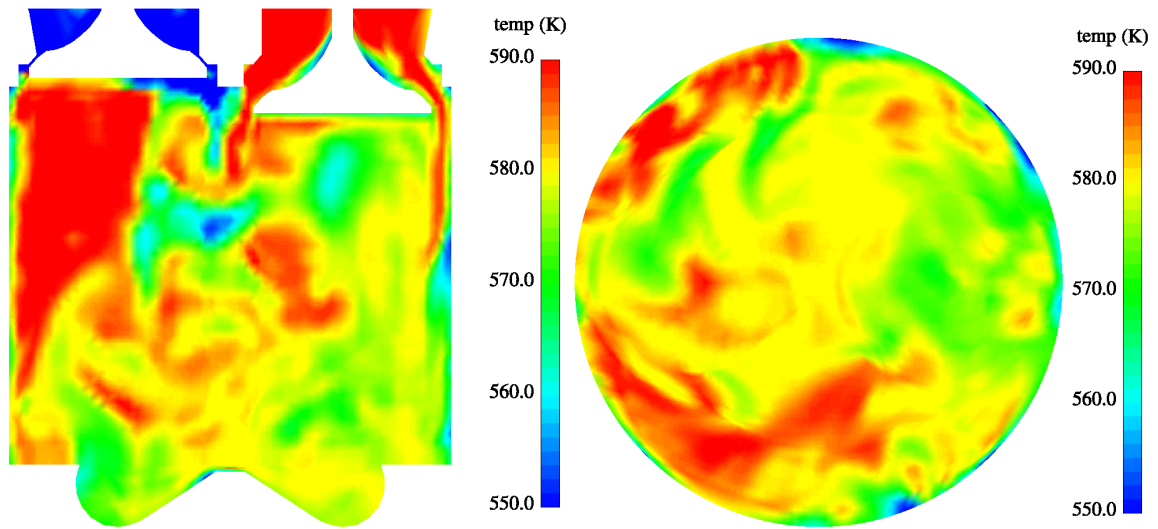
Figure 8.28 Temperature contours at a vertical cross-section through the centerline and at a horizontal cross-section 6 cm below the cylinder head at 105° CA during the intake stroke for the Smagorinsky model predictions
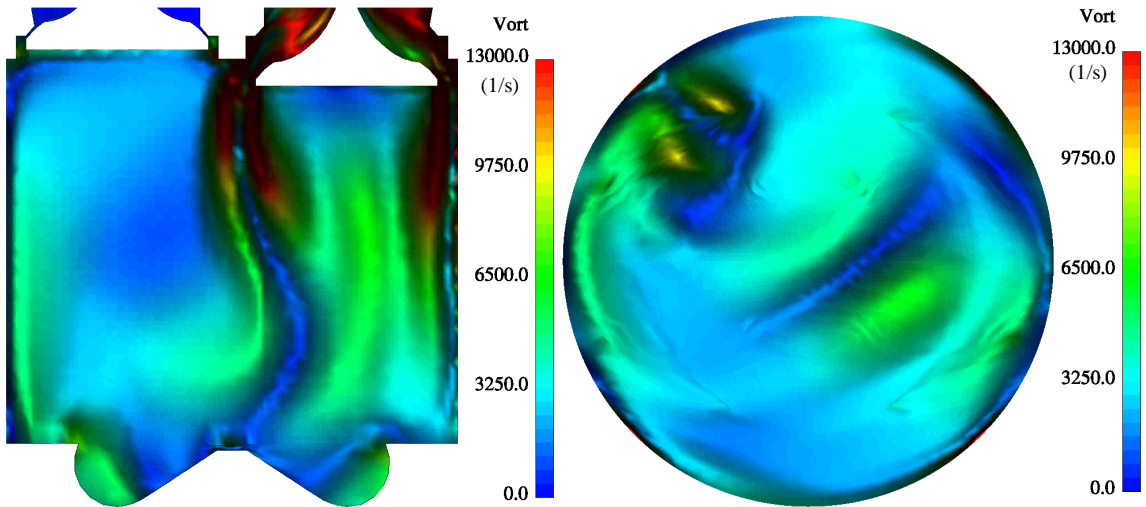
Figure 8.29 Vorticity contours at a vertical cross-section through the centerline and at a horizontal cross-section 6 cm below the cylinder head at 105° CA during the intake stroke for the k-ε model predictions
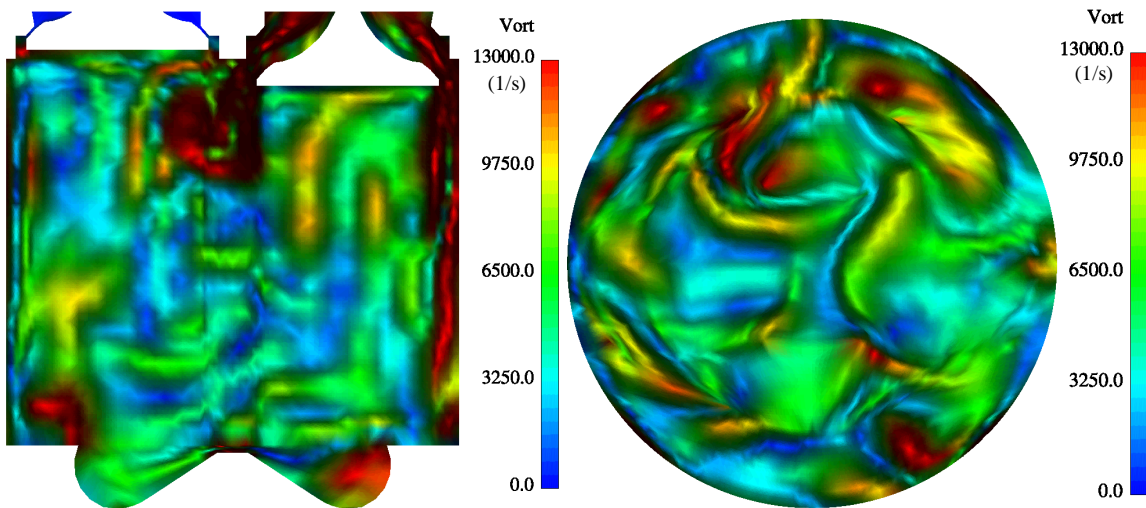
Figure 8.30 Vorticity contours at a vertical cross-section through the centerline and at a horizontal cross-section 6 cm below the cylinder head at 105° CA during the intake stroke for the Smagorinsky model predictions
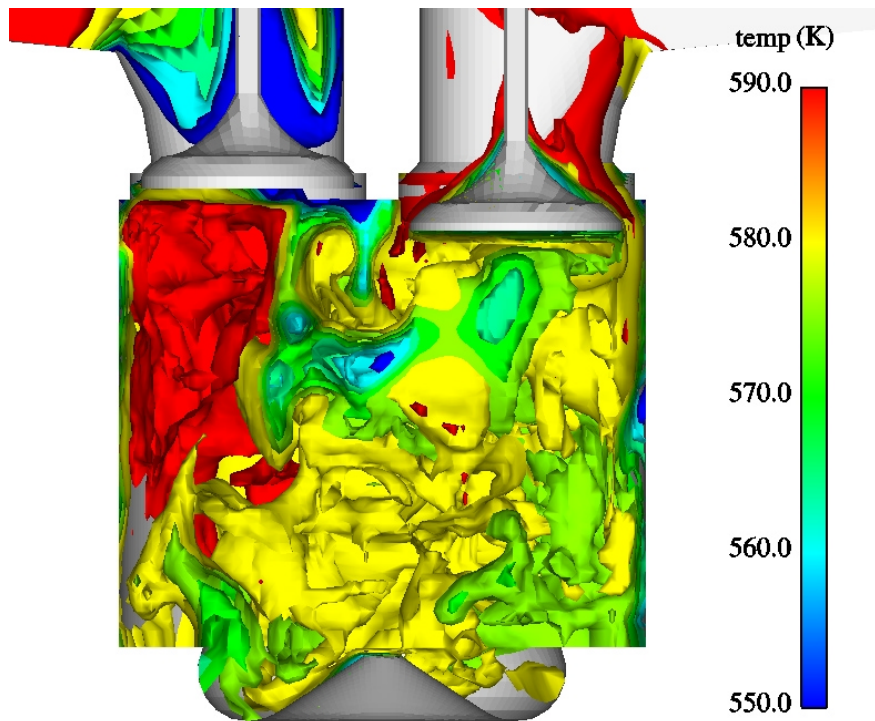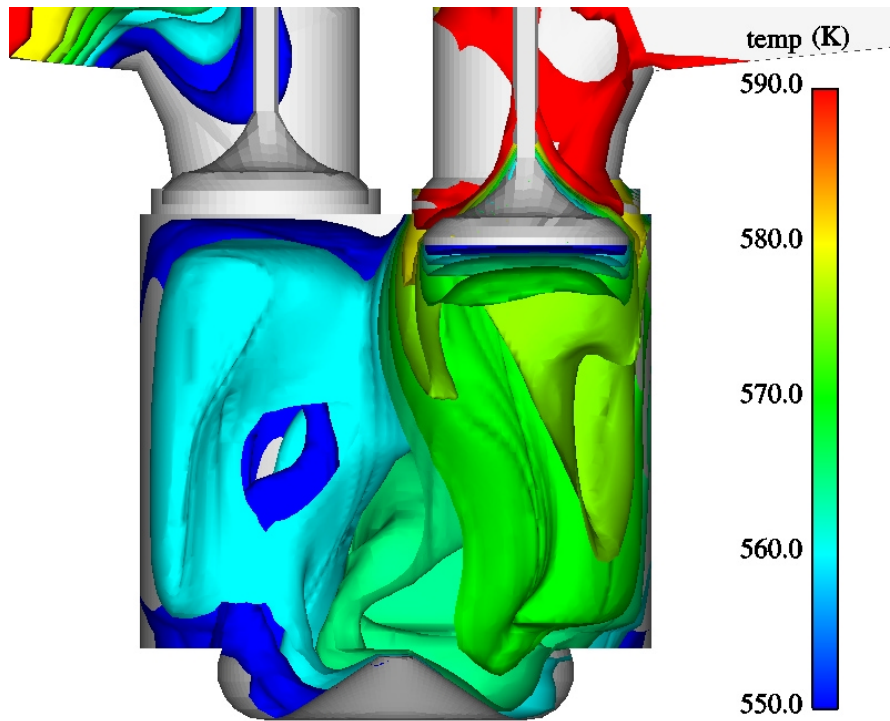
Figure 8.31 Temperature iso-contours at 105° CA during the intake stroke for the

k-ε model (top) and Smagorinsky model (bottom) predictions

The temperature contours are depicted in Figures 8.27 and 8.28. Although both models predict the inlet jet around the intake valve, the k-ε model shows again an almost uniform distribution, whereas the Smagorinsky model predictions betray a highly turbulent structure. Notice that the diffusion of the inlet jet is much higher for the k-ε model predictions. The same is true for the vorticity contours presented in Figures 8.29 and 8.30. Finally, the iso-contours of temperature are shown in Figure 8.31 for a more visual understanding.

The results presented in this section are seen as a confirmation of the fact that the present methodology is capable of resolving a significant portion of the inertial sub-range in the energy spectra. Certainly, the most energetic large coherent structures are captured by the predictions. The energy spectra display about the same energy content out to $f \approx 10^4 \, \text{Hz}$ as the same order of maximum frequency as in experiments.

Chapter 9

CONCLUSIONS AND RECOMMENDATIONS

The order of magnitudes of the important length and time scales which are relevant to both the engine geometry and speed, and the resulting turbulent flow field were established using the k-ε model predictions. A review of measured and computed scales relevant to IC engines was presented and an assessment of these was made in comparison with the self imposed scales of the engine itself. This assessment included axisymmetric calculations using the KIVA-3 code (Amsden, 1993) for a typical IC engine, and focuses on the influence of combustion, compression ratio, initial conditions and numerical mesh on predicted turbulence scales implied by the standard k- ε turbulence model. The computations reveal some unexpected and interesting trends. The compression ratio has a significant overall impact on the length scale, whereas initial turbulence intensity or three-dimensionality have a barely noticeable impact on either the length or the time scales away from the TDC.

A comparative study of the commonly used RANS models applied to internal combustion engines was conducted, using a benchmark case that resembles a motored IC-engine. As expected the models did not perform uniformly well over all flow regimes. Significant differences were observed among various models as the engine speed

increased. The RNC-k-ε (i.e. k-ε model corrected for streamline curvature) model was found to perform slightly better, and the Low-Re model seems to perform the best, with an appreciable improvement near the walls.

A new hybrid eddy viscosity model has been proposed which tends to RANS calculations and to LES with a Smagorinsky SGS model, in the limit of coarse and fine girds, respectively. This model is especially suitable for engine simulations because most engine simulations are inherently three-dimensional and transient as in LES. The results indicate that the new SEV (Smagorinsky-based eddy viscosity) model provides an alternative in predicting the mean flow field in IC engines without solving the kinetic energy and dissipation rate equations; albeit algebraic expressions are provided for these quantities. The new model involves the major engine parameters such as mean piston speed, and it also contains low Reynolds number effects. With this model some in-cylinder flow properties could be simulated better. On the other hand, the new model can also be used as a SGS model for LES in case of a sufficiently small grid size. Though, more rigorous validation studies have to be conducted to appraise the SEV model, results indicate a promising turbulence model for engine simulations.

A systematic investigation of numerical prediction of in-cylinder turbulence (i.e. instantaneous random fluctuating components of flow variables) in internal combustion engines has been performed using the KIVA code. The results of the simulated benchmark cases have revealed that by carefully controlling the numerical errors and using relatively fine grid resolution and a very small time step the unsteady dynamics of turbulent flows can be captured reasonably well.

The present engine applications show that the instantaneous large scale flow structures (i.e. coherent large eddies) can be captured, and the predicted turbulence statistics are in good qualitative agreement with the experimental data in a similar engine. In particular, the good correspondence of normalized spectra to that obtained from measurements by other authors is encouraging. It can be said that a significant portion of the energy spectra can be resolved within the range of 100 to 10,000 Hz. However, the reader should be cautioned that the cycle-to-cycle variations, which are usually significant, could not be accounted for in the present calculations. In future calculations several cycles should be simulated and an ensemble mean value for the flow variables should be obtained. The predicted trends of velocity fluctuations during the intake as a function of crank angle as well as its magnitude are also in good agreement with experimentally observed trends. Close agreement of fluctuating velocity component produced on different grids and a good comparison with experimental data indicate that the numerical diffusion errors can not be a dominant factor in the defining the dynamics of the resolved flow-field. This study should be extended to simulations with combustion to have a truly understanding of the scales present inside the engine throughout the whole cycle, which would be very appreciated from an engine design aspect.

This study has also shown that contrary to some arguments, significant turbulence is likely to be generated by a carefully designed bowl, and that the intake turbulence decays rapidly towards the TDC during compression stroke. Instability seems to be induced by the unsteady flow separation at the edge of the bowl and the squish region, although the turbulence generated by the bowl is relatively small. Current work aims at combining both mechanisms so that a fair comparison with measurements can be made.

In order to ensure practicality in engineering applications, the turnaround time for the computations should be decreased drastically. This can be accomplished by resorting to parallel programming with the appropriate numerical algorithms and the use of parallel computers. A parallel implementation of the KIVA code on workstation clusters with distributed memory seems to be a viable and cost effective alternative for research institutions as well as industry.

It is also highly desirable to obtain a good set of experimental data specifically for validation of large eddy simulations. The experiments need to be performed in conjunction with the computations, and cover a range of engine speeds with and without combustion, while keeping the valve and cylinder geometry relatively simple.

Appendix A

SHORT DESCRIPTION OF THE KIVA-3 CODE

The present calculations were performed utilizing readily available computer codes, KIVA-3 and -3V (Amsden, 1993,1997; see also Amsden et al., 1985 and 1989). KIVA-3 is a transient, multiphase, multidimensional, arbitrary-mesh, finite volume CFD program widely used for internal combustion engine simulations. It is based on the Arbitrary Lagrangian Eulerian (ALE) method (Margolin, 1997). The numerical representation of the convective/advective terms in Eulerian approach lead to both diffusion and dispersion errors, which create difficulties in resolving sharp interfaces in flow variables. The ALE method seems to remedy some of those deficiencies. The concept of the ALE approach is that mesh motion can be chosen arbitrarily. The method is typically implemented in three phases. The first phase is an explicit Lagrangian update of the equations of motion. The second phase is an optional implicit phase that allows sound waves to move many computational cells per time step if the material velocities are smaller than the fluid sound speed. This allows for greater computational efficiency. The third phase is the remapping (or rezoning) where the solution from the end of phase two is mapped back onto an Eulerian grid. This mapping is essentially one step of a conservative advection algorithm (Margolin, 1997). The special case of non-moving

boundary where the cells are always mapped back to the original grid is the Eulerian limit. The reader is referred to Amsden et al., (1993) and Hirt et al., (1997) for more details regarding the ALE method and the KIVA family of codes.

The version utilized uses the standard k-ε model, and a combustion model with a combination of finite rate and equilibrium chemistry to model the combustion processes, including a NOx formation sub-model. KIVA-3 has a fairly sophisticated spray dynamics model which tracks the droplets in a Lagrangian frame of reference while accounting for the changes in mass, momentum and energy of representative droplets. The turbulence effects on the spray droplets are modeled using the Monte Carlo method. The fluctuating fluid velocity is randomly chosen from a Gaussian distribution with a standard deviation of $(2/3 \cdot k)^{1/2}$ once every turbulence-droplet correlation time, $\tau_{tur} = \text{function}(k,\varepsilon)$.

The standard k-ε model that is implemented in KIVA-3 consists of the following equations

$$\frac{\partial \rho k}{\partial t} + \nabla \cdot (\rho \underline{u} k) = -\frac{2}{3}\rho k \nabla \cdot \underline{u} + \underline{\underline{\sigma}} : \nabla \underline{u} + \nabla \cdot \left[\left(\frac{\mu}{Pr_k}\right)\nabla k\right] - \rho \varepsilon \tag{A.1}$$

$$\frac{\partial \rho \varepsilon}{\partial t} + \nabla \cdot (\rho \underline{u} \varepsilon) = -(\frac{2}{3}C_{\varepsilon_1} - C_{\varepsilon_3})\rho \varepsilon \nabla \cdot \underline{u} + \nabla \cdot \left[\left(\frac{\mu}{Pr_\varepsilon}\right)\nabla \varepsilon\right] + \frac{\varepsilon}{k}\left[C_{\varepsilon_1} \underline{\underline{\sigma}} : \nabla \underline{u} - C_{\varepsilon_2} \rho \varepsilon\right] \tag{A.2}$$

with the model constants $C_{\varepsilon_1} = 1.44$, $C_{\varepsilon_2} = 0.92$, $C_{\varepsilon_3} = -1.0$, $Pr_k = 1.0$ and $Pr_\varepsilon = 1.3$. The SGS heat flux vector is calculated from SGS stresses by using a constant turbulent Prandtl number. KIVA-3 allows for a SGS model, which utilizes the k-equation given above along with constraining the ε values to satisfy the following inequality:

$$\varepsilon \geq \left[\frac{C_\mu}{Pr_\varepsilon (C_{\varepsilon_2} - C_{\varepsilon_1})} \right]^{\frac{1}{2}} \frac{k^{\frac{3}{2}}}{L_{SGS}} \qquad (A.3)$$

L_{SGS} is an input length scale whose value is typically some measure of the computational cell dimension. In this study L_{SGS} was taken to be equal to the grid related length scale, $L_G = (\Delta x \Delta y \Delta z)^{1/3}$, and used as a constant with a typical cell size. This model will be referred to as the k-$\varepsilon |_{SGS}$ model.

The above turbulence models were used in conjunction with the commonly used law-of-the-wall boundary condition which is implemented in KIVA-3. The basic assumption here is that the interaction between the modeled near wall region and the outer region is weak (Brooke and Hanratty, 1993).

All spatial derivatives other than the convective terms are approximated with central differencing. Spatial accuracy of the convective terms is limited to several choices including first-order upwinding (FOUP), not used in this study, central differencing (CD), a user defined scheme that combines the previous two choices, and a flux-limiting scheme known as Quasi-Second-Order Upwinding (QSOU). Both the first-order upwinding and the QSOU schemes are monotonic.

Further justification to the numerical scheme can be provided by an order of magnitude analysis of the truncation error. It can be shown that in the considered cases the normalized truncation error is given by

$$T.E. = C_1 \underbrace{\frac{\overline{V}_p \Delta t}{d_v}}_{I} + C_2 \underbrace{\frac{\Delta x^2}{d_v^2}}_{II} + \vartheta \left(\Delta t^2, \Delta x^3 \right)$$

where a typical mean piston speed is $\overline{v}_p \cong 500$ cm/sec, $d_v \cong 3$ cm is the valve diameter and C_1, C_2 are assumed to be well behaving functions of space and time and $\vartheta(C_1) \cong \vartheta(C_2)$. Then, for $\Delta t = 1.0 \times 10^{-7}$ sec, and $\Delta x = 0.1$ cm,

$$\frac{\text{Term I}}{\text{Term II}} \approx \frac{\overline{V}_p d_v \Delta t}{\Delta x^2} \approx 10^{-2}$$

which shows that spatial error will still be the dominating factor, and there is no need for further refinement of the time scheme. It should be noted that there are other successful LES studies in the literature which use first order time scheme (see the work of Tamara et al., and Onera et al. as reported by Rodi et al., 1997 in an LES Workshop; see also Naitoh et al., 1992).

REFERENCES

Aldama, A. A. (1990) "Filtering Techniques for Turbulent Flow Simulation", In Brebbia, C. A. and Orszag, S.A. ed., Lecture Notes in Engineering, pp. 1-10, Springer-Verlag, Berlin, Heidelberg.

Amsden, A. A. (1997), "KIVA-3V: A Block-Structured KIVA Program for Engines with Vertical or Canted Valves," Los Alamos National Laboratory, Los Alamos National Laboratory Report LA-13313-MS, UC-1412, Los Alamos, New Mexico 87545.

Amsden, A. A. (1993), "KIVA-3: A KIVA Program with Block-Structured Mesh for Complex Geometries," Los Alamos National Laboratory, Los Alamos National Laboratory Report LA-12503-MS, UC-361, Los Alamos, New Mexico 87545.

Amsden, A. A., O'Rourke, P. J., and Butler, T. D. (1989) "KIVA-II: A Computer Program for Chemically Reactive Flows with Sprays," Los Alamos National Laboratory Report LA-11560-MS, Los Alamos, New Mexico 87545. Also US DOE Report DE89 012805.

Amsden, A. A., T. D. Butler, P. J. O'Rourke and J. D. Ramshaw (1985), "KIVA - A Comprehensive Model for 2-D and 3-D Engine Simulations," SAE Paper 850554.

Arcoumanis, C., Whitelaw, J.H., Hentschel, W. and Schindler, K-P (1994) "Flow and Combustion in a transparent 1.9 liter direct injection diesel engine," IMechE 1994, Part D: Journal of Automobile Engineering, Proc. Instn Mech Engrs, Vol. 208, pp. 191-205.

Auriemma, M., Corcione, F.E., Macchioni, R., and Valentino, G. (1998) "Interpretation of Air Motion in Reentrant Bowl in-Piston Engine by Estimating Reynolds Stresses," SAE Technical Paper Series #980482

Bardina, J., Ferziger, J. H. and Reynolds, W.C. (1983) "Improved Turbulence Models based on Large Eddy Simulation of Homogeneous, Incompressible Turbulent Flows", Report TF-19, Dept. Mech. Engr. Stanford University, Stanford, CA.

Bashay, K.R. and Gosman, A.D. and Watkins, A.P. (1986), "Assessment of Multidimensional Diesel Spray Predictions", SAE Paper 861570.

Batchelor, G.K. (1969) "Computation of the Energy Spectrum in Homogeneous Two-Dimensional Turbulence", Phys. Fluids Suppl. II, 12, pp. 233-239.

Bo, T., Clerides, D., Gosman, A. D. and Theodossopoulos, P. (1997), "Multidimensional Modeling of Diesel Combustion and Emissions Formation", Proceedings of the First Meeting of the Greek Section of the Combustion Institute, pp. 283-292, Nov. 28-29, Athens, Greece

Boussinesq, J. (1877) "Theorie de l`Ecoulement Tourbillant", Mem. Presentes par Divers Savants Acad. Sci. Inst. Fr., Vol 23, pp.31-64.

Bradshaw, P. (1971) An Introduction to Turbulence and its Measurements, Pergamon Press, Oxford, U.K.

Brooke, J. W. and Hanratty, T. J. (1993), "Origin of Turbulence-Producing Eddies in a Channel Flow", Phys. Fluids A 5,1011.

Catania, A.E (1998) Private communication.

Catania, A.E. and Spessa, E. (1996) "Speed Dependence of Turbulence Properties in a High-Squish Automotive Engine Combustion System," SAE Technical Paper Series #960268.

Catania, A.E., Dongiovanni, C., Mittica, A., Molina, G., and Spessa, E. (1995) "A New Test Bench for HWA Fluid-Dynamic Characterization of a Two-Valved In-Piston-Bowl Production Engine," SAE Technical Paper Series #952467.

Catania, A.E., Dongiovanni, C., Mittica, A., Negri, C. and Spessa, E., (1996), "Turbulence Spectrum Investigation in a DI Diesel Engine with a Reentrant Combustion Bowl and a Helical Inlet Port", SAE Paper #962019.

Catania, A.E., Dongiovanni, C., Mittica, A., Negri, C. and Spessa, E., (1997), "Study of Turbulent Flow Components and Their Statistical Properties in a DI Automotive Diesel Engine", Proc. of SAE Int. Pacific Conference, November, Bali, Indonesia.

Celik, I. and Yavuz, I. (1997) "An Assessment of Turbulence Length Scales Relevant to IC Engines," Proceedings of the ASME-ICE Division, Spring Technical Conference, Fort Collins, CO, April 27-30.

Celik, I., Chattree, M., Singh, S. and French, W.E. (1987) "Application of the k-e Turbulence Model to Swirling Flow inside the METC Entrained-flow Reactor," in Proc. of Fifth Int. Conf. on Numerical Methods in Laminar and Turbulent Flow,

Editors: C. Taylor, W.G. Habashi, and M.M. Hafez, Montreal, Canada, July 6-10, pp. 2102-2114.

Celik, I., Wang, Y.Z., Crawford, B.G. and Lyons, D.W. (1992) "A Numerical Study of Diesel Engine Emissions from Combustion of Various Fuels," in <u>New Developments in Off-Highway Engines</u>, Edt.: B. Chrisman, ASME publications, New York, pp. 73-80.

Celik, I., Yavuz, I., Smirnov, A., Smith, J., Amin, E., Gel, A. (1999) "Prediction Of In-Cylinder Turbulence for IC Engines", Mediterranean Combustion Symposium, Antalya, Turkey, June 20-25, 1999.

Choi, W. and Guezennec, Y. G. (1998), "Experimental investigation to study convective mixing, spatial uniformity and cycle-to-cycle variation during the intake stroke in an IC engine," Proceedings of the ASME ICE Division Fall Technical Conference. September 30, 1998, Clymer, New York.

Corcione, F.E. and Valentino, G. (1990) "Turbulence Length Scale Measurements by Two-Probe-Volume LDA Technique in a Diesel Engine," SAE Paper # 902080, Society of Automotive Engineers, Int. Fuels and Lubricants Meeting and Exposition, Tulsa, Oklahoma, October 22-25.

Corcione, F.E. and Valentino, G. (1994a) "Analysis of In-Cylinder Turbulent Air Motion Dependence on Engine Speed," SAE Technical Paper Series # 940284

Corcione, F.E. and Valentino, G. (1994b) "Analysis of In-Cylinder Flow Processes by LDA," Combustion and Flame, Vol. 99, pp. 387-394

Erlebacher, G., and Hussaini, M.Y. (1993) "Direct Numerical Simulation and Large Eddy Simulation of Compressible Turbulence," in <u>Large Eddy Simulation of Complex Engineering and Geophysical Flows</u>, Editors: B. Galperin, and S. A. Orszag, Cambridge University Press.

Ferziger, J (1993) "Subgrid-Scale Modeling," Large Eddy Simulation of Complex Engineering and Geophysical Flows, edited by Galperin, B. and Orszag, S., Cambridge University Press.

Ferziger, J. H. and Peric, M. (1997) <u>Computational Methods for Fluid Dynamics</u>, 2nd ed., Springer-Verlag, Berlin, Heidelberg.

Fraser, R.A., Felton, F.G., Bracco, F.V. and Santavicca, D.A. (1986) "Preliminary Turbulence Length Scale Measurements in a Motored IC Engine," SAE Technical Paper Series #860021.

Galperin, B. and Orszag, S. A. (1993) editors, <u>Large Eddy Simulation of Complex Engineering and Geophysical Flows</u>, Cambridge Univesity Press.

Garrick, S.C. (1995) "Large Eddy Simulations of a Turbulent Reacting Mixing Layer," AIAA-95-0010, 33rd Aerospace Sciences Meeting & Sciences, Reno, NV, January 9-12.

Gosman, A. D. (1985) "Multidimensional Modeling of Cold Flows and Turbulence in Reciprocating Engines," SAE Paper # 850344, Int. Congress & Exposition, Detroit, Michigan, Feb. 25-March 1.

Han, Z. and Reitz, R.D. (1995) "Turbulence Modeling of Internal Combustion Engines using RNG k-ε Models", Comb. Sci. Tech., Vol.106, pp.207.

Han, Z., Fan, L. and Reitz, R. D. (1997), "Multidimensional Modeling of Spray Atomization and Air-Fuel Mixing in a Direct-Injection Spark-Ignition Engine, SAE Paper #952431.

Han, Z., Reitz, R.D., Corcione, F.E., and Valentino, G. (1996) "Interpretation of k-ε Computed Turbulence Length Scale Predictions for Engine Flows," 26th Symposium Int., The Combustion Institute.

Haworth, D. (1998), "Large Eddy Simulation of In-Cylinder Flows", International Conference on Multi-dimensional Simulation of Engine Internal Flows, IFP, Rueil-Malmaison, France, Dec. 3-4.

Hayasa, T. (1999) "Monotonic Convergence Property of Turbulent Flow Solution with Central Difference and QUICK Schemes", Journal of Fluids Engineering, Vol. 121, pp. 351-358

Hentschel, W. (1996) "Modern Tools for Diesel Engine Combustion Investigation," Proc. of 26th Comb. Symp. (Int.), The Combustion Institute, Naples.

Hessel, R.P. and Ruthland, C. J. (1995) "Intake flow modeling in a four-stroke diesel using KIVA-3," AIAA Journal of Propulsion and Power, 11(2), pp. 378-384.

Heywood, J.B. (1987) "Fluid Motion within the Cylinder of Internal Combustion Engines," The 1986 Freeman Scholar Lecture, ASME Journal of Fluids Engineering, Vol. 109, pp. 3-35.

Himes, M.R., Farrell, P.V. (1998) "Laser Doppler Velocimeter Measurements within a Motored Direct Injection Spark Ingnited Engine", ASME ICE Engine Division Fall Technical Conference, Sept. 23-27, Clymer, New York.

Hinze, J.O. (1975) Turbulence, 2nd edition, McGraw-Hill, New York.

Hirt, C., Amsden, A., and Cook, J. (1997) "An Arbitrary Lagrangian-Eulerian Computing method for All Flow Speeds," J. Comp. Physics, Vol. 35, pp. 203-216.

Hossain, M.S. and Rodi, W. (1982), "A Turbulence Model for Buoyant Flows and its Application to Vertical Buoyant Jets", in Turbulent Jets and Plumes, editor: W. Rodi, Pergamon Press, New York, pp.121-178.

Hoult, D.P. and Wong, V.W. (1980) "The Generation of Turbulence in an Internal-Combustion Engine," in Combustion Modeling in Reciprocating Engines, Editors: J.N. Mattavi and C.A. Amann, Plenum Press, New York, pp. 131-161.

Hunt, J. C. R. (1990) "Developments in Computational Modeling of Turbulent Flows", In Numerical Simulation of Unsteady Flows and Transition to Turbulence, Editors: Rodi, G., Pironneau, O., Proceedings of the ERCOFTAC Workshop held at EPFL, Lausanne, Switzerland, March 26-28.

Knight, D., Zhou, G., Okong'o, N. and Shukla, V. (1998) "Compressible Large Eddy Simulation Using Unstructured Grids", AIAA 36th Aerospace Sciences Meeting.

Kolmogorov, A. N. (1942) "Equations of Turbulent Motion of an Incompressible Fluid", Izvestia Academy of Sciences, USSR: Physics, Vol. 6, Nos. 1 and 2, pp. 56-58.

Lam, C.K.G. and Bremhorst, K. (1981) "A Modified Form of the k-ε Model for Predicting Wall Turbulence", Transactions of the ASME, Vol.103, Sept. 1981

Lancaster, D.R. (1976) "Effects of Engine Variables on Turbulence in Spark-Ignition Engine," SAE Paper # 760159.

Lee, J. and Farell, P.V.(1992) "Particle Image Velocimetry Measurements of IC Engine Valve Flows," Sixth Int. Symp. on Applications of Laser Techniques to Fluid Mechanics and Workshop on Computers in Flow Measurements. Lisbon, Portugal.

Leschziner, M.A., (1991) "Modeling Strongly Swirling Flows With Advanced Turbulence Closure," in Advances in Numerical Simulations of Turbulent Flows, Editors: Celik, I., Kobayashi, T., Ghia, K.N. and Kurokawa, J., ASME Publication, FED-Vol. 117, pp. 1-10, New York.

Lien, F.S. and Leschziner, M.A. (1994) " Assessment of Turbulence-Transport Models Including Non-linear RNG Eddy-Viscosity Formulation and Second-Moment Closure for Flow over a Backward-Facing Step," Computers and Fluids, Vol. 23, No. 8, pp. 983-1004.

Lilly, D. K. (1966) "On the Application of the Eddy Viscosity Concept in the Inertial Sub-range of Turbulence", NCAR Manuscript 123.

Lumley, J.L. (1999) Engines: an Introduction, Cambridge University Press, Cambridge, UK.

Margolin, L. (1997) "An Arbitrary Lagrangian-Eulerian Computing Method for All Flow Speeds", J. Comp. Physics, Vol. 135, pp. 198-202.

Menon, S. and Jou, W.H. (1991) "Large-Eddy Simulations of Combustion Instability in an Axisymmetric Ramjet Combustor," Combust. Sci. and Tech. Vol. 75, pp. 53-72.

Moin, P., Squires, K., Cabot, W. and Lee, S. (1991) "A Dynamic Subgrid Scale Model for Compressible Turbulence and Scalar Transport", Physics of Fluids A, Vol. 11, pp. 2746-2757.

Mongia, H.C., Reynolds, R.S., and Srinivasan, R. (1986) "Multidimensional Gas Turbine Combustion Modeling: Applications and Limitations," AIAA Journal, Vol. 24, No. 6, pp. 890-904.

Morse, A.P., Whitelaw, J.H., Yianneskis, M. (1979) "Turbulent Flow Measurements by Laser-Doppler Anemometry in Motored Piston-Cylinder Assemblies," Transactions of the ASME, Vol. 101.

Naitoh, K., Itoh, T., Takagi, Y. (1992), "Large Eddy Simulation of Premixed-Flame in Engine Based on the Multi-Level Formulation and the Renormalization Group Theory," SAE Tech. Paper No. 920590. International Congress & Exposition, Detroit, Michigan, Feb. 24-28.

O'Rourke, P.J. and Amsden, A.A. (1987) "Three Dimensinal Numerical Simulation of the UPS-292 Stratified Charge Engine, SAE paper # 870597.

Orszag, S.A., Yakhot, V., Flannery, W.S., Boysan, F., Choudhurry, D., Maruzevsky, J. and Patel, B. (1993) "Renormalizaton Group Modeling and Turbulence Simulations in Near Wall Turbulent Flows", page 1031. Elsevier Science Publishers B.V.

Piomelli, U. (1998) "Large Eddy Simulations: Present State and Future Directions," AIAA Paper 98-0534.

Prandtl, L. (1925) "Uber die ausgebildete Turbulenz", ZAMM, Vol. 5, pp. 136-139

Ragab, S.A. and Piomelli, U. (1993) Engineering Applications of Large Eddy Simulations, ASME Publication No. FED-Vol. 162.

Ramos, J.I. (1989) Internal Combustion Engine Modeling, Hemisphere Publishing Corp., New York.

Reitz, R.D., and Rutland, C.J. (1991) "3-D Modeling of Diesel Engine Intake Flow, Combustion and Emissions," SAE paper # 911789 (SAE Trans. Vol. 10, Sec. 3).

Reuss, D.L., Kuo, T.W., Khalighi, B., Haworth, D., and Rosalik, M. (1995), " Particle Image Velocimetry Measurements in a High-Swirl Engine Used for Evaluation of Computational Fluid Dynamics Calculations", SAE Tech. Paper #952381, SAE Fall Meeting, Oct. 16-19, Toronto, Canada.

Reuss, D. L. (2000), "Cyclic Variability of Large Scale Turbulent Structures in Directed and Undirected IC Engine Flows", SAE Paper 2000-01-0246 (SP-1529)

Reynolds, W.C. (1980) "Modeling of Fluid Motions in Engines- An Introductory Overview," in Combustion Modeling in Reciprocating Engines, Editors: J.N. Mattavi and C.A. Amann, Plenum Press, New York.

Reynolds, W.C. (1989) "The Potential and Limitations of Direct and Large Eddy Simulations," in Whither Turbulence, Turbulence at Crossroads, Edt.: J.L. Lumley, Springer-Verlag, New York, pp. 313-342.

Rodi, W., Ferziger J. H., Breuer, M. and Pourquie, M. (1997), "Status of Large Eddy Simulation: Results of a Workshop", Trans. of ASME, Vol. 119, pp. 248-262.

Rotta, J. C. (1951) "Statistische Theorie nichthomogener Turbulenz", Zeitschrift fur Physik, Vol. 129, pp. 547-572.

Schumann, U. (1993) "Direct and Large Eddy Simulation of Turbulence, Summary of the State-of-the-Art 1993", In Degrez, G. ed., Introduction to the Modeling of Turbulence, VKI Lecture Series 1993-02, VKI.

Shah, P. and Markatos, N.C. (1987) "Computer Simulation of Turbulence in Internal Combustion Engines," Int.`J. for Num. Methods in Fluids, Vol. 7, pp. 927-952.

Smagorinsky, J. (1963) "General Circulation Experiments With the Primitive Equations", Monthly Weather Review, 91, pp.99-165.

Smirnov, A.V. (1998) "Turbulent Swirl Flow Modeling for Combustor Applications", Ph.D. Thesis, Chalmers University of Technology, Sweden.

Smith, J., Celik, I. , Yavuz, I., Gel, A., and Amin, E. (1998) "Investigation of a Swirling Jet using KIVA-3", Proceeding of ASME-FEDSM, June 21-25, Washington, D.C.

Smith, J., Celik, I. and Yavuz, I., (1999) "Investigation of the LES Capabilities of An Arbitrary Lagrangian-Eulerian (ALE) Method", AIAA-99-0421, pp. 1--11.

Speziale, C. G. (1998) "Turbulence Modeling for Time-Dependent RANS and VLES: A Review", AIAA Journal, Vol. 36, No. 2.

Subramaniam, S., Ganesan, V., and Rao, P.S. (1991) "An Experimental Investigtion of the Flow Characteristics in the Swirl Chamber of a C.I. Engine," SAE Paper # 910480.

Sykes, R.I., Henn, U.S., Parker, S.F. and Lewellen, W.S. (1990), "Large-Eddy Simulation of a Turbulent Reacting Plume," Atmospheric Environment, 26A, 2565-2574.

Sykes, R. I., S.F. Parker, D.S. Henn, and Lewellen, W.S., (1994), "Turbulent mixing with chemical reaction in the planetary boundary layer", Journal of Applied Meteorology, Vol. 33, 825-834.

Tennekes, H. and Lumley, J.L. (1992) A First Course in Turbulence, MIT Press, Cambridge, Massachusetts.

Valentino, G. Auriemma, M., Corcione, F.E., Macchioni, R., and Seccia, G. (1998) "A LDV Data Refinement Technique to Improve Time Scale Estimation in Reciprocating Engines," Proceedings of the ASME-ICE Division, Fall Technical Conference, Irvine, PA, Sept. 27-30.

Wilcox, D.C. (1993) <u>Turbulence Modeling</u>, Griffin Printing, Glendale, California.

Witze, P.O. (1977) "Measurements of the Spatial Distribution and Engine Speed Dependence of Turbulent Air Motion in an I.C. Engine," SAE Trans. Vol. 86, Paper # 770220, pp. 1012-1023.

Yang, S. L., Peschke, B. D. and Hanjalic, K. (1998), "IC-Engine Like Flow Study Using a Second-Moment Closure Model," Proceedings of the ASME ICE Division Fall Technical Conference, September 30, Clymer, New York.

Yavuz, I. and Celik, I. (1999a) "Applicability of the k-ε Model for IC-Engine Simulations", 3rd ASME/JSME Joint Fluids Engineering Conference, July 18-23, 1999, San Francisco, CA.

Yavuz, I. and Celik, I. (1999b) "Assessment of Various Turbulence Models for IC-Engine Applications", ASME ICE Division 1999 Fall Technical Conference, October 16-20, 1999, Ann Arbor, Michigan.

Yavuz, I., Celik, I., Smith, J., Gel, A., and Amin, E. (1998), "Bowl Induced Flow Instability in a Typical Engine Cylinder", ASME ICE-Division Fall Conf., Sept. 27-30, Clymer, New York.